INSTITUTO POTOSINO DE INVESTIGACIÓN CIENTÍFICA Y TECNOLÓGICA, A.C.

POSGRADO EN CIENCIAS APLICADAS

Effects of Functionalization and Doping in Carbon Nanotubes for Fabricating Field Effect Transistors and Cluster-Nanotube Systems: Theory and Experiment

Tesis que presenta

Edgar Eduardo Gracia Espino

Para obtener el grado de

Doctor en Ciencias Aplicadas

En la opción de

Nanociencias y Nanotecnología

Codirectores de la Tesis:

Dr. Florentino López Urías

Dr. Mauricio Terrones Maldonado

Dr. Humberto Terrones Maldonado

San Luis Potosí, S.L.P., Agosto de 2011

Créditos Institucionales

Esta tesis fue elaborada en las instalaciones y con la infraestructura de la División de Materiales Avanzados para la Tecnología Moderna del Instituto Potosino de Investigación Científica y Tecnológica, A.C. y el Laboratorio de Investigaciones en Nanociencia y Nanotecnología, bajo la co-dirección de los doctores, Florentino López Urías, Humberto Terrones Maldonado y Mauricio Terrones Maldonado.

Durante la realización del trabajo el autor recibió una beca académica del Consejo Nacional de Ciencia y Tecnología en México (204089)

IPICYT

Instituto Potosino de Investigación Científica y Tecnológica, A.C.

Acta de Examen de Grado

El Secretario Académico del Instituto Potosino de Investigación Científica y Tecnológica, A.C., certifica que en el Acta 035 del Libro Primero de Actas de Exámenes de Grado del Programa de Doctorado en Ciencias Aplicadas en la opción de Nanociencias y Nanotecnología está asentado lo siguiente:

En la ciudad de San Luis Potosí a los 23 días del mes de septiembre del año 2011, se reunió a las 09:00 horas en las instalaciones del Instituto Potosino de Investigación Científica y Tecnológica, A.C., el Jurado integrado por:

Dr. Fernando Jaime Rodríguez Macías	**Presidente**	**IPICYT**
Dra. Yadira Itzel Vega Cantú	**Secretaria**	**IPICYT**
Dr. Facundo Ruiz	**Sinodal externo**	**UASLP**
Dr. Florentino López Urías	**Sinodal**	**IPICYT**
Dr. Vicente Rodríguez González	**Sinodal**	**IPICYT**

a fin de efectuar el examen, que para obtener el Grado de:

DOCTOR EN CIENCIAS APLICADAS
EN LA OPCIÓN DE NANOCIENCIAS Y NANOTECNOLOGÍA

sustentó el C.

Edgar Eduardo Gracia Espino

sobre la Tesis intitulada:

Effects of Functionalization and Doping in Carbon Nanotubes for Fabricating Field Effect Transistors and Cluster-Nanotube Systems: Theory and Experiment

que se desarrolló bajo la dirección de

Dr. Florentino López Urías

Dr. Humberto Terrones Maldonado y el Dr. Mauricio Terrones Maldonado, ambos hasta el 17 de diciembre de 2009 y bajo su dirección externa a partir del 18 de diciembre de 2009.

El Jurado, después de deliberar, determinó

APROBARLO

Dándose por terminado el acto a las 11:20 horas, procediendo a la firma del Acta los integrantes del Jurado. Dando fe el Secretario Académico del Instituto.

A petición del interesado y para los fines que al mismo convengan, se extiende el presente documento en la ciudad de San Luis Potosí, S.L.P., México, a los 23 días del mes de septiembre de 2011.

Dr. Marcial Bonilla Marín
Secretario Académico

INSTITUTO POTOSINO DE INVESTIGACIÓN CIENTÍFICA Y TECNOLÓGICA, A.C.
IPICYT
SECRETARIA ACADEMICA

Mtra. Ivonne Lizette Cuevas Vélez
Jefa del Departamento del Posgrado

Dedicatorias

Acknowledgments

I would like to thanks to all the people who have believed in me, to those people who have support me it would be impossible to reach this goal without them.

I am also grateful to Daniel Ramirez, Ferdinando Tristan, and Hugo Ramirez for their support and invaluable friendship. I am grateful to the entire technician from advanced material division at IPICYT Beatriz Rivera Escoto and Gladis Labrada Delgado.

I cannot let leave without acknowledge to Yadira Vega Cantú, Fernando Rodríguez, Emilio Muñoz Sandoval and specially to Florentino López Urías for their motivation and enthusiasm during the really stressful and difficult times.

Also, during my master and doctoral research, they have taught me thing not just in the nanoscience field also in other aspects of day life, I am thankful to Mauricio Terrones and Humberto Terrones for their support, guidance and motivation during the last years.

Additionally, part of the work presented in this Thesis was carried out through collaboration with other research groups. Therefore part of the credits is shared with them, I give special thanks to: Krisztián Kordás, Géza Tóth, Giovanni Sala from the University of Oulu (Oulun Yliopisto) in Finland and Robert Vajtai from Rice University in USA.

Content

Constancia de aprobación de la tesis **II**
Créditos institucionales **III**
Acta de examen **IV**
Dedicatorias **V**
Agradecimientos **VI**
Lista de tablas **IX**
Lista de figuras **X**
Resumen **XVI**
Abstract **XVII**

Chapter 1 : General Introduction **1**
1.1. References 7

Chapter 2 : Fabrication of Field Effect Transistors based on Functionalized-Single Walled Carbon Nanotubes Thin Films 11
2.1. Summary 11
2.2. Introduction: Random Networks of Carbon Nanotubes 13
2.2.1. Effect of Film Thickness and Functionalization on the Electrical Properties of Carbon Nanotubes Thin Films 14
2.3. Experimental Section: Nanotube Ink Preparation, Printing Technique and Electrical Characterization of the Single Walled Carbon Nanotubes Networks 18
2.3.1. *Preparation of Aqueous Inks based on Functionalized Single Walled Carbon Nanotube* 18
2.3.2. *Inkjet Printing of Thin Films Based on Functionalized Single Walled Carbon Nanotubes* 19
2.3.3. *Temperature Dependent Conductance Measurements of Functionalized SWCNTs Networks* 20
2.4. Results and Discussion 21

2.4.1. *Electrical Properties of Random Networks Based on Functionalized Single Walled Carbon Nanotubes Prepared by Inkjet Printing* 21

2.4.2. *Current-Voltage Characteristics and Field Effect Properties of Single Walled Carbon Nanotubes Thin Films* 25

2.4.3. *Field Effect Transistor Based on Random Networks of Functionalized SWCNTs* 30

2.5. Conclusion and Perspectives 33

2.6. References 35

Chapter 3 :Silver-decorated Nitrogen Doped Multiwalled Carbon Nanotubes as Gas Sensors 39

3.1. Summary 39

3.2. Introduction: Gas Sensor Based on Carbon Nanotubes 41

3.3. Experimental Section: Silver Decoration of Carbon Nanotubes, Material Characterization and Sensor Fabrication Procedure 44

3.4. Results and Discussion 46

3.5. Understanding the Sensing Mechanism of Silver-decorated Carbon Nanotubes from a Theoretical Approach 57

3.6. Conclusions 65

3.7. References 67

Chapter 4 : Electronic Properties of Different Configuration of Nitrogen-Doped Carbon Nanotubes 71

4.1. Summary 71

4.2. Introduction: Electronic Properties of Nitrogen-Doped Carbon Nanotubes 73

4.3. Results and Discussion 78

4.3.1. *Relaxed Geometries and Electronic Properties of Nitrogen-doped (10,0) Single-Walled Carbon Nanotubes: One vacancy case* 78

4.3.2. *Relaxed Geometries and Electronic Properties of N-doped (10,0) Single-Walled Carbon Nanotube: Two vacancies case* 83

4.3.3. Energetic Stability of Nitrogen-doped (10,0) Single-Walled Carbon Nanotube with Different Doping Configurations 88

4.4. Conclusions 93

4.5. References 94

Chapter 5 : Synthesis, Characterization, and Theoretical Studies of Hybrid ZnO Nanoparticles and Nitrogen-Doped Carbon Nanotubes 97

5.1. Summary 97

5.2. Introduction: Zinc Oxide Nanoparticles Anchored to Carbon Nanotubes 99

5.3. Materials and Methods: Zinc Oxide Decoration of Nitrogen Doped Carbon Nanotubes 101

5.4. Results and Discussion: N-Doped Carbon Nanotube Decoration and Material Characterization 102

5.5. Theoretical Study of Sulfur Passivated Zinc Oxide Cluster and Carbon Nanotube System 108

5.6. Conclusions 112

5.7. References 113

Chapter 6 : Conclusions and Perspectives 117

6.1. Conclusions 117

6.2. Perspectives 120

Appendix A : Electronic Structure Calculations and Computational tools 123

A.1. *Electronic Structure Calculation* 123

A.2. *Computational Tools: The SIESTA Code* 126

A.3. *SIESTA Computational Details* 128

Appendix B : Carbon Nanotube Growth Methods and Principles of Characterization Techniques **131**

B.1. *Carbon Nanotubes Growth Methods* 131

B.1.1. *Arc-discharge and Laser Ablation* 131

B.1.2. *Chemical Vapor Deposition* 132

B.2. *Characterization Techniques* 134

B.2.1. *X-ray powder diffraction* 134

B.2.2. *Electron microscopy* 135

B.2.3. *Energy Dispersive X-ray Analysis* 136

Appendix C : Published Works During the Ph. D. Thesis **137**

C.1. *Published research papers* 137

C.2. *Published patents* 138

C.3. *Poster Presentation in International Conferences* 138

Appendices References 140

List of Tables

Table 2-1 General characteristics of water-based SWCNT inks. **19**

Table 2-2 Calculated percolation threshold thickness t_c and critical exponent α for the deposited nanotube films. **23**

Table 2-3 Electrical characteristics of SWCNTs thin films. **27**

Table 3-1 Performance comparison of Ag-decorated and pure CN_X-MWNTs based sensor devices for four different organic vapors at room temperature. **50**

Table 4-1: Comparison of the formation energy (E_{form}) of some defects in the (10,0) semiconductor single walled carbon nanotube calculated in our work and previous reported works from other groups. **90**

List of Figures

Figure 1-1: Electronic, chemical and mechanical properties of single- and multi- walled carbon nanotube can be modulated by modifying their surface. **3**

Figure 1-2: Schematic representation of the present Ph.D thesis. **5**

Figure 2-1: Representation of a nanotube film with percolation pathway between the electrodes composed of metallic and semiconductor carbon nanotubes **15**

Figure 2-2: The decay of the conductance at the charge neutrality point appears inversely proportional to the coverage density of fucnctional groups**.** **16**

Figure 2-3: Electrical conductivity as a function of average film thickness of SWCNT networks made of four different types of functionalized nanotubes. **22**

Figure 2-4: Transmission electron micrographs of carboxylic acid and polyethylene glycol functionalized inks dried on sample holder grids. **24**

Figure 2-5: Drain-source current-voltage I_{DS}-V_{DS} sweeps for COOH-, $CONH_2$-, PEG- and PABS-functionalized SWCNTs films. **25**

Figure 2-6: Channel resistance as a function of temperature. **28**

Figure 2-7: Entirely inkjet printed field effect transistor with PEG-functionalized SWCNT thin film as channel, COOH-functionalized SWCNT film as source, drain and gate electrodes on a flexible transparency foil. **30**

Figure 2-8 I_{DS}-V_{DS} plots of a transistor showing *p*-channel behavior. **32**

Figure 3-1 Schematic representation of the experimental setup of the gas vapor sensor using carbon nanotubes. **45**

Figure 3-2 Transmission electron microscopy (TEM) images of Ag-nanoparticles anchored on the surface of nitrogen doped multiwalled carbon nanotubes (CN_X-MWNTs/Ag). **46**

Figure 3-3 X-ray diffraction pattern of nitrogen-doped multiwalled carbon nanotubes and Ag-nanoparticles anchored on the surface of CN_X-MWNTs. **47**

Figure 3-4 Analysis of the operation performance of the nanotube based CS_2 sensor at room temperature. **49**

Figure 3-5 Normalized electrical resistance of nanotube foils exposed to carbon disulfide (CS_2) vapors at three different temperatures for CN_x-MWNTs and Ag-nanoparticles anchored on CN_x-MWNTs. **52**

Figure 3-6 Normalized electrical resistance of nanotube foils exposed to acetone. **54**

Figure 3-7 Normalized electrical resistance of nanotube foils exposed ethanol and chloroform vapor. **55**

Figure 3-8 Change in electrical response (%ΔR) after the exposure to different vapors at various working temperatures of Ag-decorated CN_X-MWNT sensors. **56**

Figure 3-9 Relaxed geometries of nitrogen-doped carbon nanotube (CN_X-SWNT) with different molecules around of the nitrogen atoms. **58**

Figure 3-10 Electronic density of states (DOS) of the relaxed geometries of (5,5) nitrogen-doped carbon nanotube in contact with different molecules. **59**

Figure 3-11 Relaxed geometries of silver clusters with 13 atoms (Ag_{13}) with different molecules joined to the clusters surface. **60**

Figure 3-12 Electronic density of states (DOS) of relaxed geometries of Ag_{13} cluster with different molecules attached to the surface**.** **61**

Figure 3-13 Adsorption energy different organic molecules on pyridinic nitrogen-doped carbon nanotubes and icosahedral Ag_{13} cluster. **62**

Figure 3-14 Adsorption of carbon disulfide on an $Ag_{55}C_{80}$ cluster. **63**

Figure 4-2: Molecular models depicting the starting geometry of the single-walled carbon nanotube of (10,0) chirality with one vacancy and one or two nitrogen atoms. **79**

Figure 4-3: Electronic band structure of the relaxed (10,0) single-walled carbon nanotubes containing one vacancy and one or two nitrogen atoms. **81**

Figure 4-4: Molecular models showing the starting and relaxed geometries of the single-walled carbon nanotube (SWCNT) exhibiting the (10,0) chirality with two vacancies. **83**

Figure 4-5: Electronic band structure of the relaxed (10,0)-SWCNT containing two vacancies. **85**

Figure 4-6: Molecular models showing the diameter variations generated by vacancies and nitrogen doping in a (10,0) carbon nanotube. **86**

Figure 4-7: Relaxed geometry obtained by introducing two vacancies and one nitrogen atom into the (10,0) carbon nanotube. **87**

Figure 4-8: Formation energy of the (10,0) single walled carbon nanotubes (SWCNTs) by considering different ways of introducing nitrogen atoms and vacancies. **89**

Figure 4-9: Relaxed geometry of the (10,0) carbon nanotube by simultaneously introducing one nitrogen atom in a substitutional fashion (V_0N_1) and a V_1N_1B defect. **91**

Figure 5-1: Scheme diagram of the experimental setup used to anchor ZnO nanoparticles on the surface of nitrogen-doped carbon nanotubes (CN_X-MWNTs). **101**

Figure 5-2: Scanning electron microscopy (SEM) images of ZnO nanoparticles anchored on the surface of nitrogen-doped multiwalled carbon nanotubes (CN_X-MWNTs) by using different thiophene concentrations. **102**

Figure 5-3: Thiophene concentration dependence of average size of the ZnO nanoparticles anchored on nitrogen-doped multiwalled carbon nanotubes (CN_X-MWNTs) and sulfur:zinc ratio determined by energy-dispersive X-ray (EDX) after thermal treatment. **103**

Figure 5-4: X-ray diffraction (XRD) patterns of ZnO nanoparticles anchored on the surface of nitrogen-doped multiwalled carbon nanotubes (CNx-MWNTs) for different values of the thiophene concentration. **104**

Figure 5-5: Transmission electron microscopy (TEM) images of ZnO nanoparticles anchored on the surface of nitrogen-doped multiwalled carbon nanotubes (CN_X-MWCNTs). **106**

Figure 5-6: Linear mapping of a single nitrogen-doped multiwalled carbon nanotube decorated by ZnO nanoparticles. **107**

Figure 5-7: Spin-polarized electronic density of states of the zinc oxide cluster passivated with sulfur atoms on the surface $Zn_{15}O_{15}S_x$ (x=3, 6, 9, and 12). **109**

Figure 5-8: Relaxed structure of a sulfur passivated ZnO clusters ($Zn_{15}O_{18}S_8$) on the surface of a nitrogen-doped single walled (10,0) carbon nanotube. **110**

Effects of Functionalization and Doping in Carbon Nanotubes for Fabricating Field Effect Transistors and Cluster-Nanotube Systems: Theory and Experiment

Resumen

Este trabajo concentra resultados teóricos y experimentales sobre nanotubos de carbono modificados con diferentes grupos funcionales, dopados o decorados con distintas nanopartículas, lo cual modifica sus propiedades y su interacción con el medio circundante. En el capítulo 2, estudiamos el transporte electrónico y las propiedades de efecto de campo de redes aleatorias formadas por nanotubes de carbono de pared sencilla con diferentes grupos funcionales. Hemos confirmado la importancia de la funcionalización química en las propiedades eléctricas de redes de nanotubes de carbono. Además, se demostró la construcción y el buen funcionamiento de un transistor de efecto de campo fabricado con los nanotubos estudiados.

Los materiales híbridos como los nanotubos decorados con nanopartículas metálicas pueden mostrar propiedades mejoradas o únicas para su uso en sensores de gases. Por esta razón, en el capítulo 3, hemos propuesto el uso de nanotubos de pared múltiple dopados con nitrógeno y decorados con nanopartículas de plata como sensores para disulfuro de carbono. Los resultados muestran que al modificar la temperatura de operación es posible incrementar la sensibilidad y la selectividad sobre moléculas especificas.

El capítulo 4 esta enfocado a estudiar las propiedades electrónicas y estructurales de nanotubes de carbono de pared simple dopados con nitrógeno. Se realizaron cálculos basados en la teoría funcional de la densidad. Los resultados muestran que, los nanotubos pueden ser modificados de semiconductores a metálicos al variar la concentración y posición de los átomos de nitrógeno.

Materiales compuestos como los nanotubos de carbono decorados con nanopartículas metálicas o semiconductoras pueden ser utilizados en una gran cantidad de aplicaciones, sin embargo las interacciones entre las nanopartículas y los nanotubos no están completamente claras. En el capítulo 5, se utilizaron nanotubos de carbono de pared multiple dopados con nitrógeno como sustratos para la deposición de nanopartículas de óxido de zinc. Realizamos cálculos basados en la teoría funcional de la densidad para comprender el proceso de anclaje del óxido de zinc al nanotubo de carbono, además de estudiar el rol del azufre en la estabilización de las nanoparticulas.

PALABRAS CLAVE: Dopaje, Nanotubos de Carbono, Oxido de Zinc, Plata, FETs.

Effects of Functionalization and Doping in Carbon Nanotubes for Fabricating Field Effect Transistors and Cluster-Nanotube Systems: Theory and Experiment

Abstract

This Thesis work has the experimental and theoretical results on modified carbon nanotubes with different functional groups, doped or decorated with nanoparticles, which modify their properties and interaction with the surrounded environment. In chapter 2, we studied the electrical transport and field-effect properties of random networks made of single walled carbon nanotubes with different functional side groups. We confirmed the important role of chemical functionalization on the electrical properties of nanotube networks. In addition, we also have successfully demonstrated the construction of entirely functionalized carbon nanotube field-effect transistors.

Hybrid materials, consisting of nanotubes decorated with nanoparticles shows unique or enhanced sensitivity toward gaseous species when compared to pure nanotubes gas sensors. For this reason, in chapter 3, we propose the use of nitrogen-doped multiwalled carbon nanotubes decorated with silver nanoparticles as carbon disulfide gas sensors. Our results demonstrate that the mechanism of gas detection can be tuned from physisorption, at room temperature, to chemisorption at higher temperature. We demonstrated that the used of nanotube decorated with silver nanoparticles can significantly improve the signal response when compared to those materials without nanoparticles.

We also studied in chapter 4, the electronic and structural properties of nitrogen-doped (10,0) single walled carbon nanotubes using first-principles density functional theory. Our results demonstrated that carbon nanotubes could be changed from semiconductor to metallic, when modifying the concentration and position of nitrogen atoms.

Composite materials such as metal or metal oxide decorated carbon nanotubes could be used in many applications, but the understanding of the interactions between nanoparticles and the carbon nanotubes has not been fully addressed. Along these lines, in chapter 5, we use nitrogen doped multiwalled carbon nanotubes as an efficient substrate for the deposition of zinc oxide nanoparticles. We also performed first-principles density functional calculations to understand the anchorage process of the zinc oxide to the nitrogen-doped carbon nanotubes, and the role of sulfur in the stabilization of nanoparticles.

KEY WORDS: Doping, Carbon Nanotubes, Zinc Oxide, Silver, FETs.

Chapter 1 : General Introduction

Surface carbon nanotubes modification is a prominent approach to manipulate their chemical, mechanical and electrical properties. The surface modification can be performed by doping with foreign atoms, chemical functionalization or by decorating with metallic or semiconductor nanoparticles. A selective surface modification allows modifying and manipulating a desire property for our own benefit. The addition of foreign atoms, functional groups or nanoparticles may significantly modify the properties of the carbon nanotubes and their interaction with the surrounded environment. All controlled modifications increase the opportunity to use carbon nanotubes as building blocks for high performance devices that we can use in our day life.

Pure carbon nanotubes (i.e., as they are synthesized) are chemical inert [1], this difficult their use in variety of applications. Nowadays, it is well known that chemical doping is a feasible method to modify the electronic properties of carbon-based nanomaterials [2]. Chemical doping of carbon nanotubes is an interesting topic, since the electronic, chemical and mechanical properties are significant altered depending on the species and the location of the dopant atom in the nanotube lattice structure [2]. Generally three types of doping can be described; when atoms, molecules or crystalline materials are encapsulated inside the nanotubes, the doping is called endohedral or encapsulation [3,4,5]. Exohedral doping consists on the intercalation of certain atoms into available “free” spaces of the carbon arrangement [2,6,7]. Finally, the in-plane or substitutional doping of carbon nanostructures occurs when foreign atoms replace carbon atoms in the

ordered network [2]. Nowadays, the addition of different elements such as nitrogen [8,9,10], phosphorous [11,12], or sulfur [13] has been used as a feasible method to control the properties of carbon nanotubes. Typically, these doping increase their chemical reactivity [1,2] and modify their mechanical properties altering the original morphology [8,13,14]. In nitrogen-doped nanotubes, the nitrogen modify their original tubular structure, creating cavities along the main axis of the nanotube, this morphology is the so-called “bamboo-type” structure [8] (see figure 1-1 (b-i)). Sulfur doping in carbon nanotubes also modify their original structure by creating “Y” junctions [13] as is depicted in figure 1-1 (b-iv). All these doped nanostructures increase the possibilities to design carbon nanotube based devices, such as field emission source [15], vapor-gas sensors with increased selectivity and sensitivity [16,17], also allows their used as an efficient substrate to deposit metallic or semiconductor nanoparticles [18,19], and increase their use in biological systems, such as delivery of drugs or infectious agent inhibitors [20,21]. Some applications are illustrated in figure 1-1e.

Other important approach to modify the properties of carbon nanotubes is the chemical functionalization. The chemical surface modification of nanotubes by attaching functional groups, such as carboxylic acid [22], the addition of polymer [22,23,24] or biomolecules [25] has been employed as an important step for preparing suspensions and stable solutions [26], and also to improve the interaction with polymeric matrices [27].

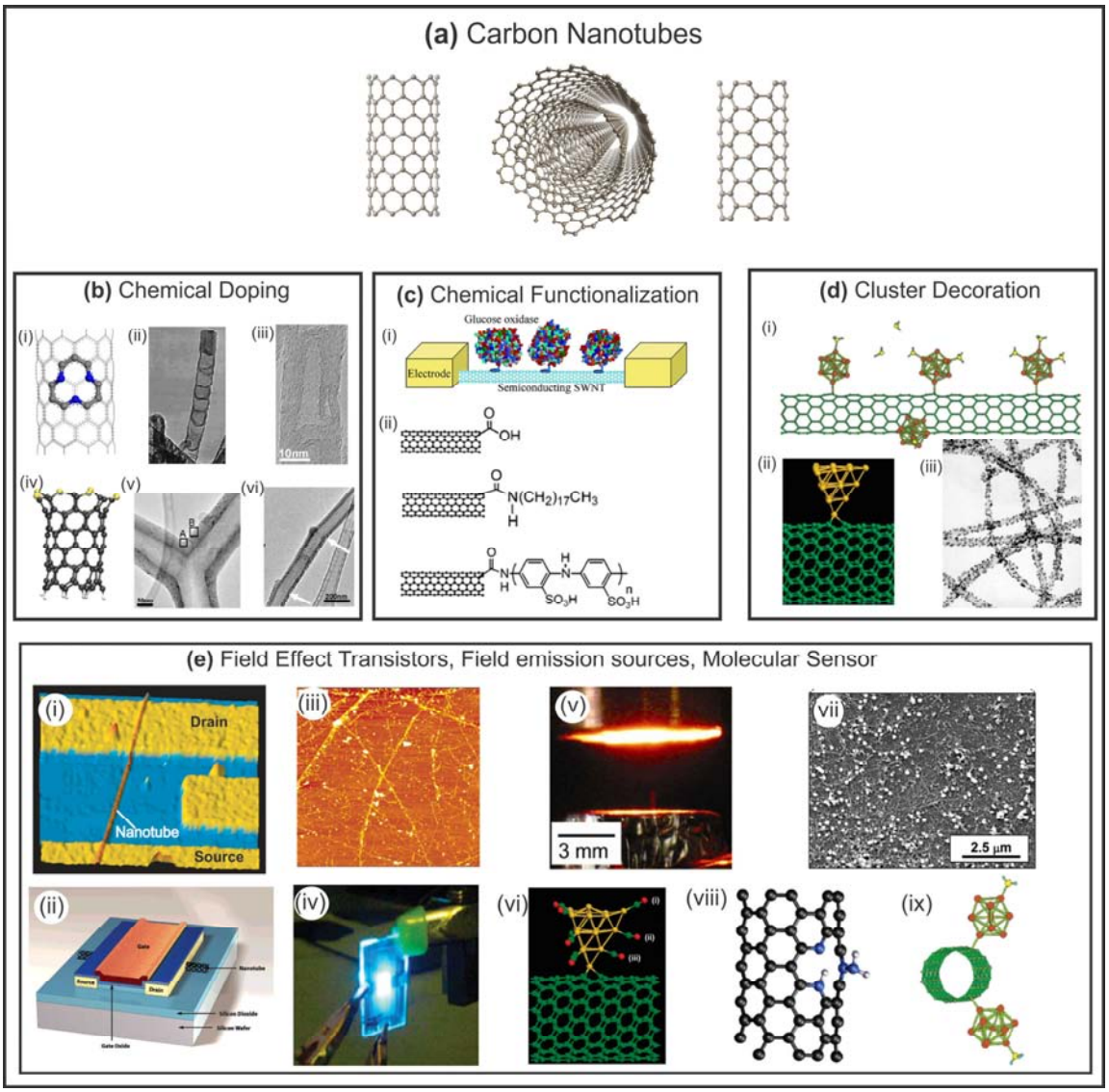

Figure 1-1: Electronic, chemical and mechanical properties of single- and multi- walled carbon nanotube can be modulated by modifying their surface. **(a)** The raw materials, Single- or multi-walled carbon nanotubes, are used as starting material. **(b)** Chemical doping of nanostructures may creates new morphologies by introducing foreing atoms; In the image, **(i-iii)** nitrogen- and sulfur- doped nanotubes with bamboo [8] and **(iv-vi)** "Y" morphologies [13], respectivelly. **(c)** Addition of functional groups such as carboxylic acid, polymers [28] or biomolecules [29] enhance the interaction with a specific materials. **(d)** The use of carbon nanotubes as an efficient subtrated for the fabrication of hybrid systems with metallic or semiconductor clusters, in the image, a scheme of gold [30] and aluminum [31] decorated SWCNTs, and MWCNTs decorated with gold nanoparticles [32]. **(e)** All these new materials increase the posibility for future applications in electronic devices, such as: **(i-iii)** field effect transitors [28,33], **(iv)** as transparent electrode for light emithing devices [34], **(v)** field emission sources [35], **(vi-ix)** selective and sensitive gas sensors [30,31,36].

However, the original electrical properties of the nanotubes are not remained intact. Side-wall covalent functionalization that change the sp^2 hybridization of carbon atoms in the tube wall could induce an impurity state in the gap region, thus leading to considerable change in electronic states as well as in the electrical properties of nanotubes [25,37]. Chemically functionalized carbon nanotubes have been widely used as an active component in sensors devices [38], polymer reinforcement [27], or biosensors [39,40]. In figure 1-1c is depicted a scheme of different functionalized nanotubes with functional groups and biomolecules.

Another important approach for surface modification is the fabrication of carbon nanotubes decorated with metal or metal-oxide nanoparticles. The addition of metallic [41] or semiconductor [42] nanoparticles modifies the properties of carbon nanotubes. These composites have been proposed as active component in gas sensing devices because they show enhanced sensitivity and selectivity [43,44] compared to pure carbon nanotubes gas sensors [45]. Also these nanocomposite can be employed in applications such as field emitters [46,47], supercapacitors [48] and hybrid solar cells [49]. In figure 1-1d are illustrated carbon nanotubes decorated with clusters and in figure 1-1e some applications.

Figure 1-2 depicts a scheme of this Ph. D. thesis, where we used carbon nanotubes as starting materials (central image), and then by a selective surface modification, we are able to modify their properties and create electronic devices that take advantage of their new properties. In Chapter 2 we studied the electrical properties of different functionalized single-walled carbon nanotubes.

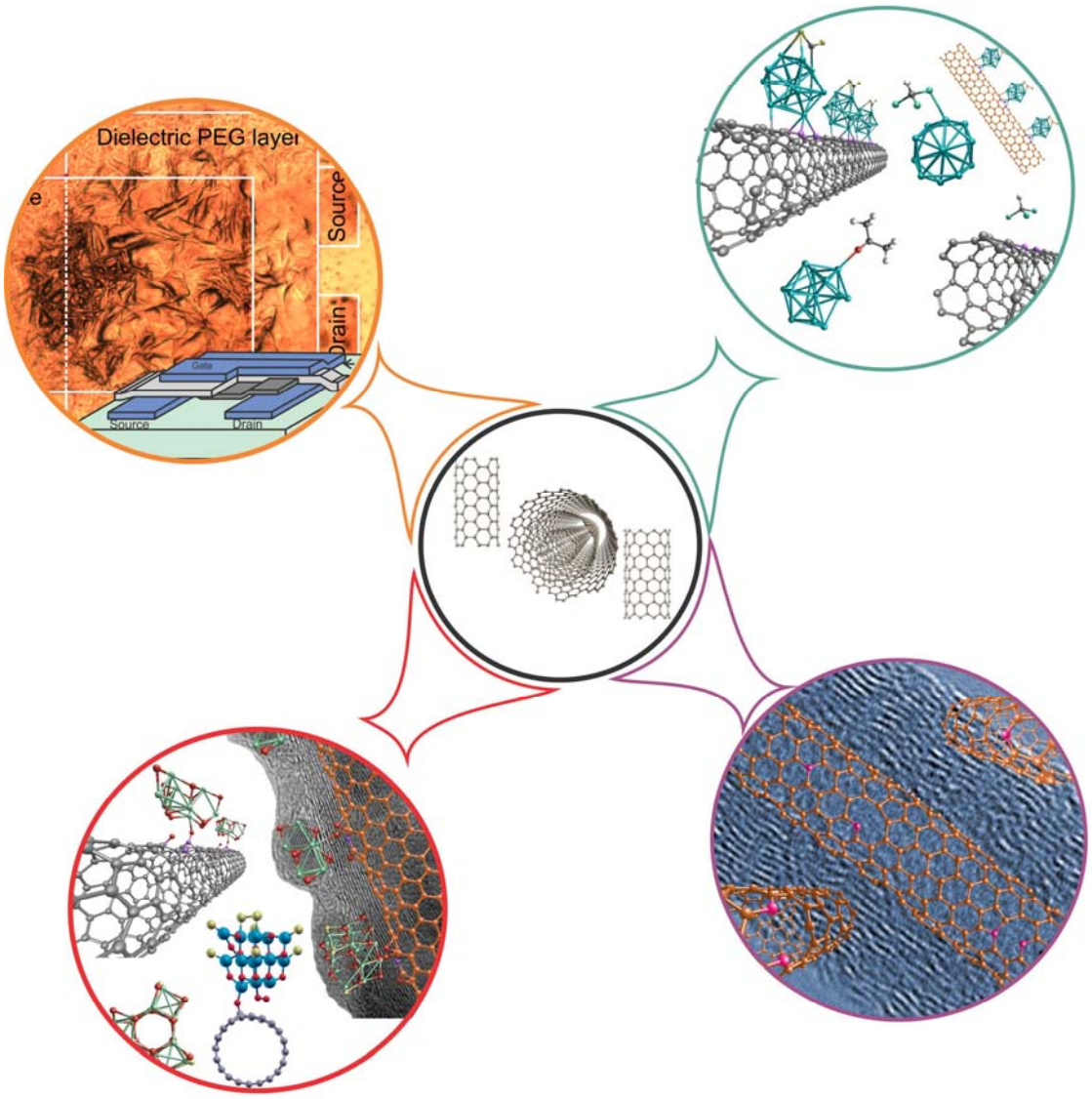

Figure 1-2: Schematic representation of the present Ph.D thesis. **(central image)** The use of carbon nanotubes as starting materials, modifying their surface (outer nanotube walls) increase the posible applications. **(top left circle)** The image depicts a field effect transistor made entirelly of functionalized nanotubes. This work is reported in Chapter 2. **(top right circle)** It shows a hybrid material made of nitrogen-doped carbon nanotubes decorated with silver nanoparticles, in Chapter 3 we built a vapor-gas sensor for carbon disulfide based on composite nanomaterials. **(botton right circle)** It depicts a TEM micrograph and some molecular model of different nitrogen doped configurations in carbon nanotubes. In Chapter 4 we studied multiple options where the nitrogen atoms can be located. Finally, in **(botton left circle)** a hybrid material made of nitrogen-doped carbon nanotubes decorated with zinc oxide nanoparticles, here we studied the interaction between the semiconductor nanoparticles, the carbon nanotubes and the passivating aggent, these results are shown in Chapter 5.

The introduction of functional groups creates materials that exhibit specific properties that give different opportunities for their applications, and by using these functionalized nanotubes we built a field effect transistor (FET), a schematic image of the resulting FET is depicted in figure 1-2 (top left circle). Also in Chapter 3, we use nitrogen-doped multiwalled carbon nanotubes decorated with silver nanoparticles as gas-vapor sensor for carbon disulfide, a molecular model of the hybrid material is depicted in figure 1-2 (top right circle). In Chapter 4 we studied by first principles calculations, the electronic properties of different configurations of nitrogen-doped carbon nanotubes. We observed that by selective nitrogen doping we can modify the electronic properties for our own benefit, a molecular representation of N-doped nanotube is depicted in figure 1-2 (bottom right circle). Finally, we modified nitrogen-doped carbon nanotubes by attaching zinc oxide nanoparticles to the outer walls, we studied the interaction between the zinc oxide cluster, the nanotube and the passivating agent, a molecular model is depicted in figure 1-2 (bottom left circle), and these results are reported in Chapter 5.

1.1. References

[1] S. Niyogi, M. A. Hamon, H. Hu, B. Zhao, P. Bhowmik, R. Sen, M. E. Itkis, R. C. Haddon, "Chemistry of Single-Walled Carbon Nanotubes", *Acc. Chem. Res.*, **35**, 1105-1113 (2002)

[2] A. Jorio, M. S. Dresselhaus, G. Dresselhaus, Ed. "Carbon Nanotubes, Advanced topics in the synthesis, structure properties and applications" Springer (2007)

[3] P. M. Ajayan, T. W. Ebbesen, T. Ichihashi, S. Iijima, K. Tanigaki, H. Hiura: "Opening carbon nanotubes with oxygen and implications for filling", *Nature* **362**, 522 (1993)

[4] Y. Tao, H. Muramatsu, T. Hayashi, Y. A. Kim, D. Shimamoto, M. Endo, K. Kaneko, M. Terrones, M. S. Dresselhaus, "Controlled growth of one-dimensional clusters of molybdenum atoms using double-walled carbon nanotube templating", *Appl. Phys. Lett.* **94**, 113105 (2009)

[5] K. Lafdi, A. Chin, N. Ali, J.F. Despres. "Cobalt-doped carbon nanotubes: preparation, texture, and magnetic properties" *J. Appl. Phys*. **79**, 6007-6009 (1996)

[6] J. Zhao, A. Buldum, J. Han, J. P. Lu, "First-Principles Study of Li-Intercalated Carbon Nanotube Ropes", *Phys. Rev. Lett.* **85**, 1706 (2000)

[7] H. Shimoda, B. Gao, X. P. Tang, A. Kleinhammes, L. Fleming, Y. Wu, O. Zhou, "Lithium Intercalation into Opened Single-Wall Carbon Nanotubes: Storage Capacity and Electronic Properties", *Phys. Rev. Lett.* **88**, 015502 (2001)

[8] R. Czerw, M. Terrones, J. C. Charlier, X. Blase, B. Foley, R. Kamalakaran, N. Grobert, H. Terrones, D. Tekleab, P. M. Ajayan, W. Blau, M. Rühle, D. L. Carroll," Identification of Electron Donor States in N-Doped Carbon Nanotubes" *Nano Lett.* **1**, 457 (2001)

[9] B. G. Sumpter, V. Meunier, J. -M. Romo-Herrera, E. Cruz-Silva, D. A. Cullen, H. Terrones, D. J. Smith, M. Terrones," Nitrogen-Mediated Carbon Nanotube Growth: Diameter Reduction, Metallicity, Bundle Dispersability, and Bamboo-like Structure Formation" *ACS Nano* **1**, 369 (2007)

[10] C.P. Ewels, M. Glerup, "Nitrogen Doping in Carbon Nanotubes", *J. Nanosci. and Nanotech*. **5**, 1345 (2005)

[11] E. Cruz-Silva, D. A. Cullen, L. Gu, J. M. Romo-Herrera, E. Muñoz-Sandoval, F. López-Urías, B. G. Sumpter, V. Meunier, J. C. Charlier, D. J. Smith, H. Terrones, M. Terrones, "Heterodoped Nanotubes: Theory, Synthesis, and Characterization of Phosphorus−Nitrogen Doped Multiwalled Carbon Nanotubes" *ACS Nano* **2**, 441 (2008)

[12] A. Chen, Q. Y. Shao, Z. C. Lin, "Effects of phosphorus-doping upon the electronic structures of single wall carbon nanotubes" *Sci China Ser G-Phys Mech Astron*, **52**, 1139 (2009)

[13] J. M. Romo-Herrera, B. G. Sumpter, D. A. Cullen, H. Terrones, E. Cruz-Silva, D. J. Smith, V. Meunier, M. Terrones," An atomistic branching mechanism for carbon nanotubes: Sulfur as the triggering agent" *Angew Chem. Int Ed,* **47**, 2948 (2008)

[14] E. Cruz-Silva, F. López-Urías, E. Muñoz-Sandoval, B. G. Sumpter, H. Terrones, J.-C. Charlier, V. Meunier, M. Terrones, "Electronic Transport and Mechanical Properties of

Phosphorus- and Phosphorus−Nitrogen-Doped Carbon Nanotubes", *ACS Nano*, **3,** 1913–1921 (2009)

[15] J.-C. Charlier, M. Terrones, M. Baxendale, V. Meunier, T. Zacharia, N. L. Rupesinghe, W. K. Hsu, N. Grobert, H. Terrones, G. A. J. Amaratung, "Enhanced Electron Field Emission in B-doped Carbon Nanotubes", *Nano Lett*, **2**, 1191–1195 (2002)

[16] F. Villalpando-Páez, A. H. Romero, E. Muñoz-Sandoval, L. M. Martínez, H. Terrones, M. Terrones, "Fabrication of vapor and gas sensors using films of aligned CNx nanotubes," *Chem. Phys. Lett.* **386**, 137-143 (2004).

[17] B. Rebollo-Plata, E. Muñoz-Sandoval, F. López-Urías, E. L. Hernández-Cortina, H. Terrones, M. Terrones, "Efficient Vapor Sensors Using Foils of Dispersed Nitrogen-Doped and Pure Carbon Multiwalled Nanotubes," *J. of Nanosci and Nanotech*, **10**, 3965–3972 (2010).

[18] X. Lepró, Y. Vega-Cantú, F.J. Rodríguez-Macías, Y. Bando, D. Golberg, M. Terrones, "Production and Characterization of Coaxial Nanotube Junctions and Networks of CNx/CNT", *Nano Lett.*,**7**, 2220–2226 (2007)

[19] X. Lepró, E. Terrés, Y. Vega-Cantú, F. J. Rodríguez-Macías, H. Muramatsu, Y. A. Kim, T. Hayahsi, M. Endo, M. Torres R.' M. Terrones, **"**Efficient anchorage of Pt clusters on N-doped carbon nanotubes and their catalytic activity", *Chem Phys Lett*, **463**, 124-129 (2008)

[20] J. C. Carrero-Sánchez, A.L. Elías, R. Mancilla, G. Arrellín, H. Terrones, J. P. Laclette, M. Terrones, "Biocompatibility and Toxicological Studies of Carbon Nanotubes Doped with Nitrogen", *Nano Lett.*, **6**, 1609-1616 (2006)

[21] A. B. Castle, E. Gracia-Espino, C. Nieto-Delgado, H. Terrones, M. Terrones, S. Hussain, "Hydroxyl-Functionalized and N-Doped Multiwalled Carbon Nanotubes Decorated with Silver Nanoparticles Preserve Cellular Function", *ACS Nano***, *5*** 2458–2466 (2011)

[22] Y.-P. Sun, K. Fu, Y. Lin, W. Huang, "Functionalized Carbon Nanotubes: Properties and Applications", *Acc. Chem. Res.*, **35,** 1096–1104 (2002)

[23] B. Zhao, H. Hu, R. C. Haddon, "Synthesis and Properties of Water-soluble Single-Walled Carbon Nanotube-Poly(aminobenzene sulfonic acid) Graft Copolymer", *Adv. Func Mater,* **14**, 71-76 (2004)

[24] B. Philip, J. Xie, J. K. Abraham, V. K. Varadan, "Polyaniline/carbon nanotube composites: starting with phenylamino functionalized carbon nanotubes", *Polymer Bulletin,* **53**, 127-138 (2005)

[25] M. Prato, K. Kostarelos, A. Bianco, "Functionalized Carbon Nanotubes in Drug Design and Discovery", *Acc. Chem. Res.* **41,** 60–68 (2008)

[26] Jie Liu, A. G. Rinzler, H. Dai, J. H. Hafner, R. K. Bradley, P. J. Boul, A. Lu, T. Iverson, K. Shelimov, C. B. Huffman, F. Rodriguez-Macias, Y.-S. Shon, T. R. Lee, D. T. Colbert, R. E. Smalley, "Fullerene Pipes", **280**,1253-1256 (2008)

[27] J. Zhu, H. Peng, F. Rodriguez-Macias, J. L. Margrave, V. N. Khabashesku, A. M. Imam, K. Lozano, E. V. Barrera, "Reinforcing Epoxy Polymer Composites Through Covalent Integration of Functionalized Nanotubes", *Adv. Func. Mater.*, **14**, 643–648 (2004)

[28] E. Bekyarova, M. E. Itkis, N. Cabrera, B. Zhao, A. Yu, J.Gao, R.C. Haddon, "Electronic properties of single-walled carbon nanotube networks", *J. Am. Chem Soc.* **127**, 5990-5995 (2005)

[29] K. Besteman, J.-O Lee, F. G. M. Wiertz, H. A. Heering, C. Dekker, "Enzyme-Coated Carbon Nanotubes as Single-Molecule Biosensors", *Nano Lett*, **3**, 727–730 (2003)

[30] D. R. Kauffman, D. C. Sorescu, D. P. Schofield, B. L. Allen, K. D. Jordan, A. Star, "Understanding the Sensor Response of Metal-Decorated Carbon Nanotubes", *Nano Lett*. **10**, 958–963 (2010)

[31] Q. Zhao, M. B. Nardelli, W. Lu, J. Bernholc, "Carbon Nanotube−Metal Cluster Composites: A New Road to Chemical Sensors?", *Nano Lett*., **5,** 847-851(2005)

[32] K. Jiang, A. Eitan, L. S. Schadler, P. M. Ajayan, R. W. Siegel, "Selective Attachment of Gold Nanoparticles to Nitrogen-Doped Carbon Nanotubes", *Nano Lett*, **3**, 275–277 (2003)

[33] P. Avouris, "Molecular electronics with carbon nanotubes", *Acc, Chem, Res*., **35**, 1026-1034 (2002)

[34] A. Kaskela, A. G. Nasibulin, M. Y. Timmermans, B. Aitchison, A. Papadimitratos, Y. Tian, Z. Zhu, H. Jiang, D. P. Brown, A. Zakhidov, Esko I. Kauppinen, "Aerosol-Synthesized SWCNT Networks with Tunable Conductivity and Transparency by a Dry Transfer Technique", *Nano Lett.* ASAP (2011)

[35] N. Perea-Lopez, B. Rebollo-Plata, J. A. Briones-Leon, A. Morelos-Gomez, D. Hernandez-Cruz, G. A. Hirata, V. Meunier, A. R. Botello-Mendez, J.-C. Charlier, B. Maruyama, E. Muñoz-Sandoval, F. Lopez-Urias, M. Terrones, H. Terrones, "Millimeter-Long Carbon Nanotubes: Outstanding Electron-Emitting Sources", *ACS Nano*, Article ASAP (May 2011)

[36] A.R. Rocha, M. Rossi, A. Fazzio, A.J.R. da Silva, "Designing real nanotube-based gas sensors" *Phys. Rev. Lett.,* 176803 (2008)

[37] J. Zhao, et al. "Electronic properties of carbon nanotubes with covalent sidewall functionalization". *J. Phys. Chem. B*, **108**, 4227–4230 (2004).

[38] W.-D. Zhang, W.-H. Zhang, "Carbon Nanotubes as Active Components for Gas Sensors", *J. of Sensors*, 160698 (2009)

[39] M. Prato, K. Kostarelos, A. Bianco, "Functionalized Carbon Nanotubes in Drug Design and Discovery", *Acc Chem Res*, **41**, 60-68 (2008)

[40] S. Kim, H. R. Lee, Y. J. Yun, S. Ji, K. Yoo, W. S. Yun, J.-Y. Koo, D. H. Ha, "Effects of polymer coating on the adsorption of gas molecules on carbon nanotube networks", *Appl. Phys. Lett.* **91**, 093126 (2007)

[41] Y. Zhang, Hongjie Dai, "Formation of metal nanowires on suspended single-walled carbon nanotubes", *Appl. Phys. Lett*., **77**,3015-3017 (2000)

[42] V. Georgakilas, D. Gournis, V. Tzitzios, L. Pasquato, D. M. Guldi, M. Prato, "Decorating carbon nanotubes with metal or semiconductor nanoparticles", *Mater. Chem*., 2007, **17**, 2679-2694 (2007)

[43] A. Star, V. Joshi, S. Skarupo, D. Thomas, J-C P. Gabriel, "Gas Sensor Array Based on Metal-Decorated Carbon Nanotubes," *J. Phys. Chem. B*, **110**, 21014–21020 (2006)

[44] S. Mubeen, T. Zhang, N. Chartuprayoon, Y. Rheem, A. Mulchandani, N. V. Myung, M. A. Deshusses, "Sensitive detection of H_2S using gold nanoparticle decorated single-walled carbon nanotubes", *Anal. Chem.* **82***,* 250–257 (2010)

[45] C. S. Yeung, L. V. Liu, Y. A. Wang, "Adsorption of small gas molecules onto Pt-doped single-walled carbon nanotubes," *J. Phys. Chem. C*, **112***,* 7401-7411 (2008)

[46] Y. S. Min, E. J. Bae, J. B. Park, U. J. Kim, W. Park, J. Song, C. S. Hwang, N. Park, "ZnO nanoparticle growth on single-walled carbon nanotubes by atomic layer deposition and a consequent lifetime elongation of nanotube field emission", *Appl. Phys. Lett.,* **90**, 263104 (2007)

[47] J.Y. Pan, C.C. Zhu, Y.L. Gao, "Enhanced field emission characteristics of zinc oxide mixed carbon nano-tubes films" *Appl. Surf. Sci.*, **254,** 3787–3792 (2008)

[48] Y. Zhang, X. Sun, L. Pan, H. Li, Z. Sun, C. Sun, B. K. Tay "Carbon nanotube–zinc oxide electrode and gel polymer electrolyte for electrochemical supercapacitors" *J. Alloys and Compounds*, **480**, L17-L19 (2009)

[49] S. Wu, Q. Tai, F. Yan, "Hybrid Photovoltaic Devices Based on Poly (3-hexylthiophene) and Ordered Electrospun ZnO Nanofiber", *J. Phys. Chem. C,* **114**,6197–6200 (2010)

Chapter 2 : Fabrication of Field Effect Transistors based on Functionalized-Single Walled Carbon Nanotubes Thin Films

2.1. Summary

In this first chapter, we studied the electrical properties of thin films of inkjet deposited single walled carbon nanotube networks with different types of functional groups: carboxylic acid (-COOH), amide (-$CONH_2$), poly(ethylene glycol) (PEG) and polyaminobenzene sulfonic acid (PABS). We then showed different device operations caused by the chemical groups. In addition, we demonstrated the construction of inkjet printed field effect transistors using thick layers of carboxyl functionalized nanotubes as source-, drain- and gate electrodes and semiconducting films of PEG-functionalized nanotubes as channel.

Chapter Content

Chapter 2 : Fabrication of Field Effect Transistors based on Functionalized- Single Walled Carbon Nanotubes Thin Films

2.1. Summary 11

2.2. Introduction: Random Networks of Carbon Nanotubes 13

2.2.1. Effect of Film Thickness and Functionalization on the Electrical Properties of Carbon Nanotubes Thin Films 14

2.3. Experimental Section: Nanotube Ink Preparation, Printing Technique and Electrical Characterization of the Single Walled Carbon Nanotubes Networks 18

2.4. Results and Discussion 21

2.5. Conclusion and Perspectives 33

2.6. References 35

2.2. Introduction: Random Networks of Carbon Nanotubes

Single walled carbon nanotubes (SWCNTs) are appealing candidates for fabricating molecular electronic devices. Depending on their chirality and diameter, SWCNTs could exhibit either metallic or semiconducting behavior, both necessary building blocks for constructing electronic circuits [1]. It has been reported the fabrication of different devices based on individual SWCNTs such as, field effect transistors and logic circuits [2], gas sensors [3] and nano-sized rectifiers [4]. Despite the impressive properties of single-tube devices, they are difficult to fabricate and virtually impossible to scale up. In addition, the assembly and connection of individual SWCNTs to contacts is challenging, and the absence of highly purified SWCNTs of specific chirality complicates the assembly of electronic devices. For the reasons explained above, carbon nanotube films have been explored as an alternative solution for constructing electronics devices. The viability of using SWCNTs networks as diodes, field-effect transistors (FETs) [5,6,7,8] and chemical sensors [9,10] have already been demonstrated. Additionally, because of their optical transparency and good electrical conduction, SWCNTs films have been suggested for conductive coatings as an alternative to transparent oxides [11,12].

2.2.1. Effect of Film Thickness and Functionalization on the Electrical Properties of Carbon Nanotubes Thin Films

The electrical properties of nanotube thin film are thickness dependent. In this way, controlling the thickness and homogeneity of the nanotube network is an important factor to increase the reproducibility in the electrical behavior of the nanotube films. By increasing the network density, the electrical current can be improved, but further increments in the film thickness generate networks with electrical transport characteristics independent of the film density [13].

The electrical current through low-density carbon nanotube networks is low and behaves as semiconductor materials. If the density of SWCNTs on the films is sufficiently high, i.e. exceeds the percolation limit, the nanotubes will interconnect and form continuous electrical paths between the electrodes. The higher the density of the network, the higher the probability of a purely metallic percolation pathway. The degree of carbon nanotube alignment can dramatically influence the performance of the network device. Whereas alignment is important in reducing carrier path lengths and hence improving mobilities, perfect alignment reduces the number of percolating paths, requiring a significantly higher density of carbon nanotubes in the network [14]. Low density (but percolated) films of SWCNTs, where a percolated network of *semiconductor*-CNT (*s*-CNT) and *metallic*-CNT (*m*-CNT) dominates, exhibit nonlinear current-voltage (*I-Vs*) behavior and show gate-modulated transport in the channel due to the Schottky-barriers forming at the interface of metallic and semiconducting nanotubes. The electrical transport could be well explained by thermionic emission taking place at the junctions forming between crossing semiconducting and metallic CNTs [15].

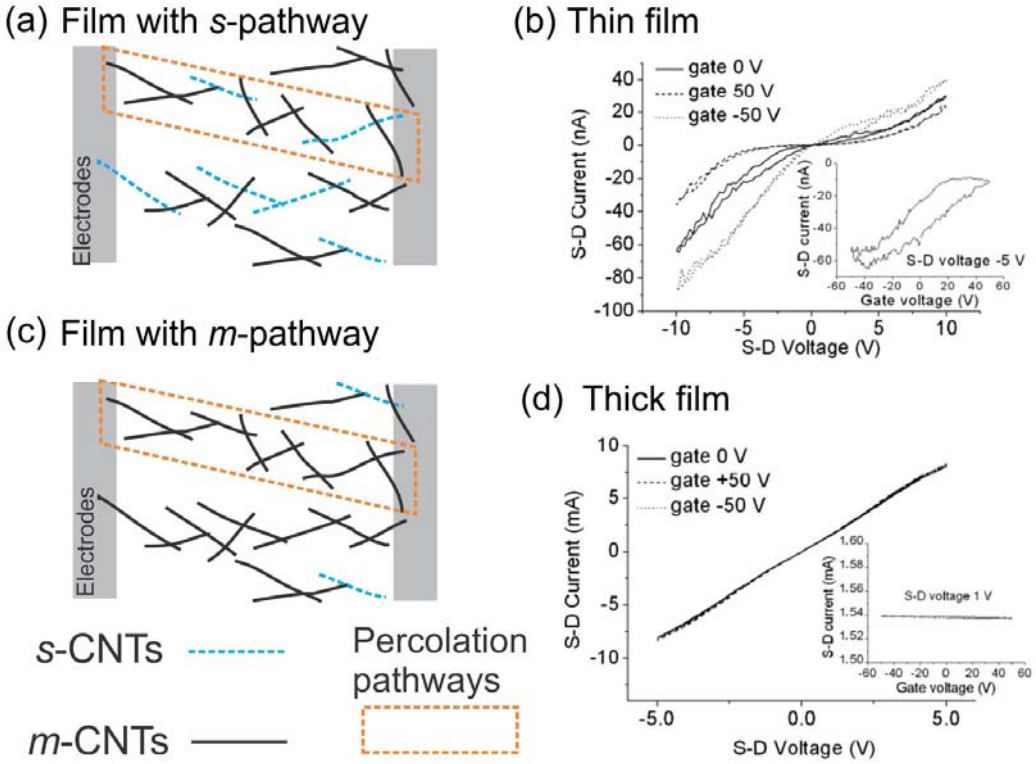

Figure 2-1 (a) Representation of a nanotube film with percolation pathway between the electrodes composed of metallic and semiconductor carbon nanotubes (*s*-CNT). **(b)** Shows the *I-Vs* and transfer characteristics of single walled carbon low-density film, showing nonlinear *I-V*'s characteristics and gate effect. **(c)** Scheme of a film containing pure metallic nanotubes (*m*-CNT) in the percolation pathway. **(d)** A chip with a dense film of nanotubes has linear $I\text{-}V_{SD}$ and a negligible gate effect could be seen [15].

A schematic representation of film containing *s*-CNTs and *m*-CNT is shown in figure 2-1a. The electrical behavior is appreciated in figure 2-1b, where the transfer characteristics low density SWCNTs thin film exhibit a no linear *I-V's* and the electrical current can be modulated with the application of a gate voltage (see inset) [15]. On the other hand, high-density nanotube networks in which the metallic nanotubes can form continuous electrical path between probe electrodes have linear transport properties without showing any gate-control [15,16,17]. Figure 2-1c shows a diagram of a nanotube network containing pure metallic nanotubes on the percolation pathways.

The electrical behavior is shown in figure 2-1d, where the inkjet printed FET with dense film of nanotubes exhibit linear I-V_{SD} and a negligible gate effect. It means that the conduction of the films becomes gradually Ohmic with increased thickness, and this can be attributed to the formation of a parallel metallic network of the deposited *m*-CNTs. These SWCNTs network can carry higher current density, but without showing any gate-control, this type of networks can be used as transparent conductive films.

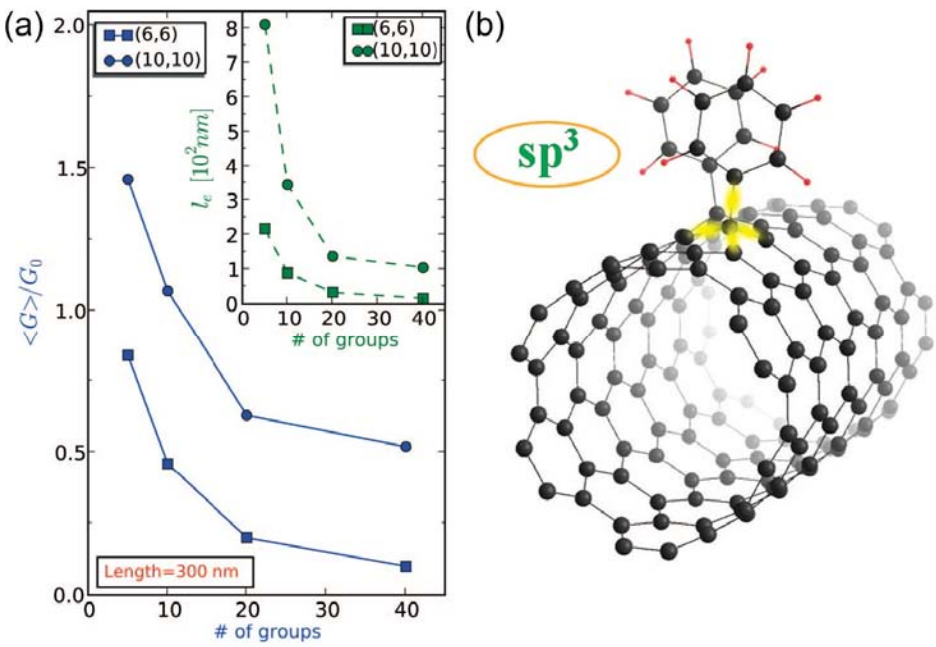

Figure 2-2 (a) The decay of the conductance at the charge neutrality point appears inversely proportional to the coverage density [18]. **(b)** Atomic structures of (6,6)-SWCNT with a paired sp^3 phenyl groups. Disorder average conductance at the charge neutrality point and estimated elastic mean free path (inset) as a function of grafted phenyl groups density for a nanotube 300 nm long.

It is also possible to modify the electrical properties of nanotube networks by introducing different chemical groups to the nanotube wall. The chemical functionalization also changes the interaction of the film with their surrounding environment. This approach has been used for the development of

high-performance composite polymeric materials [19,20], chemisensors [21,22,23], nanoelectronic devices, photovoltaic devices, as well as biosensors [24]. Covalent sidewall functionalization of SWCNTs leads to drastic changes of nanotube electronic states near the Fermi level. The sp^3 hybridization between the functional group and nanotube induces an impurity state near the Fermi level [25,26] and modify the electrical conduction properties. Figure 2-2 depicts the average quantum conductance of a 300 nm length (6,6)-SWCNT functionalized with phenyl groups. The inset shows the estimated elastic mean free path as a function of grafted phenyl groups density. The decay of the conductance appears inversely proportional to the coverage density. For small diameter semiconductor nanotubes, the addition of monovalent functional groups does not significantly modified the electrical properties, however the conductance of semiconducting tubes with standard diameter is severely damaged [27].

As we described before, it is possible to control the electrical properties of random networks of nanotubes by controlling their thickness and their chemical functionalization, a long these lines, we have studied the electrical transport properties of four different functionalized single walled carbon nanotubes. Based on the experimental results, we fabricated a field effect transistor made entirely of functionalized SWCNTs. Methods, results and discussions are presented in the following sections.

2.3. Experimental Section: Nanotube Ink Preparation, Printing Technique and Electrical Characterization of the Single Walled Carbon Nanotubes Networks

2.3.1. Preparation of Aqueous Inks based on Functionalized Single Walled Carbon Nanotube

Four types of SWCNTs with different chemical functionalization, such as carboxylic acid (-COOH), amide (-$CONH_2$), poly-(ethylene glycol) (PEG), and polyaminobenzene sulfonic acid (PABS), were used as purchased from Sigma-Aldrich. Inkjet printable aqueous dispersions of SWCNTs were prepared by sonicating 2.0 mg of nanotubes in 15 mL of deionized water for 3-5 h. Subsequently, the dispersions were centrifuged at 3500 rpm for 30 min, and the supernatant solution was collected and centrifuged again for 15 min. The centrifugation and separation steps were repeated at least four times. The as-obtained inks (Table 2-1) were then inkjet-printed on customized Si chips using a DIMATIX Fujifilm DMP-2831 with 10 pL nominal drop volume.

Boron-doped p^+ Si substrate (5-20 mΩ/cm) with a thin evaporated layer of Al on its bottom was used as back-side gate electrode. SiO_2 layer of ~1 μm (PECVD) was applied as gate dielectric on which electrodes of Pt on Ti (thickness of 300 nm and 45 nm, respectively) were defined by optical lithography. The spacing gap between adjacent source-drain electrodes was 15 μm.

Table 2-1 General characteristics of water-based SWCNT inks.

SWCNTs type	Fraction of functional group[(a)] (wt%)	Measured solid content[(b)] (µg/mL)	CNT content[(c)] (µg/mL)	Structure
Carboxyl (-COOH)	14.9	28 ± 3	~24	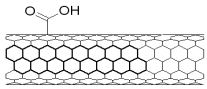
Amide ($-CONH_2$)	13.2	46 ± 5	~40	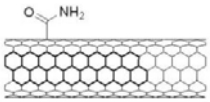
poly(ethylene glycol) (PEG)	30	35 ± 4	~25	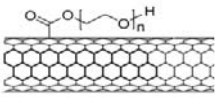
poly(amino-benzene sulfonic) acid (PABS)	65	38 ± 4	~13	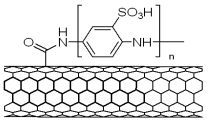

[(a)]The wt% values of functional groups are according to the specifications of Sigma-Aldrich®

[(b)] The values correspond to the whole amount of solid content in the inks measured by filtration of 100 mL ink from each sample

[(c)] The values show the nanotube concentration obtained from (a) and (b)

2.3.2. Inkjet Printing of Thin Films Based on Functionalized Single Walled Carbon Nanotubes

In order to deposit thin films with different average nanotube thickness, multiple prints over the same pattern were made. The test patterns were lines with a length of ~200 µm deposited with 9 ink droplets of 25 µm center-to-center spacing. The diameter of the dried droplets was typically ~35µm for each ink. The average layer thickness values for the nanotube films were calculated as:

$$t = \frac{C_{Ink} V_{drop} N_{drop}}{\rho_{SWCNTs} A_{Pattern}} \quad \textbf{(2-1)}$$

where C_{ink} is the ink concentration measured by weighing the mass of solid residuals after filtrating each ink (and normalizing it to the carbon content by considering the weight fraction of functional groups), V_{drop} is the nominal drop volume of 10 pL, N_{drop} is the number of drops over the printed area ($A_{pattern}$), and ρ_{SWCNT}= 1.4g/cm^3 is the mass density of a SWCNT. The electrical characterization of each sample was carried out in ambient conditions using a dual source meter (Keithley 2612) with LabView control.

2.3.3. Temperature Dependent Conductance Measurements of Functionalized SWCNTs Networks

Low-temperature measurements were performed in vacuum (base pressure ~4 x10^{-6} mbar). The sample was connected in series with a resistor (R << R_{Sample}) and a SIM928 isolated voltage source (Stanford Research Systems). As voltage was applied across the sample, the corresponding current was measured over the resistor R. The signal was amplified and detected with a SIM BJT preamplifier (Stanford Research Systems) and an Agilent 34401A digital multimeter, respectively. Optistat AC-V PT cooler system (OXFORD INSTRUMENTS) has been used in temperature control. The sample was attached to the cold head, and a vacuum was pumped with TURBO-V 70 LP MacroTorr (VARIAN) into the measurement chamber. Cooling was performed with a Pulse Tube refrigerator, whereas the heating was adjusted with an Intelligent Temperature Controller (ITC503) to reach the desired temperature. Data acquisition was performed automatically using LabVIEW 8.2.

2.4. Results and Discussion

2.4.1. Electrical Properties of Random Networks Based on Functionalized Single Walled Carbon Nanotubes Prepared by Inkjet Printing

A series of SWCNTs films with different thickness were deposited on SiO_2 substrates to form random networks of partially bundled SWCNTs. The electrical conductivity, see figure 2-3, of the films was calculated from resistance measurements carried out at 5V channel bias. By increasing the thickness of the nanotube networks, the conductivity of each film increases ~2 orders of magnitude within a narrow thickness window of the experiments; however above a certain critical thickness further significant increment of conductivity cannot be reached. Despite the equivalent nanotube coverage, the conductivities are different for each type of film.

Carboxylated and polyaminobenze sulfonic acid functionalized nanotubes exhibit always the lowest resistivity, followed by amide and poly(ethylene glycol) functionalized films having corresponding sample thickness values. The maximum achieved electrical conductivity in our experiments is ~3000 S/cm for carboxyl- and PABS-functionalized nanotubes. For Amide- and PEG-SWCNTs the conductivity is ~200 and 10 S/cm, respectively. The overall conductivity vs. thickness behavior measured for each film is similar to those of percolating networks. Near to the percolation threshold (p_c) the conductivity (σ) is expected to be related to the concentration of conducting paths (p) by the universal power law of the form $\sigma \propto (\rho - \rho_c)^{\alpha}$ [28,29].

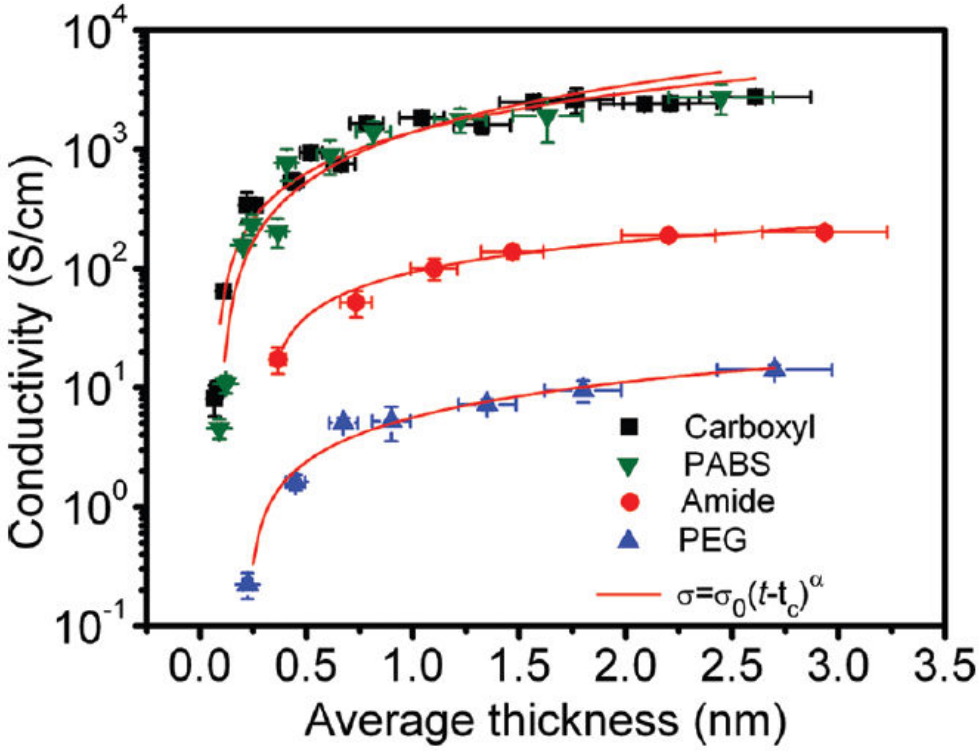

Figure 2-3 Electrical conductivity as a function of average film thickness of SWCNT networks made of four different types of functionalized nanotubes. Various thicknesses were obtained by subsequent printing over the same pattern. The electrical resistances of all networks were tested at -5 V drain-source bias. Depending on film thickness, the conductivity of the films can be varied within a window of ~2 orders of magnitude.

As the conducting paths are proportional to the film thickness, the conductivity law can be expressed as $\propto (t-t_c)^{\alpha}$ for $t \geq t_c$, where t and t_c are the thickness and the corresponding threshold value (critical thickness), and α is the critical exponent. For thicknesses lower than t_c, there is no connection between the contact electrodes. Over the threshold limit, in the SWCNTs networks, the overall resistance is dominated by the tube-tube, tube-bundle and bundle-bundle contacts as well as by the intrinsic conductivities of the nanotubes. By increasing the film thickness the number of percolated paths increases, thus the resistance decreases as more and more parallel connections form.

Table 2-2 Calculated percolation threshold thickness t_c (average thickness over the printed surface area) and critical exponent α for the deposited nanotube films.

	Carboxyl	Amide	PEG	PABS
t_c (nm)	0.07±0.01	0.31±0.05	0.23±0.38	0.09±0.02
α	1.03±0.11	0.65±0.15	0.83±0.54	1.22±0.27

However, at high film thicknesses, addition of further nanotubes to the network cannot contribute much to the improvement of conductivity because the film becomes like an ideal bulk conductor (~2 nm thickness for each sample). Films made of PEG and Amide functionalized CNTs exhibit lower conductivity with the percolation transition taking place at higher average film thicknesses of ~0.2 and ~0.4 nm respectively, compared to those of the PABS and carboxyl functionalized samples having such threshold values below 0.1 nm (see table 2-2). Note that t_c is obtained as an average thickness over the total printed area between the electrodes.

The considerably different electrical conductivity values of the films at equivalent carbon nanotube coverage are a consequence of several factors related to film morphology and functional groups linked on the nanotubes. The homogeneity of networks on the substrate surface can play an important role since the formation of CNT bundles inherently results in a partial network of metallic ropes instead of individual metallic and semiconducting nanotubes. Bundling is caused by attractive forces of tube-to-tube van der Waals interactions after the evaporation of solvent (water) from the ink. The forces can be especially strong for carboxyl and amide groups due to intermolecular H-bonding [30] between H and O or N along the side groups

of adjacent nanotubes. For polymer side groups, the polymers can cause considerable steric hindrance and limitations in direct lapping of nanotubes on each others, i.e. the nanotubes are somewhat separated from each other by the polymer chains, as it can be appreciated in figure 2-4.

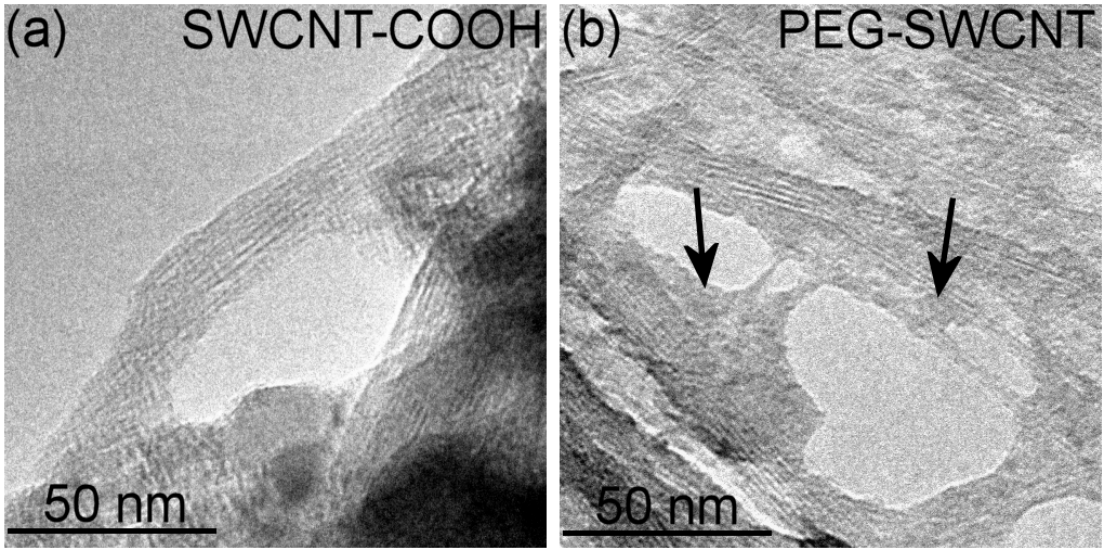

Figure 2-4 Transmission electron micrographs of **(a)** carboxylic acid and **(b)** polyethylene glycol functionalized inks dried on sample holder grids. The arrows in panel **(b)** show thin polymer layers in between the nanotubes (and bundles).

Another important factor is the acidic nature of the chemical group. Due to water adsorption on the nanotubes from the moisture of ambient air, carboxyl- [31] and sulphonic acid [32] groups can deprotonate, thus providing mobile carriers (protons and hydronium ions) for electrical transport in the film. Accordingly, nanotube films with PEG functional groups that are insulating are expected to be the least conductive, while carboxyl functionalized nanotubes are the most conductive due to possible bundling and protonic conduction. These assumptions are in qualitative agreement with the experimental results.

2.4.2. Current-Voltage Characteristics and Field Effect Properties of Single Walled Carbon Nanotubes Thin Films

Films of carboxyl functionalized SWCNTs exhibiting nonlinear *I-V* characteristics are obtained if the entangled network has low nanotube density to allow formation of continuous electrical paths [15,16,17]. We find similar nonlinear electrical transport behavior for low-density nanotube films functionalized with amide, PEG and PABS functional groups as shown in figure 2-5.

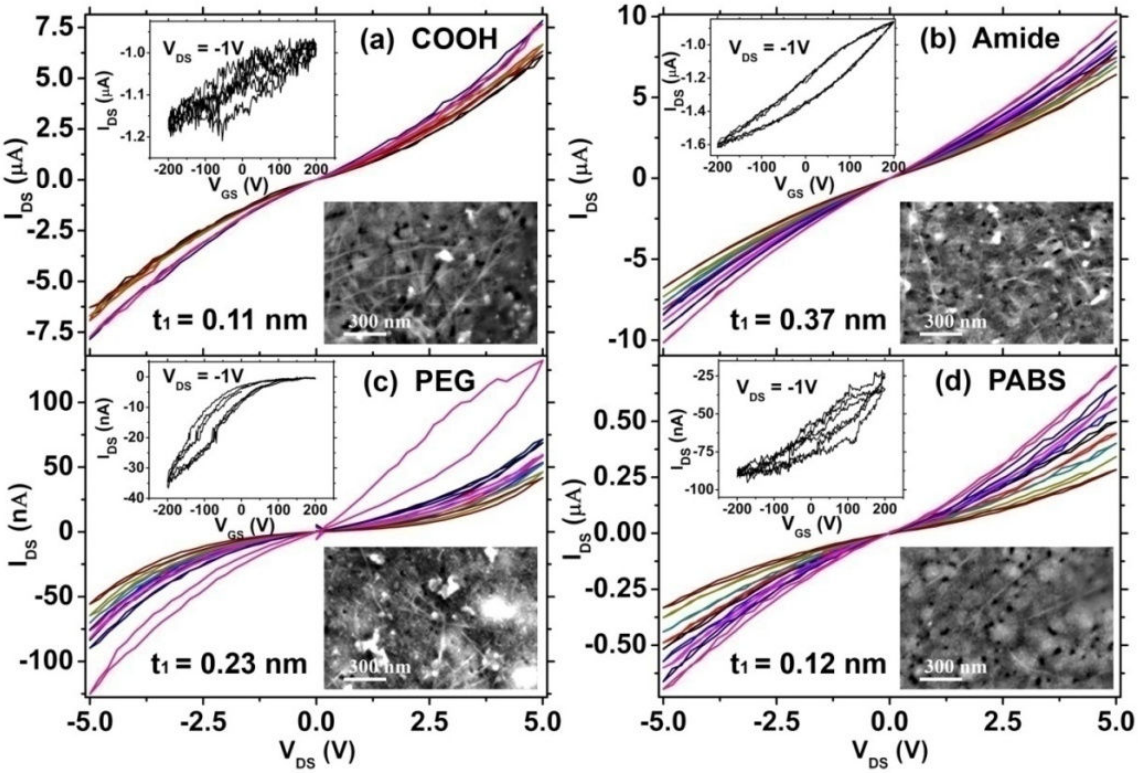

Figure 2-5 Drain-source current-voltage I_{DS}-V_{DS} sweeps for **(a)** COOH-, **(b)** $CONH_2$-, **(c)** PEG- and **(d)** PABS-functionalized SWCNTs films with thickness of 0.11 nm, 0.37 nm, 0.23 nm and 0.12 nm, respectively. The top insets are plots of I_{DS}-V_G sweeps measured at -1 V channel bias (each averaged of three subsequent measurement cycles). The bottom insets are FESEM images of the corresponding nanotube networks. Note: transistor channel with COOH-functionalized nanotubes is printed using diluted ink (50% stock dispersion and 50% deionized water).

The tunable channel transport by an external electric field (see insets in figure 2-5) supports the existence of Schottky junctions in each nanotube network. Films of PEG- and PABS-SWCNTs have considerable gate effect with channel on/off ratios of ~70 and ~4.5, respectively; while the carboxyl and amide functionalized films show moderate gate response with channel on/off ratios of ~1.3 and ~2.0, respectively (Table 2-3). The higher channel conductance at negative gate voltages for each sample suggests similar p-type field-effect transistor operation regardless of the functional group linked to the nanotubes.

In order to quantify the height of the Schottky barriers (φ_b) for the junctions of metallic and semiconducting nanotubes in each low density network, we apply a modified diode equation (Eq. 2-2) which takes into account the Ohmic losses and the series of several Schottky junctions in the percolated path. Thus the current in the nanotube networks is described as [15]:

$$I(V,T) = AA^{*}T^{2}\exp\left(-\frac{\Phi_b}{k_B T}\right)\left[\exp\left(\frac{\frac{q(V-RI)}{m}}{k_B T}\right)-1\right] \qquad \textbf{Eq. (2-2)}$$

where A is the average cross section of the films estimated by the film thickness and geometry, $A^{*}= 4\pi mqk^2/h^3$ is the Richardson constant, q is the elementary charge, $m^{*}=0.037m_e$ is the effective mass of carriers in a nanotube [33], k_B is Boltzmann's constant, h is Planck's constant, φ_b is the Schottky barrier height, R is the serial resistance of the network obtained from the I-V_{DS} slope at the large bias voltages, and m is the number of junctions along a percolated path (note: m is originally the ideality factor of

the diode, which is considered to be 1 in our calculations). The nanotube-metal electrode interfaces are assumed to be Ohmic because of the large work function of Pt film (Φ_{Pt}> 5 eV) [34,35]. Fitting Eq. 2-2 on the measured I-V_{DS} data, we get both φ_b and m parameters (summarized in table 2-3). The calculated average barrier heights from 106 to 256 meV are reasonable considering the barrier of a metal-semiconductor junction $\Phi_b = E_g - \Phi_m + \chi_S$ with a typical work function (φ_m) of 4.5-5.0 eV for metallic CNTs as well as band gap (E_g) of 0.3-0.9 eV and electron affinity (χ_s) of 3.9-4.8 eV for semiconducting CNTs [34,35,36,37,38].

Table 2-3 Electrical characteristics of SWCNTs thin films. $t_{1\ layer}$ thickness of a single print; R resistance measured at -1 V source-drain bias; transistor on/off ratio measured using -200 and +200 V gate at -1 V source-drain bias; Φ_b is the apparent average height of Schottky barriers at the junctions of metallic and semiconducting nanotubes; and m is the average number of junctions along a percolated path in the network.

	Carboxyl	Amide	PEG	PABS
$t_{1\ layer}$ (nm)	~0.11	~0.37	~0.23	~0.12
R (MΩ)	0.62 ± 0.15	0.95 ± 0.23	248.3 ± 72.6	43.8 ± 11.2
On-off ratio	1.3 ± 0.1	1.9 ± 0.4	70 ± 5	4.4 ± 1.6
Φ_b (meV)	140	106	256	176
m	16.6	20.2	21.7	11.4

The electrodes (spacing gap of 15μm) are connected with individual and bundled nanotubes having a length of ~1μm, thus the number of Schottky junctions in series we estimate from the fitting parameters (m = 11.4 to 21.7) are also reasonable. For PEG- and PABS-SWCNTs films, the resistance is governed by the sum of the series resistance of the CNT itself, the junction resistance between the CNTs, and the resistance of the polymer layer

between the CNTs. This explains the high resistance of the film while the high non-linear behavior could be explained by a high Schottky barrier (Table 2-3). In this case, not only the metallic and semiconducting CNTs form junctions (i.e. m-CNT/m-CNT, m-CNT/s-CNT and s-CNT/m-CNT) but also m-CNT/polymer/m-CNT, m-CNT/polymer/s-CNT and s-CNT/polymer/s-CNT interfaces can contribute to the nonlinear characteristics of such films.

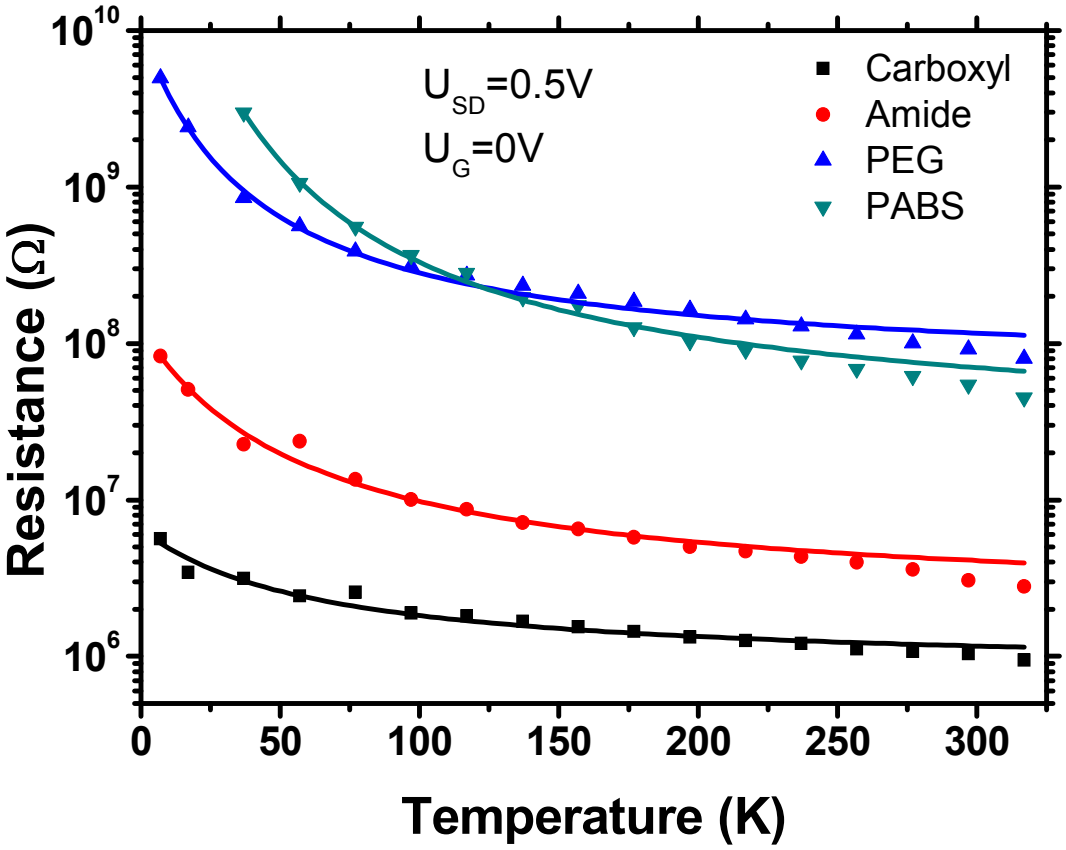

Figure 2-6 Channel resistance as a function of temperature measured using U_{SD}=0.5 V. The lines are fit to thermally-assisted tunneling with tunnel barriers of 12±6 meV, 22±5 meV, 19±1 meV and 31±2 meV for the carboxyl-, amide-, PABS- and PEG functionalized nanotube films, respectively.

The negative temperature coefficient of resistance measured for each sample from 7 K to 317 K (Figure 2-6) shows non-metallic electrical behavior similar to those results obtained by other groups [17,28]. Though a network of Schottky junctions seems to explain well the carrier transport near room temperature [15,17]. By fitting the diode equation to the low temperature data we obtain an unreasonable match. Variable-range hopping proposed for thin single-wall carbon films [17] do not explain the process either, however thermally-assisted tunneling [28]

$$R(T) = C\exp\left(\frac{T_b}{T_s + T}\right) \qquad \textbf{Eq. (2-3)}$$

where $R(T)$ is the temperature dependent resistance, C is a geometry parameter, T_b is the tunneling barrier height and T_s/T_b is the quantum induced tunneling in the absence of fluctuations - gives nearly perfect fit especially for data below ~200 K for each type of nanotube film just like in the case of pristine and carboxyl functionalized nanotube films of various thicknesses measured by another group. At low temperatures, the s-CNTs become insulating, thus electron tunneling between adjacent metallic nanotubes takes over the charge transport. The calculated apparent barrier energies are between 12 and 31 meV slightly higher than those measured for CNT bundles ~6 meV [39], mats ~9 meV [40] and ~7 meV for spray coated films [28].

2.4.3. Field Effect Transistor Based on Random Networks of Functionalized SWCNTs

Originally, semiconductor SWCNTs have been incorporated in field-effect transistors (FETs) as single nanotube on rigid substrates [2]. Recently, transistors have been fabricated from sparse networks of individual nanotubes with good mobility and an on-off ratio [5-8]. These network transistors exhibit electronic properties that are similar to those devices made of an individual *s*-CNT. For the fabrication of field effect transistors based on nanotube networks is needed low-density films with controllable electrical current by applying a gate voltage, it means that the electrical pathway must contain a mixture of *s*-CNTs and *m*-CNTs.

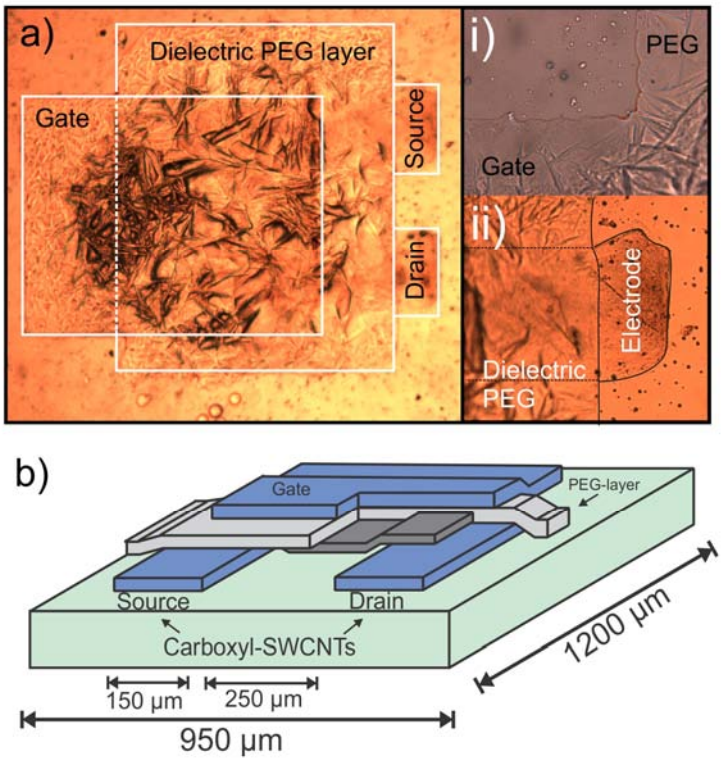

Figure 2-7 Entirely inkjet printed field effect transistor with PEG-functionalized SWCNT thin film as channel, COOH-functionalized SWCNT film as source, drain and gate electrodes. Poly(ethylene glycol) film is used as gate dielectric on a flexible transparency foil. **(a)** Optical image and **(b)** schematic drawing of the device.

Based on the results obtained for our inkjet printed thin film transistors on Si chips (section 2.4.2), we inkjet deposited entirely CNT-based FETs on a flexible polymer substrate (Figures 2-7(a-b)). Because of the measured highest on-off ratio for the channel current, PEG-functionalized nanotubes are selected to print the thin p-type channels (thickness of ~1.5 nm) on the surface of an ordinary transparency foil (Canon B-400).

Well-conducting electrodes using carboxylated nanotubes (~3.5 nm) are deposited for source and drain electrodes. These electrodes are then connected by the channel layer of PEG-functionalized CNTs. A layer of PEG (~20 µm) is then deposited on the top of channel (and partly on the source and drain electrodes too) to form the gate dielectric. Finally, on top of the PEG film, the gate electrode (~3.5 nm) is printed using carboxylated nanotubes again. An optical microscope image of the device is shown in figure 2-7a. The insets (*i-ii*) in figure 2-7a show a close up of the gate-dielectric and the source-dielectric layer limit. The lines illustrate the boundary of each FET component. The FET size is described in figure 2-7b, where it is shown a schematic drawing of the inkjet-printed FET. The FET size is around 1 mm x 1.2 mm x ~20 µm. The as-made devices exhibit nonlinear channel *I-V* behavior and p-type FET operation with a typical on-off ratio ~3 with gate voltages between -3 and 3 V as seen in figure 2-8a. When the upper and lower limits of the gate bias sweeps are increased, the transistors show ambipolar characteristics (Figures 2-8(b-d)). However when applying low gate voltages again, most of the devices operates as an *n*-channel FET shown in figure 2-8e. Similar *n-doping* was observed for individual *p-type* nanotubes by using vacuum annealing [41] or by applying large gate bias while sourcing the channel of a *p*-FET device [42].

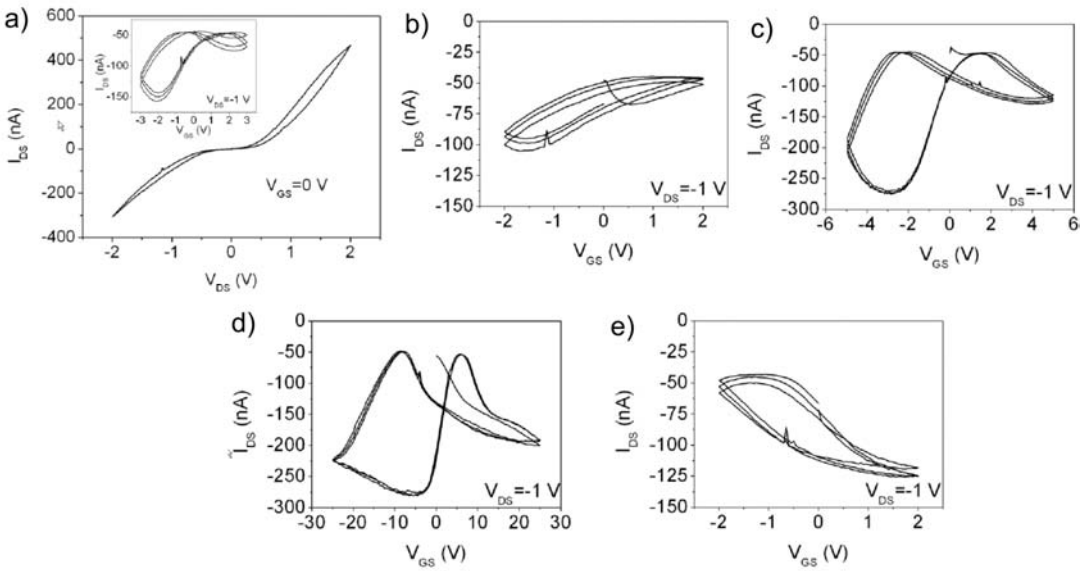

Figure 2-8 (a) I_{DS}-V_{DS} at V_{GS}= 0 V and I_{DS}-V_{GS} at V_{DS}= -1 V plots of a transistor showing *p*-channel behavior. **(b)-(e)** I_{DS}-V_{GS} plots of a device measured using different gate bias sweeps. The applied external electrical field results in gradual *n*-doping of the *p*-type channel: **(b)** *p*-FET at -2 V <V_{GS}< 2 V, **(c)** *p*-FET with slightly ambipolar behavior at -5 V <V_{GS}< 5 V, **(d)** ambipolar operation at -25 V <V_{GS}< 25 V and **(e)** *n-type* FET device operation after lowering the gate voltage sweep again to -2 V <V_{GS}< 2 V

Both processes result in desorption of O_2 and other oxidizing moieties from the surface of nanotubes that are suggested to be responsible for *p*-type doping in ambient conditions [42]. Carrier mobilities (μ) up to ~60 $cm^2V^{-1}s^{-1}$ were obtained as calculated from the transfer curves and from the geometry of transistors according to the Eq. 2-4.

$$\mu = \left(\frac{L}{WC_0}\right)\left(\frac{1}{V_{DS}}\right)\frac{\partial I_{DS}}{\partial V_{GS}} \qquad \textbf{Eq. (2-4)}$$

where L=250 µm is the channel length, W=200 µm is the channel width and C_0~$7.7\cdot10^{-6}$ $V\cdot m^2\cdot A^{-1}$ s^{-1} is the gate capacitance. These values are about an order of magnitude lower than those measured for aligned single wall nanotube array devices [43].

2.5. Conclusion and Perspectives

We have studied the electrical properties of inkjet deposited thin films of four different types of functionalized single-wall carbon nanotubes, and confirmed the important role of chemical functionalization on the electrical properties SWCNTs networks. We found that the films behave as percolating networks with a power law dependence of the conductivity on the film thickness, showing quasi-one-dimensional charge transport. The electrical transport near room temperature could be well explained by thermionic emission, taking place at the junctions between crossing semiconducting and metallic nanotubes. Polymeric functionalization show decreased conductivity by 1 to 2 orders of magnitude when compared to the amide- and carboxyl- functionalized nanotube films of the corresponding thickness, and exhibit higher apparent average Schottky barriers.

When using a proper selection of functional groups and film thickness, it is possible to obtain film conductivities in a large parameter window. By simply changing the layer thickness, networks with linear as well as nonlinear gate-controllable current-voltage transport can be made with all types of nanotubes. Though the on-off ratios obtained for functionalized SWCNT thin films transistors are moderate compared to those measured on individual nanotubes, such components can be still practical (e.g. for low-end devices that are produced in large quantities, since any pre-selection of individual semiconducting nanotubes is not necessary). Furthermore, with a proper optimization of gate dielectric material and thickness, the switching behavior might be improved further. At low temperatures, the semiconducting nanotubes become insulating, thus electron tunneling between adjacent metallic nanotubes takes over the charge transport.

Finally, we have successfully demonstrated that inkjet printed field-effect transistors could be constructed solely from thin films of functionalized carbon nanotubes (except the gate dielectric which is a layer of inkjet printed PEG). We have also showed that a p-channel thin film FET device could be transformed to n-type by simply applying a large local electrical field with the gate electrode. Because of practical reasons (to enable easy contacting with probes for electrical testing) the current size of a printed transistor is ~1×1 mm^2 which could be scaled down to a size of ~100×100 μm^2 with ~35-35 μm channel length and width considering the diameter of ~35 μm for the dried ink droplets having a nominal volume of ~10 pL ejected from the cartridge. Any further decrease of transistor size is possible only by using inkjet heads producing smaller ink drops or by applying substrates that are pretreated to have hydrophilic and hydrophobic surface areas for enabling good ink localization on the surface [44].

2.6. References

[1] P. Avouris, "Molecular electronics with carbon nanotubes". *Acc. Chem. Res.* **35**, 1026-1034 (2002)

[2] A. Bachtold, et al. "Logic circuits with carbon nanotube transistors". *Science* **294**, 1317-1320 (2001)

[3] J. Kong, J., et al. "Nanotube molecular wires as chemical sensors". *Science* **287**, 622-625 (2000)

[4] P.G. Collins, et al. "Nanotube nanodevice" *Science* **278**, 100-103 (1997).

[5] Z. Yangxin, et al. "p-channel, n-channel thin film transistors and p−n diodes based on single wall carbon nanotube networks". *Nano Lett.* **4**, 2031–2035 (2004)

[6] M. A. Meitl, et al. "Solution casting and transfer printing single-walled carbon nanotube films". *Nano Lett.* **4**, 1643-1647 (2004)

[7] K. Bradley, J-C Gabriel, G. Grüner, "Flexible nanotube electronics". *Nano Lett.* **3**, 1353-1355 (2003)

[8] E. S. Snow, et al. "Random networks of carbon nanotubes as an electronic material". *Appl. Phys. Lett*. **82**, 2145-2147 (2003)

[9] J. Mäklin, et al. "Nitric oxide gas sensors with functionalized carbon nanotubes". *Phys. Stat. Sol. (b)* **244**, 4298–4302 (2007)

[10] O.K. Varghese, P.D. Kichambre, D. Gong, K.G. Ong, E.C. Dickey, C.A. Grimes, "Gas sensing characteristics of multi-wall carbon nanotubes", *Sens. Actuator B,* **81**, 32-41 (2001)

[11] Z. Wu, et al. "Transparent, Conductive carbon nanotube films". *Science*, **305**, 1273-1276 (2004)

[12] T.M. Barnes, et al. "Single-wall carbon nanotube networks as a transparent back contact in CdTe solar cells". *Appl. Phys. Lett.,* **90**, 243503 (2007)

[13] E. Bekyarova, M. E. Itkis, N. Cabrera, B. Zhao, A. Yu, J. Gao, R. C. Haddon, "Electronic Properties of Single-Walled Carbon Nanotube Network", *J. Am. Chem. Soc* , **127**, 5990-5995 (2005)

[14] J-H Lim, N. Phiboolsirichit, S. Mubeen, Y. Rheem, M. A. Deshusses, A. Mulchandani, N. V. Myung, "Electrical and Sensing Properties of Single-Walled Carbon Nanotubes Network: Effect of Alignment and Selective Breakdown", *Electroanalysis*, **22**, 99-105 (2010)

[15] T. Mustonen, et al. "Controlled Ohmic and nonlinear electrical transport in inkjet-printed single-wall carbon nanotube films". *Phys. Rev. B*, **77**, 125430 (2008)

[16] P. Beecher, et al. "Ink-jet printing of carbon nanotube thin film transistors". *J. Appl. Phys.,* **102**, 043710 (2007)

[17] V. Skákalová, et al. "Electronic transport in carbon nanotubes: From individual nanotubes to thin and thick networks". *Phys. Rev. B,* **74**, 085403 (2006)

[18] A. Lopez-Bezanilla, F. Triozon, S. Latil, X. Blase, S. Roche, "Effect of the Chemical Functionalization on Charge Transport in Carbon Nanotubes at the Mesoscopic Scale", *Nano Lett.,* **9,** (2009)

[19] B. Zhao, H. Hu, R., C. Haddon, "Synthesis and Properties of Water-soluble Single-Walled Carbon Nanotube-Poly(aminobenzene sulfonic acid) Graft Copolymer", *Adv. Func Mater* **14**, 71-76 (2004)

[20] B. Philip, J. Xie, J. K Abraham, V. K Varadan, "Polyaniline/carbon nanotube composites: starting with phenylamino functionalized carbon nanotubes", *Polymer Bulletin* **53**, 127-138 (2005)

[21] W.-D. Zhang, W.-H. Zhang, "Carbon Nanotubes as Active Components for Gas Sensors", *Journal of Sensors*, 160698 (2009)

[22] P. Qi, O. Vermesh, M. Grecu, A. Javey, Q. Wang, H. Dai, S. Peng, K. J. Cho, "Toward Large Arrays of Multiplex Functionalized Carbon Nanotube Sensors for Highly Sensitive and Selective Molecular Detection", *Nanoletters,* **3**, 347-351 (2003)

[23] X. Feng, S. Irle, H. Witek, K. Morokuma, R. Vidic, E. Borguet, "Sensitivity of Ammonia Interaction with Single-Walled Carbon Nanotube Bundles to the Presence of Defect Sites and Functionalities", *J. Am Chem Soc*. **127**, 10533-10538 (2005)

[24] M. Prato, K. Kostarelos, A. Bianco, "Functionalized Carbon Nanotubes in Drug Design and Discovery", *Acc Chem Res*, **41**, 60-68 (2008)

[25] J. Zhao, et al. "Electronic properties of carbon nanotubes with covalent sidewall functionalization". *J. Phys. Chem. B*, 108, 4227–4230 (2004).

[26] H. Park, et al., "Effects of sidewall functionalization on conducting properties of single wall carbon nanotubes", *Nano Lett.* **6**, 916–919 (2006)

[27] A. Lopez-Bezanilla, X. Blase, S. Roche, "Quantum Transport Properties of Chemically Functionalized Long Semiconducting Carbon Nanotubes", *Nano Res*, **3**, 28-295 (2010)

[28] E. Bekyarova, et al. "Electronic properties of single-walled carbon nanotube networks". *J. Am. Chem. Soc.*, **127**, 5990-5995 (2005)

[29] D. Stauffer, A. Aharony, "Introduction to Percolation Theory", London: Taylor & Francis (1994)

[30] D.F. Shriver, P.W. Atkins. "Inorganic chemistry": Oxford University Press, (2006)

[31] H. Hu, et al., "Chemically functionalized carbon nanotubes as substrates for neuronal growth". *Nano Lett*. **4**, 507–511 (2004)

[32] S.J. Paddison, "Proton conduction mechanisms at low degrees of hydration in sulfonic acid–based polymer electrolyte membranes". *Annu. Rev. Mater. Res.* **33**, 289–319 (2003)

[33] P. Jarillo-Herrero, et al. "Electron-hole symmetry in a semiconducting carbon nanotube quantum dot". *Nature* **429**, 389 – 392 (2004)

[34] H.M. Manohara, et al. "Carbon nanotube schottky diodes using Ti−Schottky and Pt−Ohmic contacts for high frequency applications". *Nano Lett.* **5**, 1469–1474 (2005)

[35] W.S. Su, T.C. Leung, C.T. Chan, "Work function of single-walled and multiwalled carbon nanotubes: First-principles study". *Phys. Rev. B* **76**, 235413 (2007)

[36] J. Appenzeller, et al., “Tunneling versus thermionic emission in one-dimensional semiconductors”, *Phys. Rev. Lett.* **92**, 048301 (2004)

[37] F. Buonocore, et al. “Ab initio calculations of electron affinity and ionization potential of carbon nanotubes”. *Nanotechnology* **19**, 025711 (2008)

[38] S. Kazaoui, et al., “Electrochemical tuning of electronic states in single-wall carbon nanotubes studied by in situ absorption spectroscopy and ac resistance”. *Appl. Phys. Lett.* **78**, 3433-3435 (2001)

[39] A.B. Kaiser, G. Düsberg, S. Roth, “Heterogeneous model for conduction in carbon nanotubes”, *Phys. Rev. B*, **57,** 1418-1421 (1998)

[40] A.B. Kaiser, et al. “Some problems in understanding the electronic transport properties of carbon nanotube ropes”. *Curr. Appl. Phys.* **1**, 50-55 (2001)

[41] Ph. Avouris, “Carbon nanotube electronics”. *Chem. Phys.* **281**, 429-445 (2002)

[42] A. Javey, Q. Wang, A.Li. Ural, H. Dai, “Carbon nanotube transistor arrays for multistage complementary logic and ring oscillators”. *Nano Lett.* **2**, 929-932 (2002)

[43] S.J. Kang, et al., “High-performance electronics using dense, perfectly aligned arrays of single-walled carbon nanotubes”, *Nature Nanotech.* **2**, 230-236 (2007).

[44] H. Sirringhaus, et al., “High-resolution inkjet printing of all-polymer transistor circuits”, Science **290**, 2123 (2000)

Chapter 3 : Silver-decorated Nitrogen Doped Multiwalled Carbon Nanotubes as Gas Sensors

3.1. Summary

Sensors based in foils of silver nanoparticles (Ag-NPs) anchored on the surface of nitrogen-doped multiwalled carbon nanotubes (CN_X-MWNTs) were fabricated and tested with vapor-gas of carbon disulfide, acetone, ethanol and chloroform. Firstly, the CN_x-MWNTs were produced using the chemical vapor deposition method and then mixed with silver nitrate in ethanol solvent, thus producing carbon nanotubes decorated with Ag nanoparticles. These samples were characterized using scanning electron microscopy, transmission electron microscopy, and X-ray diffraction. The foils were obtained by dispersing the decorated nanotubes using the vacuum filtration method, and then were collocated inside a quartz tube in a tubular furnace, under controlled temperature and atmosphere. Our results on electrical resistance for various cycles demonstrated that the Ag-nanoparticles anchored on CN_X-MWNTs are better sensors than when only CN_x-MWNTs are used. The temperature effects on the performance of the sensors are discussed. We found that the mechanism of vapor detection can be tuned from physisorption, at room temperature, to chemisorption at higher temperature. In order to understand the different interactions between the systems involved in the sensors first-principles density functional calculations were carried out.

Chapter Content

Chapter 3 : Silver-decorated Nitrogen Doped Multiwalled Carbon Nanotubes as Gas Sensors

3.1. Summary 39

3.2. Introduction: Gas Sensor Based on Carbon Nanotubes 41

3.3. Experimental Section: Silver Decoration of Carbon Nanotubes, Material Characterization and Sensor Fabrication Procedure 44

3.4. Results and Discussion 46

3.5. Understanding the Sensing Mechanism of Silver-decorated Carbon Nanotubes from a Theoretical Approach 57

3.6. Conclusions 65

3.7. References 67

3.2. Introduction: Gas Sensor Based on Carbon Nanotubes

Carbon nanotubes (CNTs) have proved to be excellent candidates for sensing applications [1,2]. Multiwalled carbon nanotube (MWCNTs)-based sensors are sensitive to a variety of gases such as NH_3, NO, NO_2, H_2, SF_6, and Cl_2 [3-5]. Different devices have been used to fabricate CNTs sensors for the detection of vapors and gases; the most common configurations are field effect transistors (FETs) and resistors [6]. Because their simplicity and easy fabrication, the resistor is a frequently used arrangement, where the change in electrical conductivity is monitored when the sensor is exposed to various atmospheres. One common disadvantage of carbon nanotubes based gas sensors is the potential interference from relative humidity at room temperature, the slow recovery and poor selectivity [6]. There have been a variety of attempts to overcome these limitations, such as heat treatment, ultraviolet light irradiation, increasing carrier gas flux, and modification of CNTs with functional groups or other additives [7].

Chemically functionalized CNTs have been used as an active component in sensors devices the addition of functional groups such as carboxylic acid in singlewalled carbon nanotubes (SWCNTs) or MWCNTs has demonstrated enhanced sensitivity to ethanol [8] and NO gas [9]. Others approaches involve the incorporation of carbon nanotubes into polymers [10,11], such as polypyrrole that shows an enhanced sensitivity [12], also SWNTs with covalently attached poly- (*m*-aminobenzene sulfonic acid) have shown improved sensor performance for detection of NH3, and allow detection at concentrations as low as 5 ppm. In this context, nanocomposite materials such as nanotubes decorated with metal or metal-oxide nanoparticles have been proposed as active component in gas sensing devices. These

nanoparticles-nanotube systems have attracted much attention because they show enhanced sensitivity toward gaseous species such as H_2, H_2S [13,14], NO_2 [15,16], NH_3 and CO [16,17] compared to pure nanotubes gas sensors [18].

Nitrogen-doped multiwalled carbon nanotubes (CN_X-MWNTs) have shown to be an excellent approach to overcome some limitations that exhibit pure carbon nanotubes systems in gas sensing applications [19-21]. Due to their important chemical reactivity at the surface, these materials are very good candidates for anchoring nanoparticles [22]. For instance, carbon nanotubes with Ag-nanoparticles have proved to be an excellent active component for sensing biological materials [23,24] and hydrogen peroxide [25]. Additionally, the decoration of carbon nanotubes with silver nanoparticles has been extensively explored [26-29] increasing the possibility for future applications.

By taking advantage of the facility to deposit metallic nanoparticles on nitrogen-doped nanotubes and the high affinity that silver exhibit to sulfur containing molecules; we fabricated a carbon disulfide (CS_2) gas sensor. We have selected CS_2 as a targeting gas because of its potential hazard to human health as alternative technique for the analysis of reduced sulfur compounds (RSC) in air. Nowadays gas chromatography (GC) is the most used technique to that [30]. CS_2 is one of the most abundant RSCs in the environment [31]. Pure CS_2 is highly volatile, the vapor can explode in air, and the exposure affects the nervous system and developing fetus, it chronic exposure may lead kidney and liver damage [32]. In order to overcome the difficulty on the detection and quantification of CS_2 and the time-consuming and tedious processes of sampling and offline analytical protocols in the laboratory, the developing of portable, sensitive and selective sensors are needed. There have been done considerably efforts to detect CS_2 using

nanomaterials such as CeO_2 [33]. However, the CS_2 vapor detection is still a challenge, and there is a need for the development of portable and better sensors materials.

In the present chapter, we proposed the use of nitrogen-doped multiwalled carbon nanotubes (CN_X-MWCNTs) decorated with silver nanoparticles as vapor-gas sensors materials. Different fabricated sensors are tested using CS_2, we also tested ethanol, acetone and chloroform vapor. Thermal effects are also studied on the sensors performance. In addition, first-principles calculations are carried out in order to understand the interaction between carbon nanotubes, silver nanoparticles and the involved organic molecules.

3.3. Experimental Section: Silver Decoration of Carbon Nanotubes, Material Characterization and Sensor Fabrication Procedure

3.3.1. Synthesis of Silver-decorated Nitrogen-doped Multiwalled Carbon Nanotubes

The nitrogen-doped multiwalled carbon nanotubes (CN_X-MWNTs) were synthesized by chemical vapor deposition (CVD) process [34,35,36]. The anchorage process of silver nanoparticles was carried out following the next steps: Firstly, the CN_X-MWNTs were heated at 300 ^{0}C in air during 5 min. After that, 35mg of nanotubes were added to 20 ml of acetone containing silver nitrate (166µl of a solution 0.1 N, J.T. Baker®) in a flask. The suspension was dispersed ultrasonically by one hour and the resultant solution is placed in a water bath to increase the temperature up to 52 $^{\circ}$C; the temperature was maintained during 60 minutes. Finally, the solution is filtered using a PTFE membrane with 0.2µm pore size, washed with distilled water and dried at 110 ^{0}C in a furnace.

3.3.2. Fabrication Procedure of Gas Sensor Based on Carbon Nanotubes and Their Electrical Characterization

Foils formed by dispersed pristine CN_X-MWNTs and CN_X-MWNTs decorated with Ag nanoparticles (CN_X-MWNTs-Ag) were obtained by vacuum filtration using acetone as a solvent. The concentration of the suspension was selected to provide a homogeneous foil thickness. The foil sensors were cut to obtain a film dimension of 0.5x4.0 mm. The films were supported on alumina plates with copper electrodes using silver paint. Finally, the electrodes were connected to the source-meter and control

system. The sensor device was collocated within a quartz tube inside a tubular furnace; a schematic diagram of the setup used in the experiments is shown in figure 3-1. We then plotted the normalized resistance (R_N) which is defined by $R_N = (R-R_0)/R_0$, in which R represents the electrical resistance obtained in the measurement; R_0 is the initial value of the resistance.

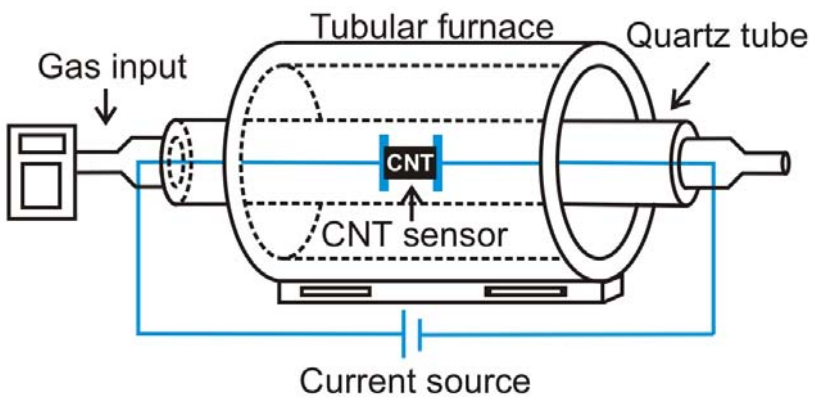

Figure 3-1 Schematic representation of the experimental setup of the gas vapor sensor using carbon nanotubes. Two types of foils were constructed by using: **(1)** nitrogen-doped multiwalled carbon nanotubes decorated by Ag-NPs (CN_X-MWNTs-Ag) and **(2)** only CN_X-MWNTs. The foils were collocated inside a quartz tube in a tubular furnace, under controlled temperature and atmosphere. Five cycles have been chosen, allowing 80 s for the solvent vapor to enter in the reaction chamber, and 100 s for purging the system with pure Ar.

3.3.3. Material Characterization Techniques

The characterization of the nanotubes films was carried out using a scanning electron microscopy (FEG-SEM, FEI XL30 FEG/SFEG) operated at 3-20kV. The X-ray powder diffraction patterns of all samples were performed using a XRD D8 ADVANCE – BRUKER AXS, with a Cu K_α radiation (λ = 1.54060 Å). The operating current and voltage were maintained at 35 kV and 25 mA. High-resolution images were taken with a HRTEM -field emission Tecnai F30 operated at 300 kV. The electrical characterization of each sample was carried out using a SourceMeter (Keithley 2400) with Labview ® environment.

3.4. Results and Discussion

3.4.1. Nanocomposite Characterization and Carbon Nanotube Sensor Fabrication

Firstly, the samples were characterized using transmission electron microscopy (TEM). Figure 3-2 depicts the images of silver nanoparticles (Ag-NPs) anchored on the surface of nitrogen-doped multiwalled carbon nanotubes (CN_X-MWNTs). Note that the sample exhibits a homogeneous distribution of Ag-NPs with an average size of 14 nm. High magnification images (see figure 3-2(b-c)) show that Ag-NPs present a small amorphous layer on its surface. These amorphous layers could be formed by carbonaceous material derived from the decoration process.

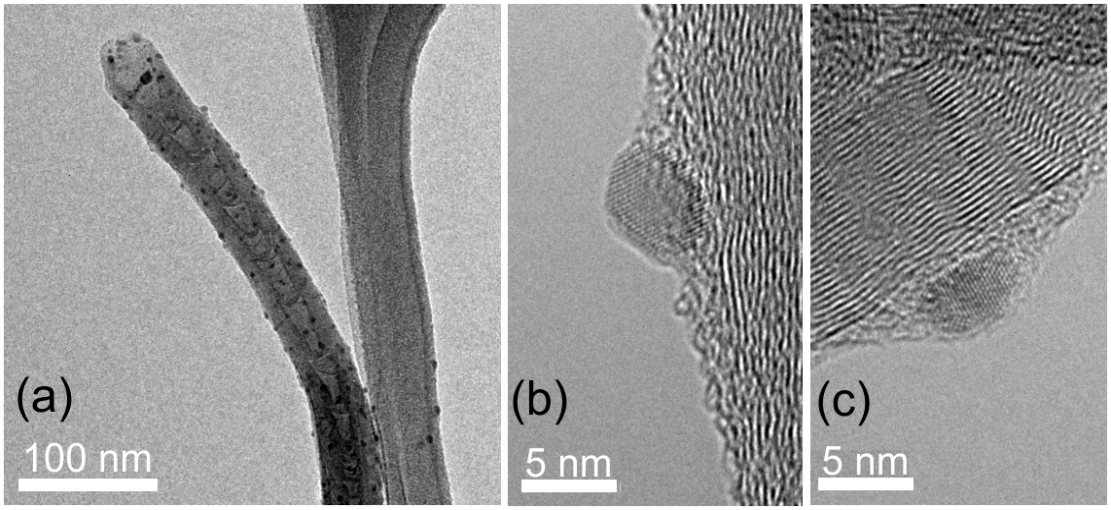

Figure 3-2 Transmission electron microscopy (TEM) images of Ag-nanoparticles anchored on the surface of nitrogen doped multiwalled carbon nanotubes (CN_X-MWNTs/Ag). In **(a)** it is possible to observe a homogeneous distribution of Ag-nanoparticles surrounded the carbon nanotube surface**. (b-c)** High magnification images showing silver nanoparticles anchored on the surfaces of the multiwalled carbon nanotubes, the average size is 14 nm. Note that an amorphous thin layer covers the Ag-nanoparticle´s surface.

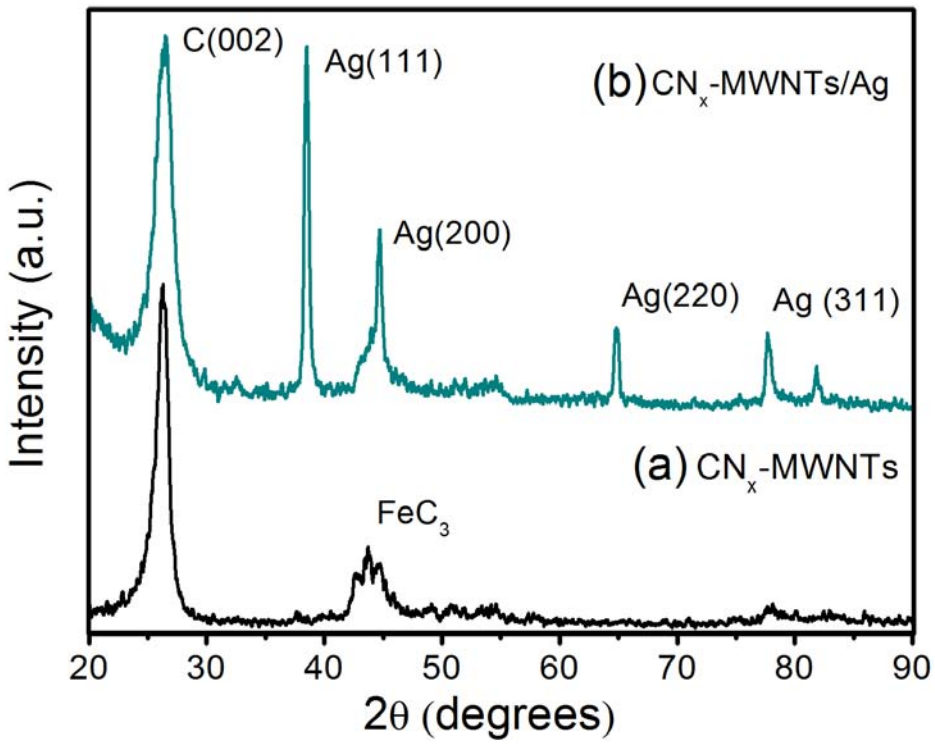

Figure 3-3 X-ray diffraction pattern of **(a)** nitrogen-doped multiwalled carbon nanotubes (CN_X-MWNTs) and **(b)** Ag-nanoparticles anchored on the surface of CN_X-MWNTs (CN_X-MWNTs/Ag). The sample contains only CN_X-MWNTs exhibits a peak C(002) in 26 degree corresponding to carbon nanotube (typical of graphite systems). The different signals observed beyond of 30 degree correspond to the encapsulated materials (FeC_3 and α-Fe) by the carbon nanotubes. The sample CN_X-MWNTs/Ag exhibits additional peaks, which correspond to the Ag-nanoparticles.

Figure 3-3 depicts X-ray diffraction characterization which reveals that the sample containing only CN_X-MWNTs exhibits a peak C(002) in 26 degree corresponding to carbon nanotube (typical of graphitic systems). Also, different signals were observed beyond of 30 degree that corresponds to the encapsulated materials (FeC_3 and alpha-Fe) by the carbon nanotubes. These encapsulated materials are small nanoparticles or nanowires generally found at samples of carbon nanotubes obtained by chemical vapor deposition. The sample corresponding to Ag-NPs on CN_X-MWNTs exhibit

different additional peak intensities, due to the Ag-nanoparticles, the indexed planes in the plot correspond to Ag-bulk with a face centered cubic structure (fcc), which match to the intensities obtained by this sample, suggesting that the Ag-NPs exhibit a fcc type structure. Foils made of samples characterized above, were fabricated by vacuum filtration of solutions containing dispersed Ag-NPs on CN_X-MWNTs or pure CN_X-MWNTs. Scanning electron microscopy characterization revealed that the foils show a homogenous dispersion. In order to measure the sensing capacity of the foils, these were placed inside a quartz tube (illustrated in figure 3-1) with a controlled temperature and atmosphere. Thus two channels are used for introducing the gas to be sensed and the argon gas flow was used to purge or clean the foils. Two different time of exposure were used: 80 s for the gas to be sensed and 120 to argon gas, this process is repeated for five or more cycles. Thus different plots of the electrical resistance as a function of the time (s) were obtained. All these result are explained in the following section.

3.4.2. *Sensing Properties of Silver Decorated Nitrogen-doped Carbon Nanotubes at Different Operation Temperatures*

The efficiency of the sensing capacity of the different foils were tested when a vapor flow formed by carbon disulfide (CS_2), acetone ($(CH_3)_2CO$), ethanol (C_2H_5OH) or chloroform ($CHCl_3$) were passing thought the quartz tube. We determine the sensor performance by analyzing the response (%ΔR), which is defined as:

$$\%\Delta R = \left(\frac{R_2 - R_1}{R_1} \right) * 100 \qquad \textbf{Eq. (3-1)}$$

where R_1 is the electrical resistance before the gas exposure, and R_2 is the maximum electrical resistance reached after the gas exposure. We also determined the response and recovery time.

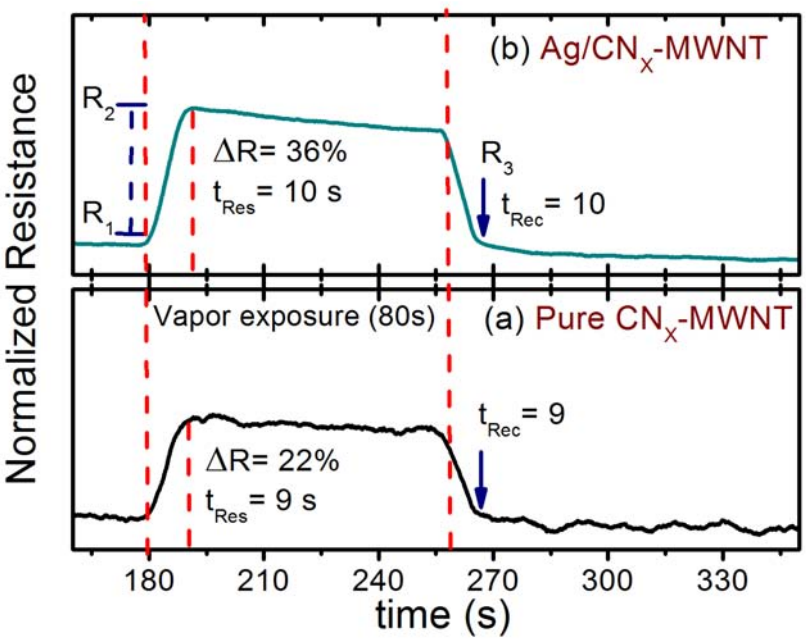

Figure 3-4 Analysis of the operation performance of the nanotube based CS_2 sensor at room temperature. **(a)** pure CN_X-MWNTs, and **(b)** CN_X-MWNT/Ag composite. Both materials exhibit similar response and recovery times, ~10 s. However, the change in electrical response (ΔR) of the sensor based on CN_X-MWNT/Ag composite show larger sensitivity compared to pure CN_X-MWNTs sensor material.

Table 3-1 Performance comparison of Ag-decorated and pure CN_X-MWNTs based sensor devices for four different organic vapors at **room temperature**.

	Response (%ΔR)	Response time (s)	Recovery time (s)
CN_X-CS_2	20	9	10
Ag-CN_X-CS_2	35	10	11
CN_X-$(CH_3)_2CO$	20	11	10
Ag-CN_X-$(CH_3)_2CO$	40	12	11
CN_X- C_2H_5OH	20	12	11
Ag-CN_X-C_2H_5OH	25	17	14
CN_X-$CHCl_3$	30	15	11
Ag-CN_X-$CHCl_3$	60	15	11

Here, $\%\Delta R=[(R_2-R_1)/R_1]$, where R_1 and R_2 are the electrical resistance before and after the exposure respectively. Response time, it is the necessary time to reach the maximum electrical resistance after the exposure of the targeted analyte. Recovery time, it is defined as the necessary time to recover the 95% of the initial electrical resistance.

The response time is defined (t_{Res}) as the necessary period to reach the maximum electrical resistance (R_2 in figure 3-4) when the sensor is exposed with the targeted analytes. The recovery time was defined as the needed time to recover 95% of its initial electrical resistance (R_1 in figure 3-4). In all systems, the electrical resistance increases when the samples were exposed to the vapors and decreases during the purging cycles. At room temperature (25°C), when the sensors are exposed to any of the targeted analytes, the maximum electrical resistance of the nanotubes foils is reached (the sensor material is saturated, denoted as R_2 in figure 3-4) and it remains practically constant until the purging cycle is applied. Then, the system decreases its electrical signal (R_3 in figure 3-4), returning to the response measured before the vapor exposure (denoted as R_1 in figure 3-4). This indicates that the adsorbed molecules on the carbon nanotubes during the contact with the vapor flow are detached. After various testing cycles, we notice that the electrical resistance corresponding to the base line of the

systems remain constant, this suggest that the sensor exhibit a good stability, a desire characteristic for a good sensor material.

Figure 3-4 depicts the analysis of the operation performance for nanotube based CS_2 vapor sensor at room temperature (25 °C). In figure 3-4 can be observed that both nanomaterials, pure and Ag-decorated nanotubes, exhibit similar response and recovery times (~10 s for the case of CS_2 vapor), however the variation in electrical resistance (ΔR) generated by the exposure to the organic vapor is larger for the Ag-decorated CN_X-MWNTs (ΔR = 36 %) compared to pure CN_X-MWNTs (ΔR = 22%), these results suggest better sensitivity for CS_2 vapor in the case of the metal-nanotube systems. Similar results were obtained when the targeted analytes were acetone, ethanol or chloroform; these results are summarized in table 3-1. The response time for all sensors is in the range of 10-20 s, and the recovery time is 10-15 s. All the sensors based on Ag-decorated CN_X-MWNTs exhibit larger change in electrical resistance (%ΔR) compared to pristine CN_X-MWNTs. Results on the sensor response in presence of CS_2 vapor at different temperatures are shown in figure 3-5. The two different curves refer to foils formed by pure CN_X-MWNTs and CN_X-MWNTs/Ag. Notice that the CN_X-MWNTs-Ag exhibits larger change in electrical resistance than CN_X-MWNTs.

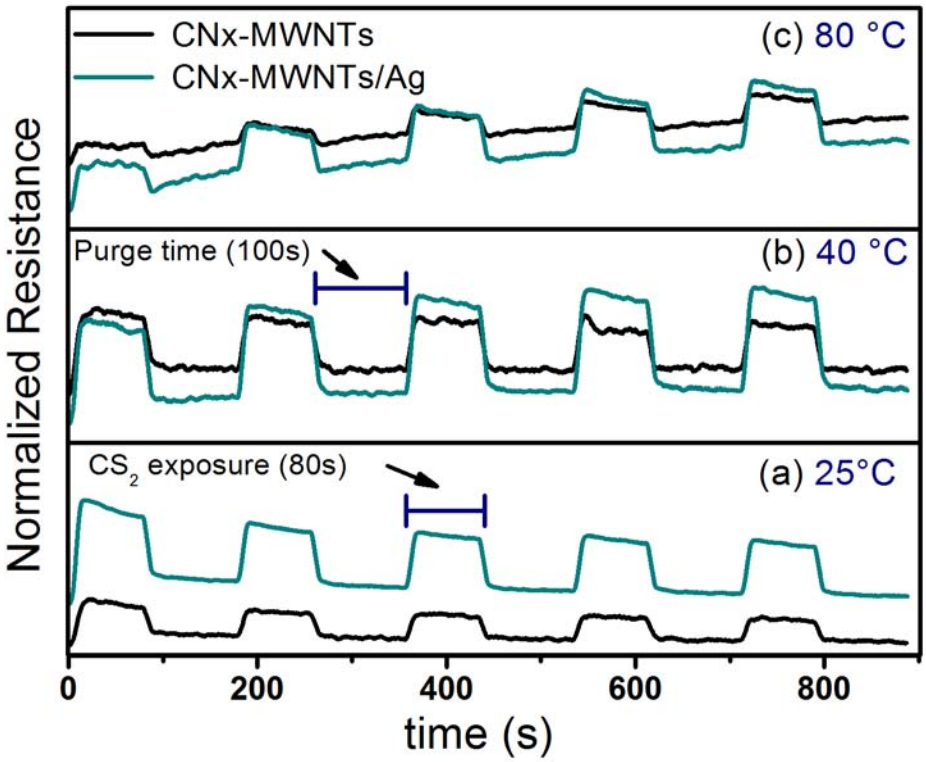

Figure 3-5 Normalized electrical resistance of nanotube foils exposed to carbon disulfide (CS_2) vapors at three different temperatures for CN_x-MWNTs (black line) and Ag-nanoparticles anchored on CN_x-MWNTs (blue line). **(a)** At 25°C a good performance is observed, however, after each purge cycle, base line remains constant, suggesting a weak interaction between vapor and sensor material (physisorption). **(b)** 40°C, chemisorption and physisorption are both important. **(c)** 80°C the Ag decorated nanotubes are still showing a good. The slope of the base line suggests that at 80°C, chemisorption process is the mean mechanism of gas detection. The CN_X-MWNTs-Ag exhibit larger change in electrical resistance when it's exposed to the CS_2 vapor. Note that the foils formed by CNx-MWNTs-Ag exhibit larger electrical resistance. The shadow areas indicate the exposure cycles to the CS_2 vapor, equivalent to 80s.

This effect could be related that CN_X-MWNTs/Ag samples exhibit more superficial area due to the Ag-NPs and consequently the vapor molecules found more active sites for attaching, which could increase the electrical resistance. At room temperature (25 °C), the sensors display an excellent performance, after the purge cycle the foils are cleaned, decreasing its electrical resistance, revealing a weak interaction between the CS_2

molecules and sample. This fact is understood for foils formed by only CN_X-MWNTs, but not for CN_X-MWNTs-Ag composite since one expects that the sulfur atoms should be strongly attached to the Ag-nanoparticles and consequently the sensors exhibit a chemisorption behavior. This effect could be explained, by suggesting that Ag-NPs does not interact directly with the CS_2 molecules. As it is already found by TEM characterization the Ag-NPs exhibit small amorphous layer on its surface. However, a chemisorption effect is observed when the sensors are tested at higher temperatures. At 40 °C (figure 3-5b) the base line remains practically constant, where the chemisorption starts to appear. For 80 °C (figure 3-5c), the base line of the sensor signal is increasing slightly, suggesting that chemisorption of CS_2 vapor is the mean adsorption process. This event can be related with the amorphous layer surrounding the Ag-nanoparticles, which could be removed by thermal effects.

Once cleaned the surface of the Ag-nanoparticles, the sulfur atoms are attached covalently with the silver atoms. It is important to observe the difference in the intensity of the normalized electrical resistance in the two nanomaterials, possibly indicates that, in the case of the CN_X-MWNTs-Ag a larger number of active sites exists where molecules can interact with the composite surface. This could explain the substantially increment of several orders of magnitude in the electrical resistance, compared with the pure CN_X-MWNTs. Our results are in good agreement with the previous reported data, where metal decorated nanotube systems show an improvement in sensitivity [13,15-17].

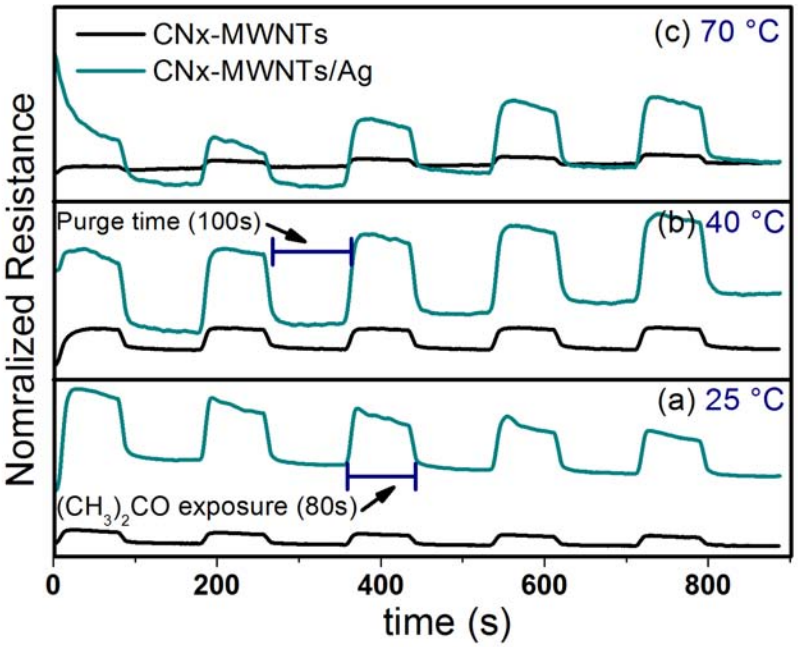

Figure 3-6 Normalized electrical resistance of nanotube foils exposed to acetone. The CN_X-MWNTs/Ag exhibit larger change in electrical resistance and at higher temperatures the CN_X-MWNTs/Ag shows a better signal response. At 70°C, the pure CN_X-MWNTs show almost a null signal response.

We have tested our sensor devices with other three different solvent, acetone, ethanol and chloroform. Figure 3-6 displays the sensor response with the acetone vapor gas for 25, 40 and 70 ^{o}C. We observe that similar results, at low temperatures (25 and 40 °C) the adsorption process is dominated by physisorption. At higher temperatures, 70 °C in this case, chemisorption is relevant. As we can observe, in all the working temperatures, the CN_X-MWNTs-Ag exhibit always better sensitivity for acetone.

Figure 3-7 depicts the results of change in the electrical resistance when ethanol (C_2H_5OH) and chloroform ($CHCl_3$) were introduced. We observed a similar behavior; at room temperature the sensors exhibit a weak interaction,

suggesting a physisorption process, between nanomaterials and the vapors. These results also find that the intensity of the change in electrical resistance of the CN_X-MWNTs/Ag composites is larger by several orders of magnitudes compared to the pristine nanotubes. At higher temperatures, when the pristine CN_X-MWNTs does not show a clear response, the CN_X-MWNTs/Ag improves the sensing signal and a chemisorption become relevant.

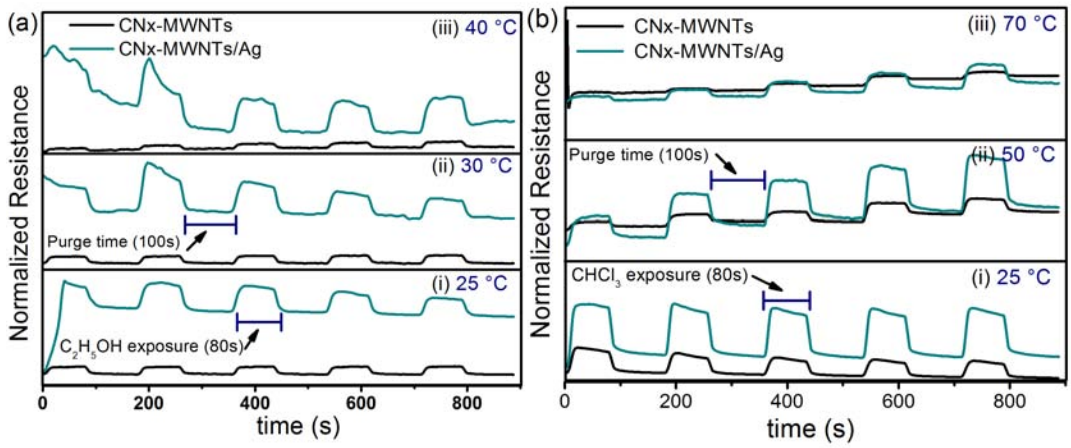

Figure 3-7 Normalized electrical resistance of nanotube foils exposed **(a)** ethanol and **(b)** chloroform vapor. The CN_X-MWNTs/Ag exhibit larger change in electrical resistance and at higher temperatures the CN_X-MWNTs/Ag shows a better signal response. After 40°C no clear signal response was observed for ethanol. By varying the operation temperatures, it can select the vapor that will be detected.

As we can see from figures 3-5 to 3-7, the operation temperature depend s of the vapor to be detected. The obtained results with Ag-decorated CN_X-MWNTs are summarized in figure 3-8, where it is monitored the response (%ΔR) versus operation temperature of the sensor device. It is observed that the sensor response increase with the operation temperature for all tested vapor. However at higher temperature the response starts to decreases, this temperature depend of the targeted analyte, being the lowest for ethanol,

then chloroform, acetone and finally for carbon disulfide vapor. For ethanol, after 40°C there is no clear response, but for chloroform, exhibit a very nice response with good sensitivity. By increasing the operation temperature (80°C) the electrical change generated by introduction of chloroform is almost null, while for acetone or carbon disulfide still exhibit clear response and good sensitivity. At 130°C the response for acetone and carbon disulfide decrease near to zero. These results suggest that by varying the operation temperature, it is possible to control the detection of the desired vapor and improve the selectivity of the sensor device.

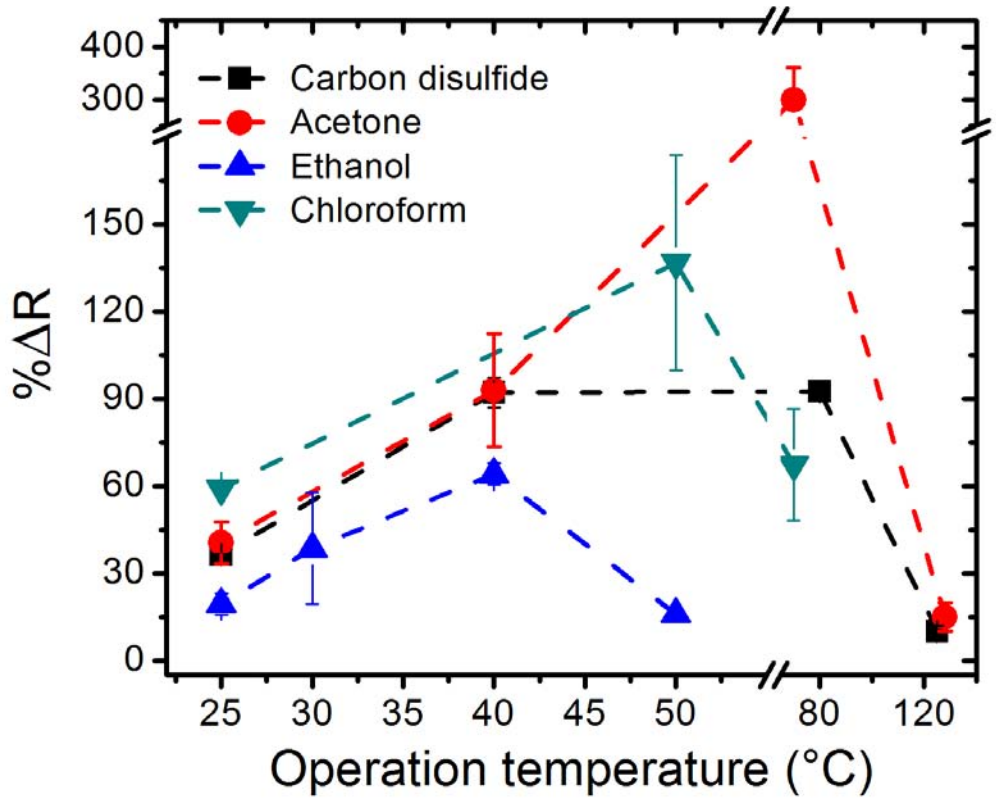

Figure 3-8 Change in electrical response %ΔR (see Eq. 3-1) after the exposure to different vapors at various working temperatures of Ag-decorated CN_X-MWNT sensors. The response of the sensor for different analytes increases with the operation temperature, however, after certain temperature the response start to decrease depending of the targeted analytes. It suggests that controlling the working temperature it is possible to discriminate the analytes to be detected, improving selectivity of the sensor material.

3.5. Understanding the Sensing Mechanism of Silver-decorated Carbon Nanotubes from a Theoretical Approach

We have performed density functional theory calculations in order to understand the interaction between the nitrogen-doped nanotubes and carbon disulfide, ethanol, acetone and chloroform molecules. For the calculations, the metallic (5,5) carbon nanotubes with a pyridine-type nitrogen-doped have been considered. The pyridine doping consists in removing a carbon atom (creating a vacancy) and the carbon atoms surrounding the vacancy are substituted by nitrogen atoms (see figure 3-9a). Different molecules were set around the doping sites and relaxed using conjugated gradient method.

The electronic calculations were performed using density functional theory (DFT) [37,38] in the framework of the LSDA with a basis of linear combination of atomic orbitals (LCAO) as implemented in the SIESTA code [39]. The systems were constructed by using a supercell of 100 atoms taking 5 units of the (5,5) nanotube (20 atoms per unit cell) and different organic molecules. Periodic boundary conditions were used and the inter-tube distance was kept to a minimum of 30 Å to avoid lateral interactions. The adsorption energy (E_a) was calculated through the formula $E_a=E_m+E_c-E_s$, where E_m and E_c are the energies associated to the isolated molecule (adsorbate: carbon disulfide, ethanol, acetone, chloroform) and the substrate material (adsorbent: carbon nanotube) respectively, and E_s is the energy associated to the complex system (molecule + nanotube). For further information see Apendix A.

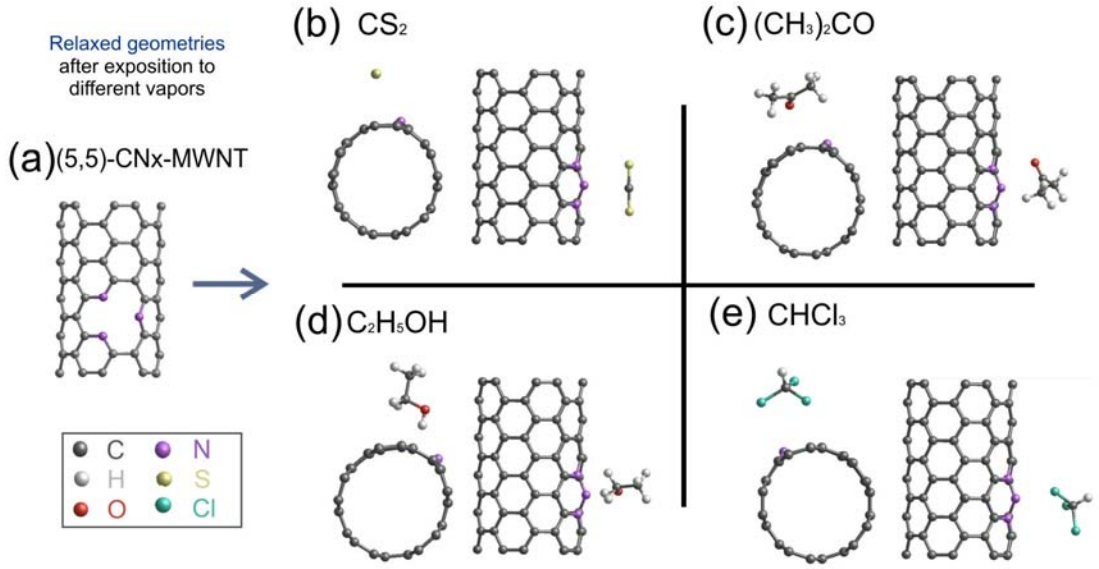

Figure 3-9 Relaxed geometries of nitrogen-doped carbon nanotube (CN_X-SWNT) with different molecules around of the nitrogen atoms. Here, the nitrogen atoms are introduced in pyridine fashion in the nanotube´s lattice. Results for: **(a)** single nanotube, **(b)** nanotube-carbon disulfide (CS_2), **(c)** nanotube-acetone ($(CH_3)_2CO$), **(d)** nanotube-ethanol (C_2H_5OH), and **(e)** nanotube-chloroform ($CHCl_3$). Notice that in all cases, a non covalent bonds were found, which suggest a physisorption state.

Figure 3-9 depicts the relaxed structures of the nitrogen-doped (5,5) carbon nanotubes joined to the carbon disulfide, ethanol, acetone, and chloroform molecules. Notice that the molecules exhibit a weak interaction with the carbon nanotubes, suggesting that the molecules are joined via a physisorption mechanism, which is in qualitatively agreement with the sensing capacity at room temperature of foils made of only CN_X-MWNTs. The electronic density of states of all systems is shown in figure 3-10. It is observed that when the nanotube is in contact with the different molecules, there is almost null contribution around of the Fermi level. These results are in according with the experimental results when only CN_X-MWNTs are used. Experimental results shown above for sensors fabricated with CN_X-MWNTs with Ag-NPs demonstrated that the different molecules could be attached in a chemisorptions fashion.

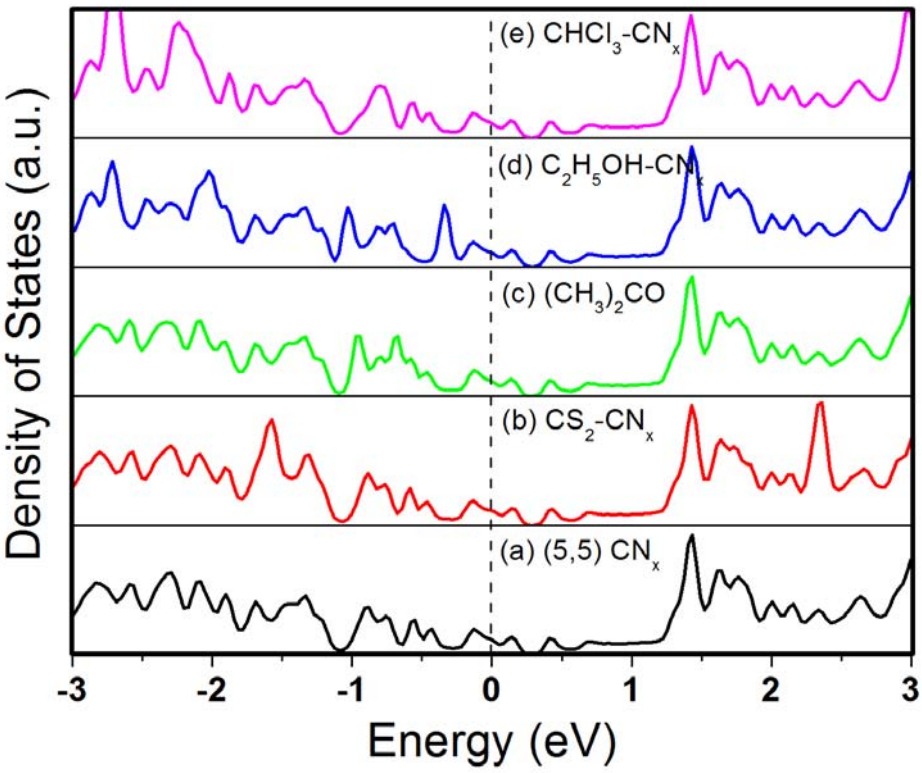

Figure 3-10 Electronic density of states (DOS) of the relaxed geometries of (5,5) nitrogen-doped carbon nanotube in contact with different molecules. **(a)** Single nanotube, **(b)** nanotube-carbon disulfide (CS_2), **(c)** nanotube-acetone ($(CH_3)_2CO$), **(d)** nanotube-ethanol (C_2H_5OH), and **(e)** nanotube-chloroform ($CHCl_3$). Note that there exists a poor contribution of the different organic molecules to the DOS around of the Fermi level compared to the single nanotube. The relaxed structures can be seen in figure 3-9.

In order to understand these systems, we performed another calculation using an icosahedral Ag_{13} cluster as a substrate material and different molecules were attached to its surface. The calculation was performed with an Ag_{13} cluster and the organic molecules with an intercell separation of 30 Å. All the structures were relaxed by conjugated gradient minimization until the maximum force was less than 0.04eV/Å. For further information please see Apendix A.

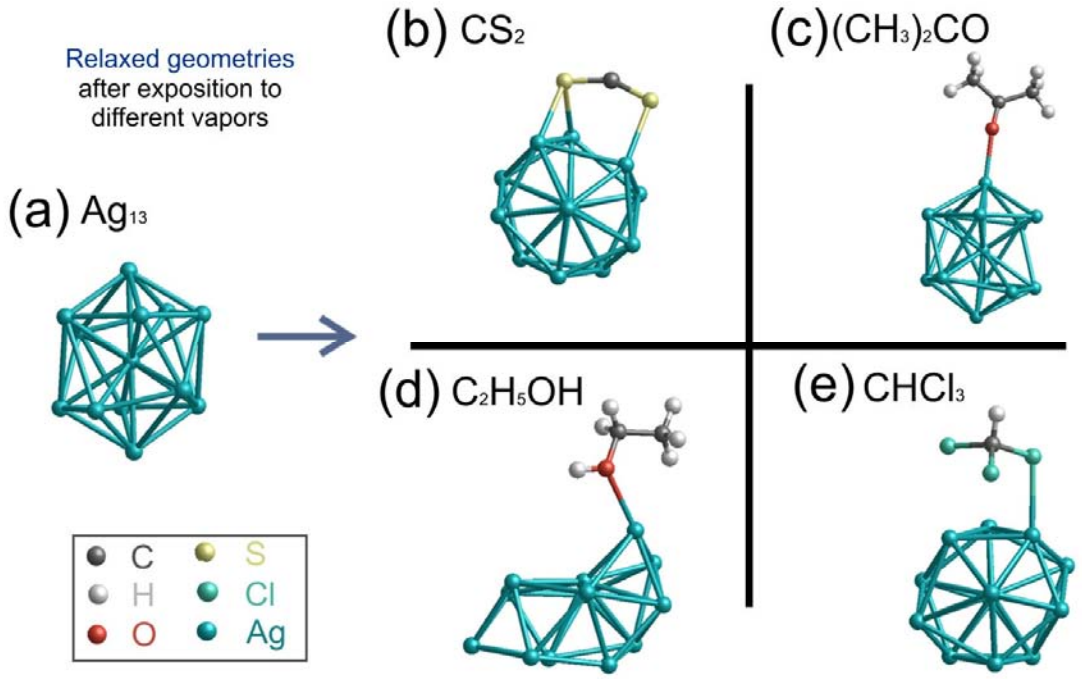

Figure 3-11 Relaxed geometries of silver clusters with 13 atoms (Ag_{13}) with different molecules joined to the cluster´s surface. All calculations have been initialized with icosahedral geometry for the silver clusters. **(a)** isolated Ag_{13} cluster**, (b)** Ag_{13}-carbon disulfide (CS_2), **(c)** Ag_{13}-acetone ($(CH_3)_2CO$), **(d)** Ag_{13}-ethanol (C_2H_5OH) and **(e)** Ag_{13}-chloroform ($CHCl_3$).

The resulting structures exhibit a bonding between the adsorbed molecules and the metallic cluster. The relaxed structures are shown in figure 3-11. The electronic density of states of the obtained geometries are shown in figure 3-12. We can observe that the states around the Fermi level in some cases decrease; it could suggest the increment in the electrical resistance. In this case, all the molecules exhibit a bonding with the substrate material.

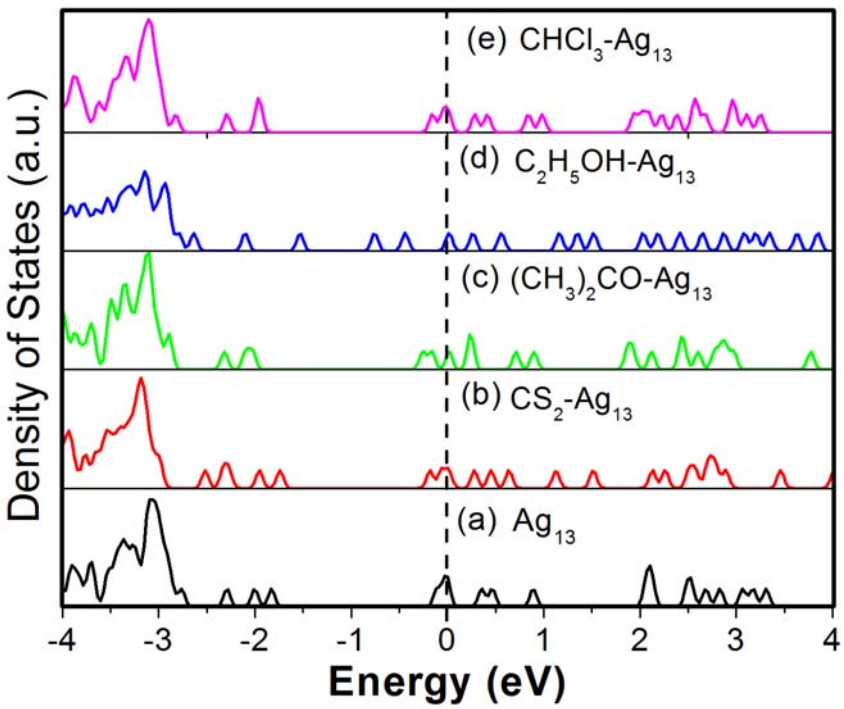

Figure 3-12 Electronic density of states (DOS) of relaxed geometries of Ag_{13} cluster with different molecules attached to the surface**. (a)** isolated Ag_{13} cluster, **(b)** Ag_{13}-carbon disulfide (CS_2), **(c)** Ag_{13}-acetone ($(CH_3)_2CO$), **(d)** Ag_{13}-ethanol (C_2H_5OH) and **(e)** Ag_{13}-chloroform ($CHCl_3$). The relaxed structures can be seen in figure 3-11.

These results are in agreement with our experimental data, where exists higher change in the electrical resistance when the nanocomposite CN_X-MWNTs-Ag is exposed to the vapors and we observe, in this case, that chemisorption could be the main mechanism of adsorption when Ag-NPs are involved. We determine the adsorption energy (E_{ads}) of all systems, as we define our reference system, a positive energy signifies a stable configuration. When a pyridine-like N-doped (5,5) SWNT is used as an adsorbent material, the E_{ads} of the different molecules is low. In the case of acetone and chloroform the adsorption energy is slightly negative, -0.082 and -0.053 eV, while the E_{ads} for CS_2 and ethanol is positive, 0.120 and 0.195 eV, these results can be observed in figure 3-13. When the

icosahedral Ag_{13} cluster is used, as we observe previously, there are bonds between systems. In this case the E_{ads} is higher, the oxygenated species such as acetone and ethanol exhibit the lowest E_{ads}, 0.338 and 1.059 eV respectively however, when the chloroform and carbon disulfide are used the adsorption energy is equal to 56.31 and 56.96 eV. The results are shown in figure 3-13.

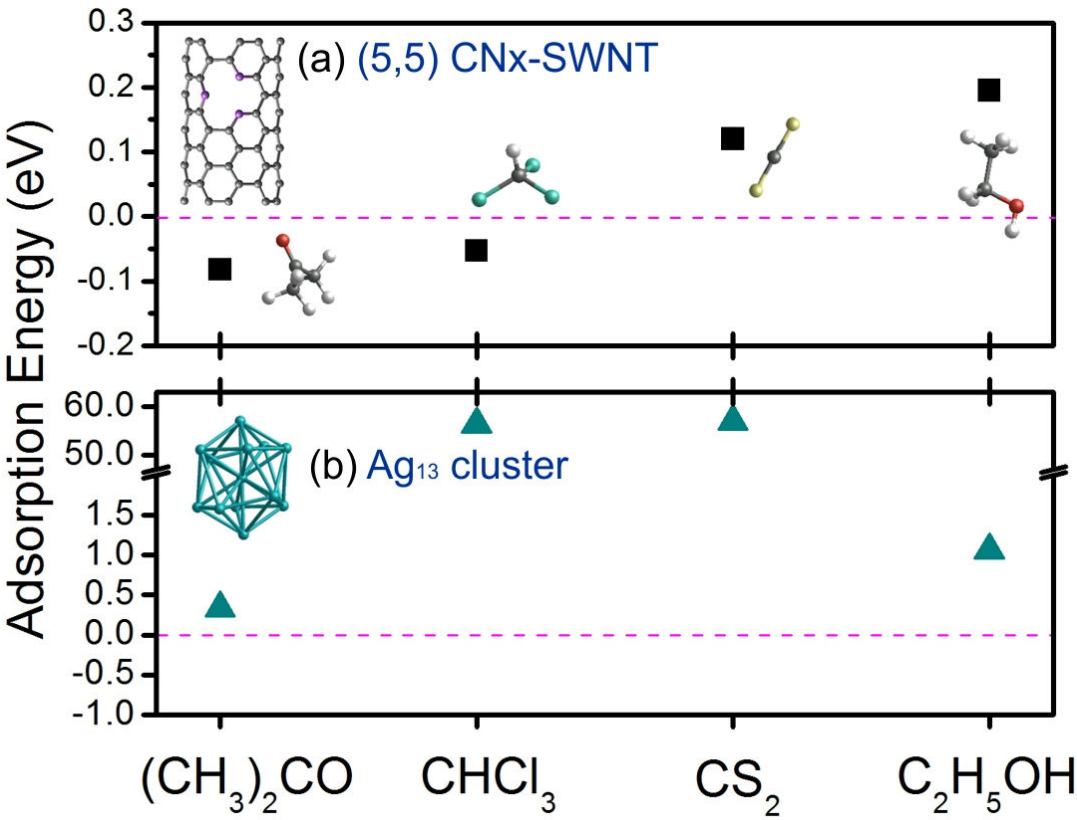

Figure 3-13 Adsorption energy different organic molecules on pyridinic nitrogen-doped carbon nanotubes and icosahedral Ag_{13} cluster. In **(a)** the adsorption energy (E_{ads}) of the molecules on a CN_X-SWNT. Acetone and chloroform exhibit slightly negative E_{ads}, -0.082 and -0.053 eV respectively, while carbon disulfide and ethanol exhibit a E_{ads} equal to 0.120 and 0.195 eV. **(b)** E_{ads} when an Ag_{13} cluster is used as a adsorbent material. In this case, the oxygenated species (acetone and ethanol) exhibited the lowest but positive E_{ads}, 0.338 and 1.059 eV respectively. In the case of $CHCl_3$ and CS_2, they exhibit a similar and large E_{ads} equal to 56.31 and 56.96 eV. All the organic molecules exhibit larger E_{ads} when are adsorbed on the icosahedral Ag cluster compared to the nanotube case. Note, positive adsorption energy means a stable configuration.

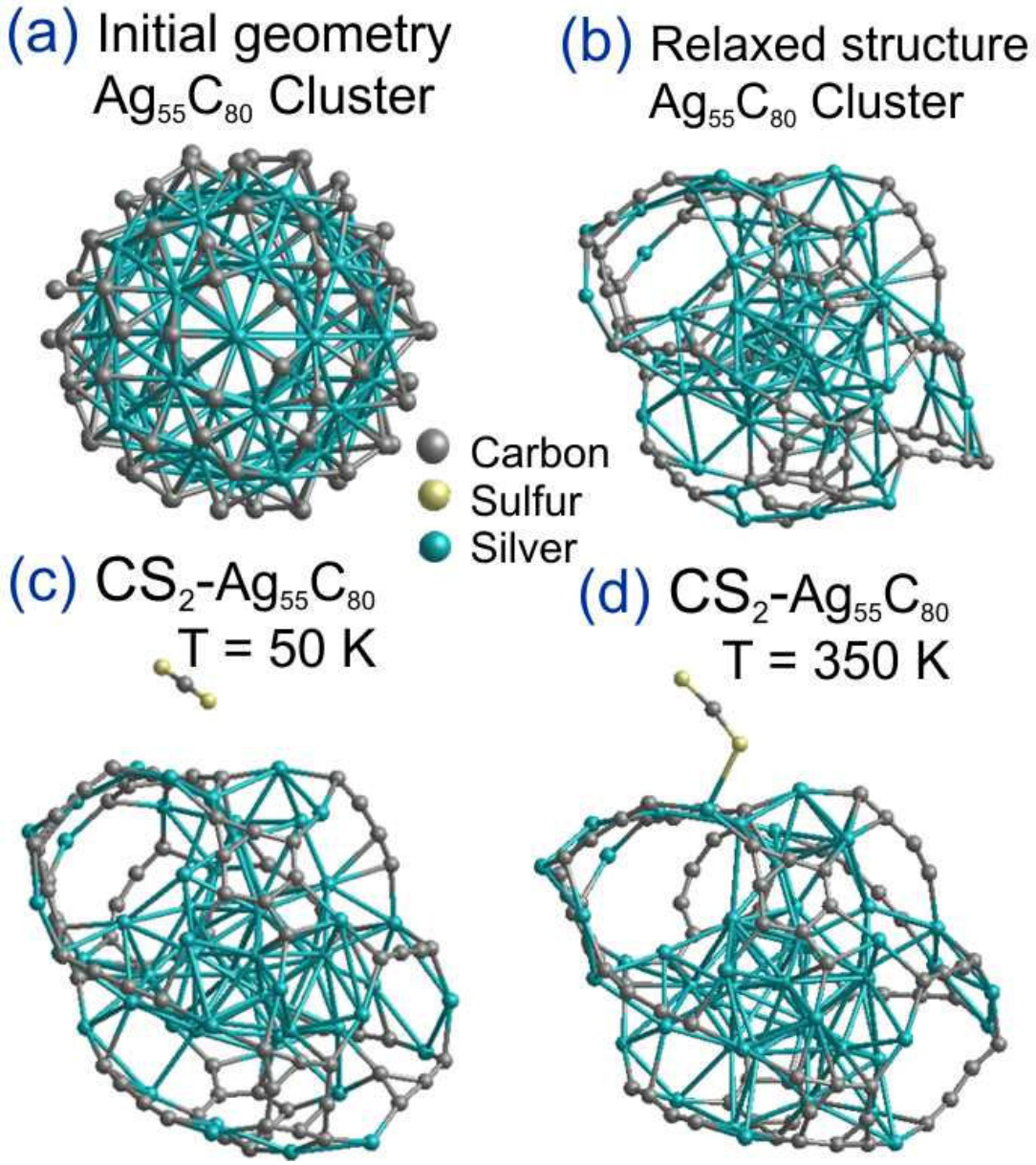

Figure 3-14 Adsorption of carbon disulfide on an $Ag_{55}C_{80}$ cluster. **(a)** Initial geometry of an icosahedral Ag_{55} cluster surrounded by carbon layer (C_{80}). **(b)** Relaxed structure of $Ag_{55}C_{80}$ cluster. **(c)** Depicts the final geometry after a molecular dynamics simulation at T = 50 K during 1 ps. After the exposure to CS_2 molecule it does not exist a chemical bond between systems suggesting a physisorption state. **(d)** Final geometry after molecular dynamics at T=350 K during 1 ps. As we can observe, it exhibit a bond between CS_2 molecule and the $Ag_{55}C_{80}$ cluster, suggesting that it's possible to obtain a chemisorption state at higher temperatures. These results are in good agreement with the experimental data.

We return to the case related with the carbon disulfide gas-vapor sensed at room temperature by foils made of Ag-NPs on CN_x-MWNTs. The electrical resistance as a function of the number of cycles suggests that the CS_2 molecules are attached to system (Ag-NPs or nanotube surface) via a physisorption mechanism. Sulfur atoms should be joined via a chemisorption mechanism (covalent bond) with Ag-NPs. Here, we address this problem and propose a possible mechanism. From the TEM images (figure 3-2), the CN_X-MWNTs decorated with Ag nanoparticles exhibit a small layer composed by amorphous carbon. In order to understand the role of this amorphous layer on Ag nanoparticles in the sensing capacity, we construct an Ag_{55} icosahedral nanoparticle surrounded by a carbon layer (C_{80}). Each carbon atom was three-coordinated with Ag atoms; the initial structure and the relaxed geometry can be seen in figure 3-14a and 3-14b. Subsequently, we placed a CS_2 molecule on the surface of the $Ag_{55}C_{80}$ nanoparticle, the entire system was relaxed using molecular dynamics simulations at 50 Kelvin during 1 ps with 1 femtosecond steps (figure 3-14c), and it is observed that there is no bonds between the systems (creating a physisorption state). Using the latest structure (figure 3-14c), similarly the system was relaxed at 350 Kelvin during 1 ps. The final geometry is shown in figure 3-14d exhibiting a covalent bond between CS_2 molecule and the $Ag_{13}C_{20}$ cluster (chemisorption). These results reveal a good agreement with our experimental data. During the molecular dynamics at T=350 K, the CS_2 molecule formed various non-stable bonds with Ag atoms, however, for final steps of the relaxation process, the molecules is stably joined to a low-coordinated Ag atom.

3.6. Conclusions

The gas sensors based on Ag-nanoparticles anchored on the surface of nitrogen-doped multiwalled carbon nanotubes were fabricated and tested with different chemical substances: carbon disulfide, acetone, chloroform and ethanol. Our results were compared with sensors performed with only nitrogen-doped multiwalled carbon nanotubes. The temperature dependence of the sensor performances was monitored; the results revealed that the sensor response and selectivity depend strongly of the temperature, promoting in some cases that gas molecules are attached to the nanotubes surface via a covalent bond. Typically, at room temperature, the sensors exhibit stable and constant changes of the electrical resistance, indicating that the gas molecules are weakly attached (physisorption) to the CNx-MWNTs surface making easy the removal of these molecules during the purging system. However, when the temperature increases, the sensors efficiency is affected. In some cases, the electrical resistance increases monotonously with the number of cycles, suggesting the existence of covalent bonds (chemisorption) between the carbon nanotubes and the gas molecules.

We demonstrated using density functional calculations that the carbon disulfide, ethanol, acetone, and chloroform are weakly linked to the nitrogen doped carbon nanotubes, however when these molecules were set at the surface of a Ag-cluster, the molecules are attached to the surface via a covalent bond, promoting in some cases, severe changes in the original cluster structure. Finally, an intriguing case is the related with carbon disulfide gas, here at room temperature the sensor efficiency is excellent, one would expect that the sulfur atoms would stick to the Ag-nanoparticles via a covalent bonds since the good affinity of the silver and sulfur, however the results show otherwise. Based on the TEM images (see figure 3-2), we attributed this effect to that the Ag-nanoparticles exhibit an amorphous carbon layer on its surface preventing the free interaction between the sulfur and silver atoms. Based in our DFT molecular dynamics calculations, we demonstrated

that at low temperature, CS_2 molecule did not attach to the surface of an Ag-cluster covered by an amorphous carbon layers, however with the increase of the temperature, covalent bonds between the CS_2 and the Ag-cluster were observed.

3.7. References

[1] J. Wang, "Carbon-nanotube based electrochemical biosensors: A review", *Electroanalysis*, **17**, 7-14 (2005)

[2] C. Li, E.T. Thostenson, T.–W. Chou, "Sensors and actuators based on carbon nanotubes and their composites: A review", *Comp Sci and Tech,* **68,** 1227–1249 (2008)

[3] D. R. Kauffman, A. Star, "Carbon nanotubes gas and vapor sensors," *Angew. Chem. Int. Ed.* **47**, 6550 – 6570 (2008).

[4] N. Sinha, J. Ma, J. T. W. Yeow, "Carbon nanotubes-based sensors," *J. Nanosci. Nanotech.* **6**, 573-590 (2006).

[5] O. K. Varghese, P. D. Kichambre, D. Gong, K. G. Ong, E. C. Dickey, C. A. Grimes, "Gas sensing characteristics of multi-wall carbon nanotubes," *Sensors and Actuators B*, **81**, 32–41 (2001).

[6] Q. Cao, J. A. Rogers, "Ultrathin films of single-walled carbon nanotubes for electronics and sensors: A review of fundamental and applied aspects", *Adv. Mater.* **21**, 29–53 (2009).

[7] W-D Zhang, W-H Zhang, "Carbon nanotubes as active components for gas sensors," *J. Sensors*, 160698 (2009).

[8] H.-L. Hsu, J.-M. Jehng, Y. Sung, L.-C. Wang, S.-R. Yang, "The synthesis, characterization of oxidized multi-walled carbon nanotubes, and application to surface acoustic wave quartz crystal gas sensor," *Mater Chem and Phys*, **109**, 148–155 (2008).

[9] J. Maklin, T. Mustonen, K. Kordas, S. Saukko, G. Toth, J. Vahakangas, "Nitric oxide gas sensors with functionalized carbon nanotubes," *Phys. Stat. Sol. B*, **244**, 4298–4302 (2007).

[10] K. H. An, S. Y. Jeong, H. R. Hwang, Y. H. Lee, "Enhanced sensitivity of a gas sensor incorporating single-walled carbon nanotube-polypyrrole nanocomposites," *Adv Mater*, **16**, 1005–1009 (2004).

[11] E. Bekyarova, M. Davis, T. Burch, M. E. Itkis, B. Zhao, S. Sunshine, R. C. Haddon "Chemically Functionalized Single-Walled Carbon Nanotubes as Ammonia Sensors", *J. Phys. Chem. B*, **108**, 19717-19720 (2004)

[12] K. H. An, S. Y. Jeong, H. R. Hwang, Y. H. Lee, "Enhanced sensitivity of a gas sensor incorporating single-walled carbon nanotube-polypyrrole nanocomposites" *Adv. Mater.* **16**, 1005-1009 (2004)

[13] A. Star, V. Joshi, S. Skarupo, D. Thomas, J-C P. Gabriel, "Gas Sensor Array Based on Metal-Decorated Carbon Nanotubes," *J. Phys. Chem. B*, **110**, 21014–21020 (2006).

[14] S. Mubeen, T. Zhang, N. Chartuprayoon, Y. Rheem, A. Mulchandani, N. V. Myung, M. A. Deshusses, "Sensitive detection of H_2S using gold nanoparticle decorated single-walled carbon nanotubes", *Anal. Chem.* **82***,* 250–257 (2010).

[15] M. Penza, R. Rossi, M. Alvisi, G. Cassano, E. Serra, "Functional characterization of carbon nanotube networked films functionalized with tuned loading of Au nanoclusters for gas sensing applications," *Sensors and Actuators B: Chemical,* **140**, 176-184 (2009).

[16] C. Bittencourt, A. Felten, E.H. Espinosa, R. Ionescu, E. Llobet, X. Correig J.-J. Pireaux, "WO_3 films modified with functionalised multi-wall carbon nanotubes: morphological, compositional and gas response studies," *Sensors and Actuators B: Chemical,* **115**, 33-41 (2006).

[17] D. R. Kauffman, D.C. Sorescu, D. P. Schofield, B. L. Allen, K. D. Jordan, A. Star, "Understanding the sensor response of metal-decorated carbon nanotubes," *Nano Lett.,* **10**, 958–963 (2010).

[18] C. S. Yeung, L. V. Liu, Y. A. Wang, Adsorption of small gas molecules onto Pt-doped single-walled carbon nanotubes," *J. Phys. Chem. C*, **112***,* 7401-7411 (2008).

[19] F. Villalpando-Páez, A. H. Romero, E. Muñoz-Sandoval, L. M. Martínez, H. Terrones, M. Terrones, "Fabrication of vapor and gas sensors using films of aligned CNx nanotubes," *Chem. Phys. Lett.* **386**, 137-143 (2004).

[20] B. Rebollo-Plata, E. Muñoz-Sandoval, F. López-Urías, E. L. Hernández-Cortina, H. Terrones, M. Terrones, "Efficient Vapor Sensors Using Foils of Dispersed Nitrogen-Doped and Pure Carbon Multiwalled Nanotubes," *J. of Nanosci and Nanotech*, **10**, 3965–3972 (2010).

[21] S. Peng, K. Cho, "Ab Initio Study of Doped Carbon Nanotube Sensors," *Nanolett,* **3**, 513-517 (2003)

[22] A. Zamudio, A. L. Elías, J. A. Rodríguez-Manzo, F. López-Urías, G. Rodríguez-Gattorno, F. Lupo, M. Rühle, D. J. Smith, H. Terrones, D. Díaz, M. Terrones, "Efficient Anchoring of Silver Nanoparticles on N-Doped Carbon Nanotubes," *Small*, **2**, 346 – 350 (2006).

[23] Y.-C. Tsai, P.-C. Hsua, Y.-W. Lin, T.-M. Wu, "Silver nanoparticles in multiwalled carbon nanotube–Nafion for surface-enhanced Raman scattering chemical sensor," *Sensors and Actuators B: Chemical,* **138**, 5-8 (2009).

[24] M. Sanles-Sobrido, L. Rodríguez-Lorenzo, S. Lorenzo-Abalde, A. Gonzalez-Fernandez, M. A. Correa-Duarte, R. A. Alvarez-Puebla, L. M. Liz-Marzán "Label-free SERS detection of relevant bioanalytes on silver-coated carbon nanotubes: The case of cocaine", *Nanoscale*, **1**, 153–158 (2009)

[25] W. Zhao, H. Wang, X. Qin, X. Wang, Z. Zhao, Z. Miao, L. Chen, M. Shan, Y. Fang, Q. Chen, "A novel nonenzymatic hydrogen peroxide sensor based on multi-wall carbon nanotube/silver nanoparticle nanohybrids modified gold electrode", *Talanta,* **80**, 1029-1033 (2009).

[26] N. Tanakaa, H. Nishikioria, S. Kubotaa, M. Endo, T. Fujii, "Photochemical deposition of Ag nanoparticles on multiwalled carbon nanotubes" *Carbon,* **47**, 2752-2754 (2009).

[27] Y. Lin, K. A. Watson, S. Ghose, J. G. Smith, Jr., T. V. Williams, R. E. Crooks, W. Cao, J. W. Connell, "Direct Mechanochemical Formation of Metal Nanoparticles on Carbon Nanotubes", *J. Phys. Chem. C,* **113** 14858–14862 (2009).

[28] Y.-C. Chen, R. J. Young, J. V. Macpherson, N. R. Wilson, "Single-Walled Carbon Nanotube Networks Decorated with Silver Nanoparticles", *J. Phys. Chem. C,* **111***,* 16167-16173 (2007).

[29] Y. Lin, K. A. Watson, M. J. Fallbach, S. Ghose, J.G. Smith, Jr. D. M. Delozier, W. Cao, R. E. Crooks, J. W. Connell, "Rapid, Solventless, Bulk Preparation of Metal Nanoparticle-Decorated Carbon Nanotubes", *ACSnano,* **3**, 871–884 (2009).

[30] S. K. Pandey, K.-H. Kim, "A Review of Methods for the Determination of Reduced Sulfur Compounds (RSCs) in Air" *Environ. Sci. Technol.* **43***,* 3020–3029 (2009).

[31] W. Wardencki, "Problems with the determination of environmental sulfur compounds by gas chromatography", *J. Chromatography A*, **793**, 1-19 (1998).

[32] Agency for Toxic Substances and Disease Registry. "Toxicological Profile for Carbon Disulfide", Department of Health and Human Services, Atlanta*, GA* (1996).

[33] Y. Xuan, J. Hu, K. Xu, X. Hou, Y. Lv, "Development of sensitive carbon disulfide sensor by using its cataluminescence on nanosized-CeO_2" *Sensors and Actuators B: Chemical*, **136**, 218-223 (2009).

[34] R. Czerw, M. Terrones,J.-C. Charlier,X. Blase,B. Foley,R. Kamalakaran, N. Grobert, H. Terrones, D. Tekleab, P. M. Ajayan, W. Blau,M. Ruhle, D. L. Carroll. "Identification of Electron Donor States in N-Doped Carbon Nanotubes", *NanoLett*, **1**, 457-460 (2001).

[35] M. Pinault, H. Mayne-L'Hermite, C. Reynaud, O. Beyssac, J.N. Rouzaud, C. Clinard, "Carbon nanotubes produced by aerosol pyrolysis: growth mechanisms and post-annealing effects", *Diamond Relat. Mater*, **13**, 1266-1269 (2004)

[36] M. Mayne, N. Grobert, M. Terrones, R. Kamalakaran, M. Rühle, H.W. Kroto, D. R. M. Walton, "Pyrolytic production of aligned carbon nanotubes from homogeneously dispersed benzene-based aerosols", *Chem. Phys. Lett.,* **338**, 101–107 (2001)

[37] P. Hohenberg, W. Kohn, Inhomogeneous Electron Gas, *Phys. Rev*. **136**, B864 (1964).

[38] W. Kohn, L. J. Sham, "Self-Consistent Equations Including Exchange and Correlation Effects", *Phys. Rev*, **140**, A1133 (1965).

[39] J.M. Soler, E. Artacho, J.D. Gale, A. García, J. Junquera, P. Ordejón, D.J. Sánchez-Portal, *" The SIESTA method for ab initio order-N materials simulation" Phys.: Condens. Matter*, 14, 2745 (2002)

Chapter 4 : Electronic Properties of Different Configuration of Nitrogen-Doped Carbon Nanotubes

4.1. Summary

The electronic properties of (10,0)-semiconducting single-walled carbon nanotubes (SWCNTs) containing structural defects such as vacancies (single and di-vacancies), and pyridinic Nitrogen atoms, are investigated using first-principles density functional theory. The band structure, electronic band gap, formation energy, structural relaxation, and HOMO-LUMO wave functions, were systematically calculated using various combinations of vacancies and nitrogen concentrations. It is found that depending on the concentration and location of Nitrogen atoms with respect to the vacancy-sites, semiconducting (10,0)-SWCNTs could become metallic. After relaxation, di-vacancies, with pyridine-like Nitrogen atoms, undergo a reconstruction so as to form pentagonal and octagonal rings in which Nitrogen behaves as a substitutional atom (not pyridinic) within the graphitic lattice. Interestingly, some Nitrogen doped configurations exhibit a *p-type* doping characteristics. The possibility of having *p-n* junctions in SWCNTs by doping with just one element as dopant is also discussed.

Chapter Content

Chapter 4 : Electronic Properties of Different Configuration of Nitrogen-Doped Carbon Nanotubes

4.1. Summary 71

4.2. Introduction: Electronic Properties of Nitrogen-Doped Carbon Nanotubes 73

4.3. Results and Discussion 78

4.4. Conclusions 93

4.5. References 94

4.2. Introduction: Electronic Properties of Nitrogen-Doped Carbon Nanotubes

The study and control of defects on doped carbon nanotubes is of technological relevance because during synthesis, different types of defects could result (intentionally or unintentionally) within the structures. Nowadays, it has been found that the addition of different elements such as nitrogen [1,2], phosphorous [3,4], or sulfur [5], results in the chemical modification of carbon nanotubes, as well as changes in their electronic and mechanical properties. Depending on the foreign atom (dopant), it is possible to observe different tubular morphologies. For example, bamboo-type morphologies could be generated in the presence of nitrogen [6], and Y-junctions could be produced when S is present in the synthesis [5]. These and others nanotube architectures have attracted the attention of numerous researchers because of the possibility of tailoring their band gap. Therefore, it is essential to understand the role and dynamics of the chemical dopants and defects when embedded in the lattice of carbon nanotubes. During the first analysis and theoretical study of N-doped carbon nanotubes (CN_X-MWCNTs) reported by Czerw *et al.* [6], it was found that the nitrogen atom exhibited two types of chemical bonding: 1) *substitutional* when the nitrogen atom replaces a C atom in the hexagonal carbon lattice (N bonded to three carbon atoms), and 2) *pyridine-like* in which a N atom is only bonded to two carbon atoms in vacancy locations generated in the hexagonal tubular lattice. The triple pyridine-like model proposed by Czerw *et al.* [6] consisted of a vacancy embedded in the carbon nanotube surrounded by three nitrogen atoms with double coordination to the C atoms, a schematic diagram is depicted in figure 4-1(a-b).

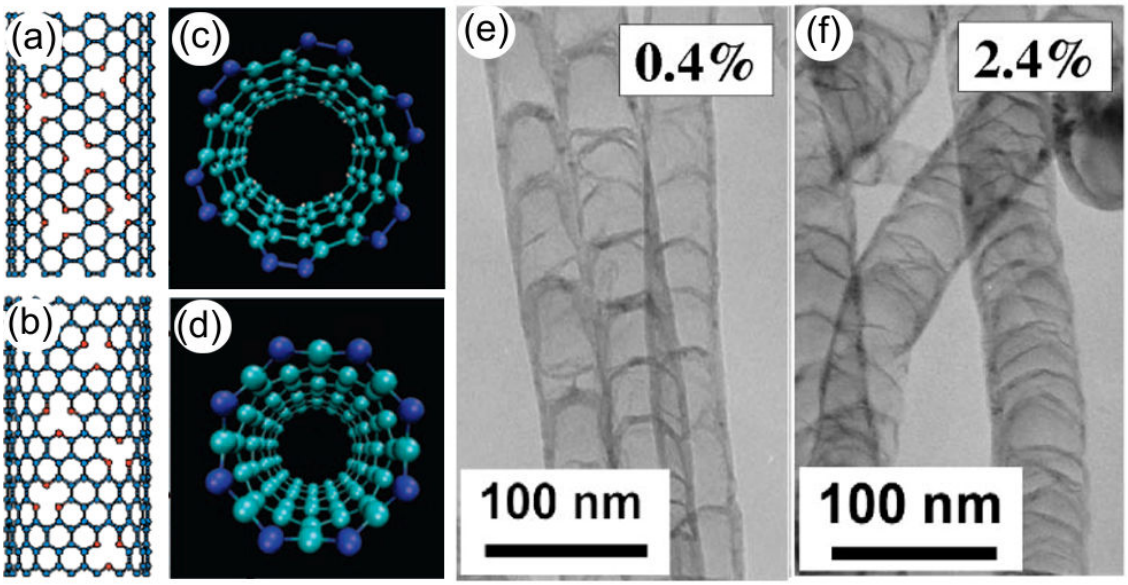

Figure 4-1: Structure of nitrogen-doped carbon nanotubes. **(a)-(b)** Pyridinic-like structure of armchair and zig-zag nanotubes [6]. **(c)-(d)** Nitrogen rings located at the tip of the nanotube may be the responsible for closing the tubular structure, thus generating the so-called "bamboo-like" structure [1]. **(e)-(f)** Shows TEM images of nitrogen-doped nanotubes, the compartment (bamboo-like) structures dependent on the nitrogen concentration. the compartment distance of the CN_X-MWCNTs decreases with increasing nitrogen concentration [7].

Nitrogen rings located at the tip of the nanotube have been suggested to be the responsible for closing the tubular structure, thus generating the so-called "bamboo-like" structure [1] (see figure 4-1(c-d). These compartments increase at higher nitrogen concentration; figure 4-1(e-f) depicts TEM images of CN_X-MWCNTs where is observed the differences between two nitrogen concentrations [7]. Using tight binding calculations the authors determined that N-doping was responsible for the metallic behavior by the addition of electronic states at the Fermi level. In addition, they reported experimental evidence indicating that N-doping islands exhibited strong electron donor states near the Fermi level and proposed that all N-doped

nanotubes needed to be metallic [8,9]. Generally speaking, when doping occurs within a carbon nanotube, shifts in the Fermi energy are observed and the sites could enhance its chemical activity [10,11]. The induced electronic states in the vicinity of the Fermi energy and therefore, the transport properties of doped-nanotubes are sensitive not only to the concentration of nitrogen atoms, but also to their distribution and nanotube chirality [12,13].

Effect of nitrogen-vacancy on the transport properties of single-walled carbon nanotubes (SWCNTs) study was performed by Wei *et al.* [14]. They demonstrated that one vacancy with one or three N-atoms on the metallic (4,4) and semiconducting (8,0) carbon nanotubes generates a half-filled impurity band, which is favorable to the transport of semiconducting nanotubes but not favorable for metallic one. Transport properties studies of substitutional nitrogen doping on zigzag and armchair nanotubes were reported by Kaun *et al.* [15]. They found that for (7,0) zigzag semiconducting nanotube, doping with a single N impurity increases current flow and for a (10,10) armchair metallic nanotube, a reduction of current is observed with substitutional doping due to elastic backscattering by the impurity. Also, substitutional nitrogen-doping and nitrogen adatom impurity via N_2 molecules effect on the electronic and magnetic properties of graphite and carbon nanotubes were studied by Ma *et al.* [16]. They found that N adatom forms a bridge-like structure on the nanotube surface. Experimental and theoretical calculations on electrical transport characteristics of nitrogen-doped single-walled carbon nanotubes, N-doped SWCNTs, were performed by Min *et al.* [17]. They found that contrary to the expectation that the nitrogen atoms may induce *n-type* doping, the electrical transports through the N-doped SWCNTs are either ambipolar in vacuum or *p-type* in air. Their first-principles electronic structure calculations on the nitrogen-doped

semiconducting (10,0) nanotubes demonstrated that the nitrogen dopant indeed favors the pyridine-like configuration and the Fermi level of the pyridine-like N-doped SWCNT is almost at the intrinsic level. Recent first-principles density functional calculations performed by Fujimoto *et al.* [18] demonstrated that the pyridine-type defects in the nitrogen-doped (10,0) carbon nanotube are energetically preferred to the substitutional nitrogen defect under the existence of the vacancy in the nanotube. They also found that pyridine-type defects promote localized states near the valence-band, which acts as an acceptor state. Other studies have demonstrated the possibility of controlling the nanotube growth and simultaneously the nanotube properties by adding nitrogen, phosphorus, and sulfur atoms in small concentrations were performed by Sumpter *et al.* [19]. Also, studies on the adsorption of metal atoms or molecules on a graphite 0001 [20], graphene [21], nanotubes [22] surface with defects and nitrogen-doping have been reported as well as the influence of the nitrogen doping on the radial breathing mode in carbon nanotubes [23]. In the mentioned studies above, the nitrogen-doping on graphite or carbon nanotubes was generally introduced via substitutional, triple pyridine-like or four-nitrogen atoms by generating one or two vacancies respectively.

Additional to these nitrogen-doping fashions, in this chapter, we have investigated new different ways of nitrogen doping on carbon nanotubes. One and two adjacent vacancies were introduced in a semiconducting (10,0) carbon nanotube lattice and all possibilities were explored by replacing systematically low-coordinated carbon atoms (C-atoms surrounded the vacancy) by nitrogen atoms. The density functional theory (DFT) in conjunction with the local density approximation has been used to predict the structure, formation energy, and the electronic properties of these doped systems. We found that the electronic properties are very sensitive to the

nitrogen concentration, its configuration and the number of vacancies introduced in the systems. In addition, the carbon nanotubes tend to avoid dangling bonds and its surface self reconstructs.

4.3. Results and Discussion

4.3.1. *Relaxed Geometries and Electronic Properties of Nitrogen-doped (10,0) Single-Walled Carbon Nanotubes: One vacancy case*

Firstly, we focus on the introduction of a single vacancy in a (10,0) semiconductor carbon nanotube, and the different ways of accommodating one or two N atoms around the vacancy. The electronic calculations were performed using Density Functional Theory [24,25] within the Local Density Approximation (DFT-LDA) as implemented in the SIESTA code [26]. The systems were constructed by using a supercell of 160 atoms taking 4 unit cell of a (10,0) nanotube. All nanotubes were relaxed by conjugate gradient minimization until the maximum force was less than 0.04 eV/Å. For further information please see Apendix A.

Figure 4-2 depicts all the non-equivalent geometries of the (10,0) carbon nanotube generated by removing a carbon atom (creating one vacancy), and replacing the low coordination carbon atom by nitrogen atoms. The unrelaxed system is shown in figure 4-2a, which corresponds to the starting geometry used in our calculations. The A, B and C labels in figure 4-2a represent the type of site; notice that sites A and C are equivalent. In order to dope carbon nanotubes, we have removed one or more carbon atoms located at sites A, B, and C, and replaced them by nitrogen atoms. For an individual nitrogen atom, we have two non-equivalent configurations as shown in figure 4-2b and 4-2c. In this case, the nitrogen atom was either located in site B (V_1N_1B configuration) or in site C (V_1N_1C configuration). It should be noted that the configuration V_1N_1A is equivalent to the configuration V_1N_1C.

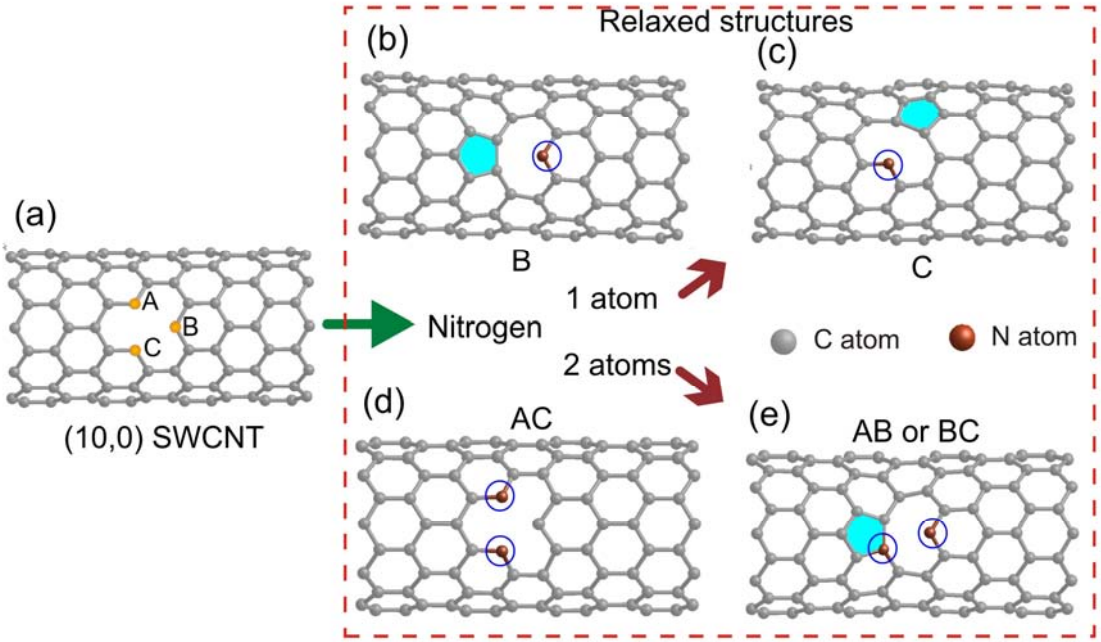

Figure 4-2: Molecular models depicting: **(a)** The starting geometry of the single-walled carbon nanotube (SWCNT) of (10,0) chirality with one vacancy, **(b)** and **(c)** relaxed structures when the carbon atom is replaced by a nitrogen atom in site B (V_1N_1B) and C (V_1N_1C) respectively. The cases of two nitrogen atoms replacing the carbon atoms are shown in **(d)** V_1N_2AC and **(e)** V_1N_2BC configuration. The case shown in (e) has two equivalent configurations. All the relaxed structures have at least one pyridine-like site.

After structural relaxation, significant structural changes were observed: In both cases, one pentagonal ring appears (in front of the nitrogen atom), and the nitrogen atom remains with a pyridine-like structure. Similar V_1N_1B structure was obtained in Ref. [18]. For two nitrogen atoms introduced in the vacancy, we have two different configurations (see figure 4-2d, and 4-2e). When the nitrogen atoms are located in sites A and C (V_1N_2AC configuration), the carbon nanotube keeps the original morphological structure with slight changes in the inter-atomic distances for atoms surrounding the vacancy (see figure 4-4d), and the two nitrogen atoms

remain doubly coordinated. However, if the two nitrogen atoms are incorporated to the system and located in sites B and C (V_1N_2BC configuration, which is equivalent to the configuration AB (V_1N_2AB)), the formation of a pentagonal ring is again observed with a triply-coordinated nitrogen atom, and the other nitrogen atom remains doubly-coordinated (pyridine-like). This result is in according to previous calculations [18]. Notice that this structure is similar to that obtained for an individual nitrogen case shown in figure 4-2b (V_1N_1B configuration). However, the electronic properties of these systems are completely different as discussed below. We have also studied the nitrogen pyridine-like V_1N_3ABC, substitutional doping (without vacancy) V_0N_1, and one vacancy (without doping) V_1N_0 cases. In general, we observed that the introduction of one vacancy with or without pyridine-like nitrogen atoms makes it difficult to have a self-reconstruction of the nanotube surface. Kotakoski *et al.* [27] studied the role of vacancies in undoped carbon nanotubes. These authors used a nonorthogonal density-functional-theory-based tight-binding model, and removed 1-6 carbon atoms from the carbon nanotubes. They demonstrated that the formation energies of small vacancy clusters from single vacancies are energetically more favorable in comparison to large “holes”. Another recent study on multi-vacancies in undoped carbon nanotubes demonstrated that the formation of pentagons eliminates the dangling bonds thus lowering the formation energy [28]. Regarding nitrogen-doped nanotubes, Yu *et al.* [29] reported using *ab initio* density functional theory calculations the effects of substitutional doping nitrogen atoms on the structure and electronic properties of zigzag carbon nanotubes. They introduced two nitrogen atoms in the nanotube lattice and demonstrated that the electronic properties depend on the sites that the two nitrogen atoms occupy in the hexagons.

The band structure and wave functions at the Γ-point for the top valence (HOMO: the highest occupied molecular orbital) and lowest conduction band (LUMO: the lowest unoccupied molecular orbital) are shown in figure 4-3 (the corresponding relaxed structures can be seen in figure 4-2). Calculations on the nanotube (10,0) without defects or dopants demonstrate that it exhibits a semiconducting behavior with an electronic band gap (Eg) of 0.754 eV in according with previous calculations [18,30].

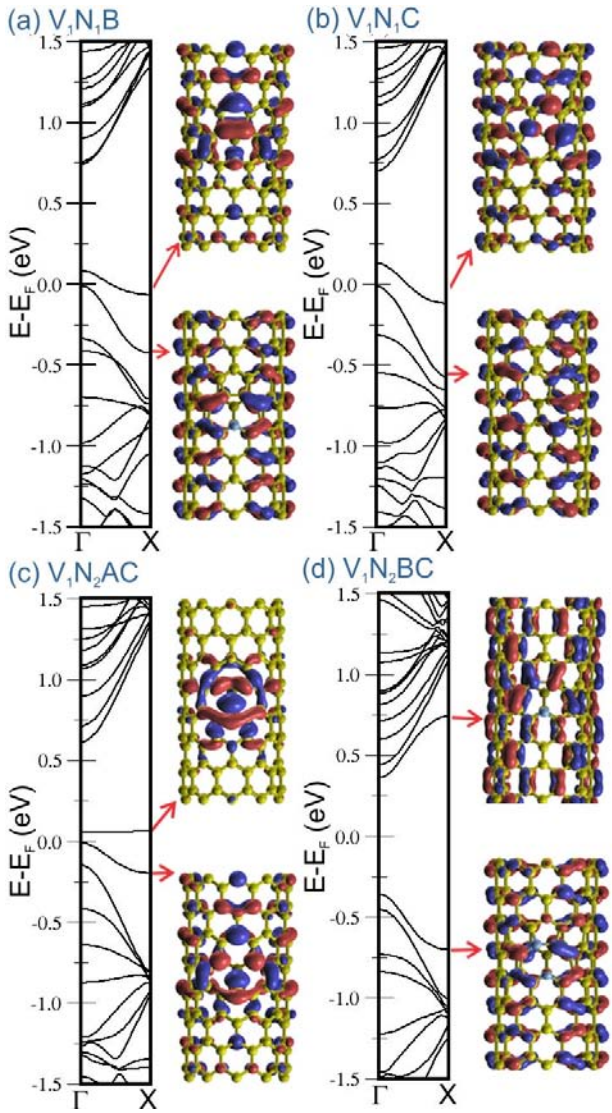

Figure 4-3: Electronic band structure of the relaxed (10,0) single-walled carbon nanotubes containing one vacancy and one or two nitrogen atoms. In all cases, the Fermi level is set to zero. The cases **(a)** V_1N_1B and **(b)** V_1N_1C correspond to one-nitrogen systems whose structures are shown in figure 4-2b and c, respectively; these systems exhibit a metallic behavior and a *p-type* doping. The cases shown in **(c)** and **(d)** correspond to the V_1N_2AC and V_1N_2BC configurations (two nitrogen atoms), respectively. The corresponding relaxed geometries can be seen in figure 4-2d and e. The V_1N_2AC system exhibits a small band gap and a *p-type* doping, whereas the V_1N_2BC system shows a band gap similar to the pristine tube. In all cases, the wave functions are plotted at the gamma point with an isosurface value of ±0.05 $Å^{-3/2}$.

If a nitrogen atom is introduced in the nanotube lattice as depicted in figures 4-2b and 4-2c (V_1N_1B and V_1N_1C configurations), the Fermi energy (which is located at zero) is shifted towards the valence band, see figure 4-3a and 4-3b, showing a metallic behavior with a partially filled band. The wave functions for these structures are also shown in figure 4-3; in both cases the LUMO wave function exhibits states mainly located in the pentagonal ring, being most localized for the V_1N_1B configuration, whereas the HOMO wave function exhibits states along of the entire body of the carbon nanotube in both structures. Opposite results were obtained for two nitrogen atoms; the V_1N_2AC configuration exhibits a small electronic band gap (0.064 eV), and the Fermi energy is shifted close to the valence band showing a *p-type* doping (see figure 4-3c). The corresponding LUMO wave function exhibits highly localized states near the vacancy and nitrogen atoms (non dispersive band). In addition, the HOMO wave function exhibits localized states in the vicinity of the vacancy defect. The V_1N_2BC system shows an Eg equal to 0.723 eV, which is slightly reduced when compared to the pristine nanotube (see figure 4-3d). Note that all systems presented in figure 4-3 exhibit significant changes around of the Fermi level, however, far away from the Fermi level the bands remain almost similar, independently of defects or doping concentration.

4.3.2. Relaxed Geometries and Electronic Properties of N-doped (10,0) Single-Walled Carbon Nanotube: Two vacancies case

The case for two vacancies and two nitrogen atoms systems is shown in figure 4-4. It is important to mention that the vacancies were generated by removing two adjacent carbon atoms (di-vacancy) along the tube axis (see figure 4-4a). The initial configuration (figure 4-4a: not relaxed geometry) provides four options (site A, B, C, or D) in which nitrogen atoms could replace the carbon atoms.

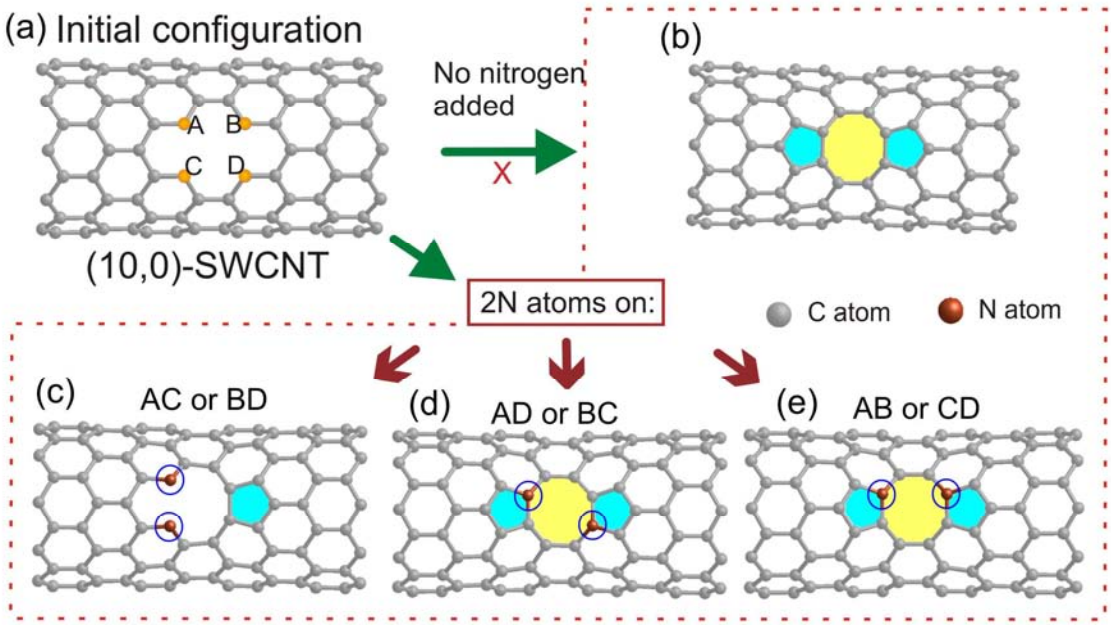

Figure 4-4: Molecular models showing: **(a)** The starting and **(b)** relaxed geometries of the single-walled carbon nanotube (SWCNT) exhibiting the (10,0) chirality with two vacancies. The relaxed structures of the three non-equivalent cases of accommodating two nitrogen atoms are shown in **(c)** V_2N_2AC, **(d)** V_2N_2AD, and **(e)** V_2N_2AB. Note that for the case shown in **(c)**, the nitrogen atoms remain as a pyridinic type, whereas for **(d)** and **(e)**, the N-atoms adopt three nearest neighbors (substitutional-like behavior).

After geometry relaxation, it was observed a reduction in diameter of the tube around the vacancy defect. For the relaxed structure with only two vacancies, V_2N_0 configuration (without nitrogen), the carbon nanotube healed its surface, by forming two pentagonal and one octagonal rings (5-8-5 defect) in order to avoid dangling bonds (see figure 4-4b). The octagonal ring creates a saddle point in the structure and in consequence local negative Gaussian curvature is observed. In this region, the nanotube diameter is reduced. *Ab initio* calculations performed by Amorim *et al.* [31] reported a study on the role of divacancies in the transport properties of carbon nanotubes. They also demonstrated that the 5-8-5 defects are energetically favorable for a large range of nanotube diameters. By introducing two nitrogen atoms, there are three non-equivalent configurations (see figure 4-4c, d, and e). When nitrogen atoms were located in site AC or equivalently BD (V_2N_2AC configuration), the resulting relaxed structure exhibits a pentagonal ring, which contains only carbon atoms. The two nitrogen atoms remain with a pyridine-like configuration, thus avoiding the closure of the local structure (see figure 4-4c). However, if the two nitrogen atoms are located in sites A and D (V_2N_2AD configuration), which is equivalent to the V_2N_2BC configuration, the resulting structure exhibits a 5-8-5 defect (pentagonal-octagonal-pentagonal rings), see figure 4-4d. Similar results have been obtained when nitrogen atoms are placed in sites A and B sites (V_2N_2AB or equivalently V_2N_2CD configuration). We have also studied the divacancy containing four nitrogen atoms occupying the A, B, C, and D sites (see figure 4-4a, configuration V_2N_4ABCD). After geometry relaxation non-important changes on the structure of the carbon nanotube were observed in according with previous calculations [22,32].

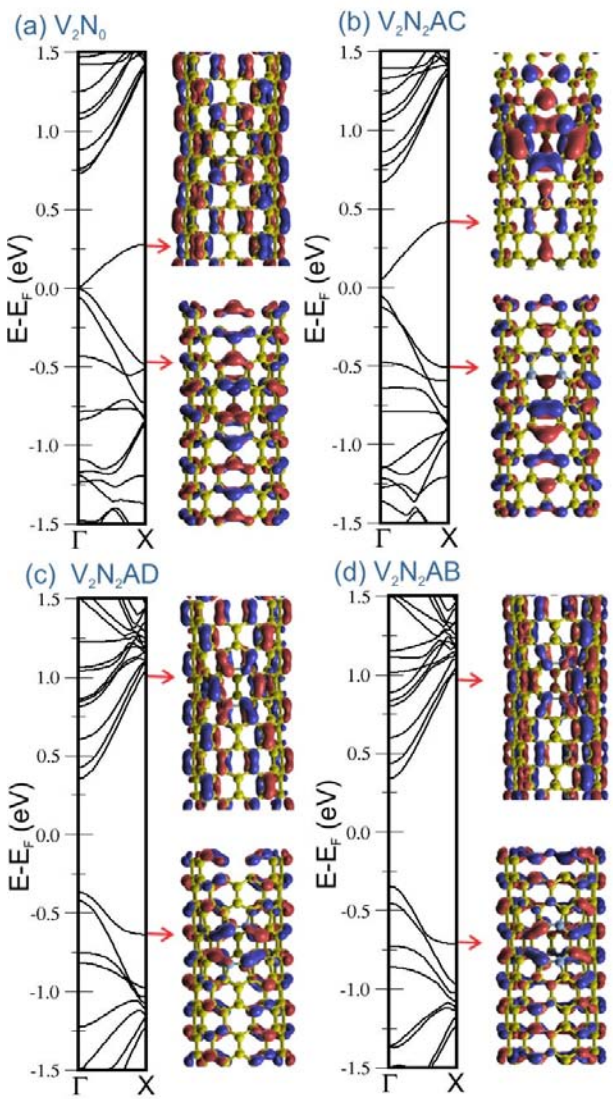

Figure 4-5: Electronic band structure of the relaxed (10,0)-SWCNT containing two vacancies. In all cases, the Fermi level is set to zero. The frame shown in **(a)** corresponds to the case without nitrogen, where the Fermi energy has been shifted to the valence band, exhibiting a very small band gap (0.012 eV). Frames **(b)**, **(c)**, and **(d)** correspond to two nitrogen system whose structures are shown in figure 4-4 c, d and e, respectively. For V_2N_2AC, the structure exhibits a small band gap of 0.106 eV and a *p-type* characteristic. For the last two cases (V_2N_2AD and V_2N_2AB configurations), similar band structures and band gaps are obtained when compared to the pristine carbon tubule. In all cases, the wave functions were plotted at gamma point with an isosurface value of ±0.05 $Å^{-3/2}$.

Figure 4-5 depicts results on the band structure and HOMO and LUMO wave function plots for the different systems shown in figure 4-4. The nanotube with two adjacent vacancies, V_2N_0 (without nitrogen) exhibits a small band gap (0.012 eV) and its corresponding wave functions displays states distributed along the nanotube waist (see figure 4-5a). The cases concerning the introduction of two nitrogen atoms in non-equivalent sites are shown in figures 4-5 b-d. For the system exhibiting a V_2N_2AC configuration, the Fermi energy (located at zero) has been shifted to the valence band and they exhibit a small Eg equal to 0.106 eV (figure 4-5b). The wave function of

V_2N_2AC configuration exhibits localized states in the atoms surrounding the nitrogen atoms and the pentagonal ring (see figure 4-5b). However, for the V_2N_2AD and V_2N_2AB configurations, the carbon nanotube exhibits a semiconductor behavior with an electronic band gap of 0.719 and 0.685 eV, respectively. Both configurations exhibit wave functions with states distributed on the entire nanotube lattice (see figure 4-5 c and d).

In order to understand the corrugation effect and the diameter variation due to the presence of vacancies and nitrogen doping, we analyzed five representative cases (see figure 4-6). The nanotube diameters experience a diameter reduction at the vacancy followed by a slight increase near to the defect, thus resulting in corrugation. We have also observed that the diameter reduction significantly depends of the position and concentration of the dopant atoms.

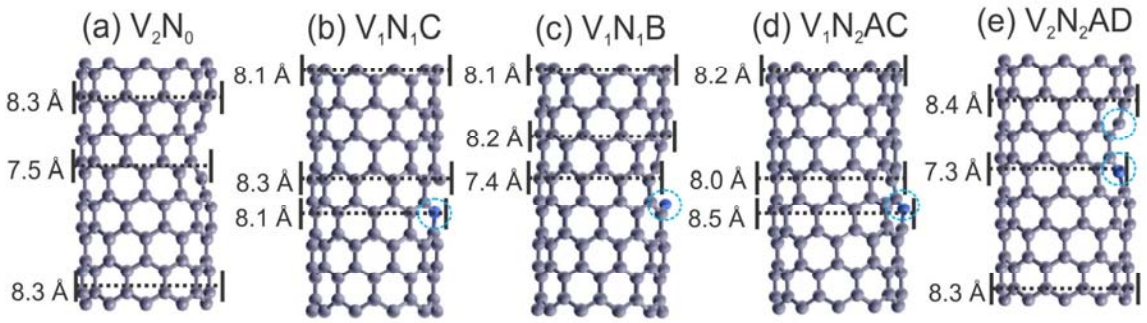

Figure 4-6: Molecular models showing the diameter variations generated by vacancies and nitrogen doping in a (10,0) carbon nanotube. Side views images reveal the diameter variation along the nanotube axis for different representative cases: **(a)** Two vacancies without nitrogen (V_2N_0), **(b)** V_1N_1C, **(c)** V_1N_1B, **(d)** V_1N_2AC, and **(f)** V_2N_2AD. The nitrogen atoms are indicated by the open cycles. In **(b)** the diameter is slightly varied, but for **(c)**, **(d)**, and **(f)**, it is observed a difference of ~0.8 Å between the larger and smaller diameters, these values are similar to the V_2N_0 case. These changes in diameter result in corrugated surfaces, characteristics of the nitrogen-doped nanotubes. It is important to mention that the diameter of a pristine (undoped and without vacancies) (10,0) carbon nanotubes is around 7.99 Å.

In addition, we studied two more configurations for two vacancies with one and three nitrogen atoms (V_2N_1C and V_2N_3ABD); the different site types can be seen in figure 4-4a. The relaxed structures and the band structure calculations are shown in figure 4-7. The system corresponding to the V_2N_1C exhibits 5-8-5 defects (see figure 4-7a), similar to nanotubes with only two vacancies and without nitrogen doping (see configuration V_2N_0 in figure 4-7b), this vacancy-nitrogen system also exhibit a *p-type* behavior, see figure 4-7b. The relaxed structure corresponding to V_2N_3ABD exhibits only one pentagonal ring, which contains a nitrogen atom; the other two nitrogen atoms remain as pyridine-like sites (see figure 4-7c) and the corresponding band structure can be seen in figure 4-7d. Here, a *p-type* behavior was also observed. Both configurations (V_2N_1C and V_2N_3ABD) exhibit a diameter variation of ~1 Å near the defective region.

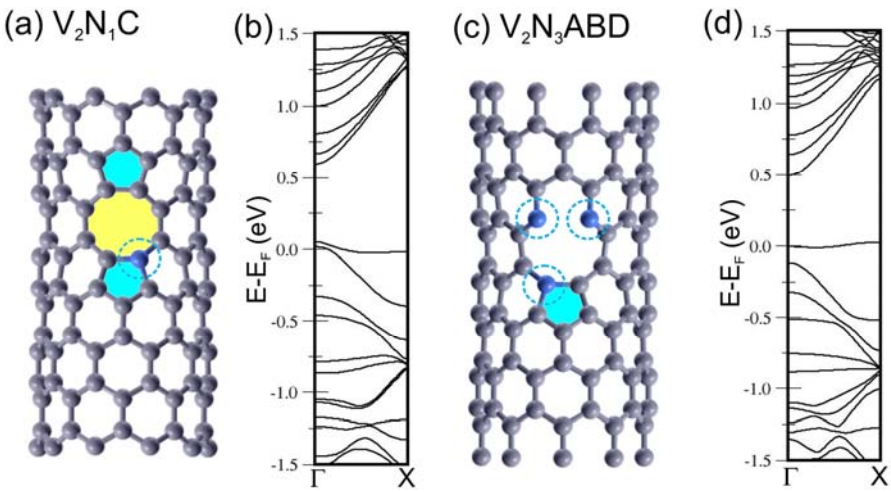

Figure 4-7: (a) Relaxed geometry obtained by introducing two vacancies and one nitrogen atom (configuration V_2N_1C) into the (10,0) carbon nanotube. Note that the final structure exhibits a 5-8-5 defect; the corresponding band structure is shown in **(b)**. **(c)** Relaxed structure obtained by introducing two vacancies and three nitrogen atoms (configuration V_2N_3ABD) into the (10,0) carbon nanotube. This structure exhibits a pentagonal ring defect, and the corresponding band structure calculations are shown **(d)**. In both cases, the Fermi level shifted to the valence band, thus exhibiting a *p-type* doping behavior, and localized states at the Fermi level. The open circles indicate the position of the nitrogen atoms.

4.3.3. Energetic Stability of Nitrogen-doped (10,0) Single-Walled Carbon Nanotube with Different Doping Configurations

As we have observed from our results, various pyridine-like N-doped (10,0)-SWCNTs configurations exhibit a *p-type* doping behavior (electron acceptor), contrary to our expectations, in which the nitrogen-dopant within carbon nanotubes causes *n-type* doping behavior (electron donor). We have observed a *p-type* behavior in the systems corresponding to the V_1N_1B, V_1N_1C, V_1N_2AC, V_1N_3ABC, V_2N_1C, and V_2N_3ABD, and V_2N_4ABCD configurations. Our results are in agreement with previous reports indicating that pyridine-like configurations exhibit a *p-type* doping nature [8,30,32]. In addition, experimental electrical-transport measurements on metallic nitrogen-doped SWNTs have shown both *p-* and *n-type* doping characteristics [17,33].

Figure 4-8a shows the formation energy (see Appendix A) of all studied configurations, and figure 4-8b depicts the electronic band gaps (Eg) of the corresponding configurations. In figure 4-8a, the energies were referred to the pristine nanotube (undoped and without vacancies). It is interesting to observe that generally the role of nitrogen doping in the carbon nanotubes with one or two vacancies is reduce the formation energy. In most cases, the undoped configurations V_2N_0 and V_1N_0 exhibit higher energy than its corresponding doping cases. In figure 4-8a, we observe that next to the pristine tube, the most stable configuration is the V_0N_1 system (substitutional doping) followed by the nanotube with four-nitrogen divacancy (V_2N_4ABCD). Similar trend was reported by Li *et al.* [32] by using density functional calculations and DMOL package. In addition, they investigated these defects as a function of the nanotube chirality, showing that these are more stable in armchair nanotubes.

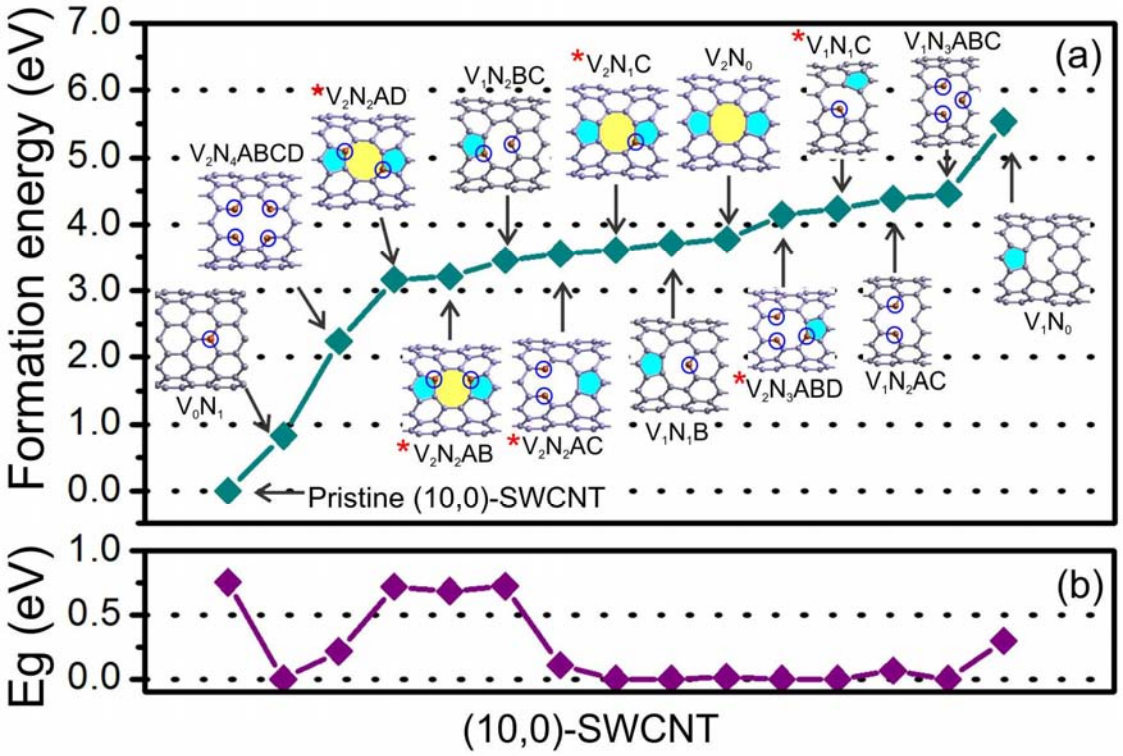

Figure 4-8: **(a)** Formation energy (see Appendix A) of the (10,0) single walled carbon nanotubes (SWCNTs) by considering different ways of introducing nitrogen atoms and vacancies (all structures were relaxed). The circles indicate the nitrogen atoms and all energies are referred to the pristine (10,0) nanotube (undoped and without vacancies). The attached symbol (*) corresponds to new N-doped configurations. The most stable doped nanotube corresponds to the substitutional nitrogen doping V_0N_1 configuration followed by the V_2N_4ABCD configuration. Notice that the less stable configuration correspond to the one-vacancy nanotube without nitrogen (V_1N_0). The corresponding electronic band gaps (Eg) are shown in **(b)**. Notice that the modified (10,0)-SWCNTs exhibits a reduced Eg, which become metallic in some cases.

In figure 4-8a, several configurations were observed in the range of 3 to 5 eV; here some structures experience self-surface reconstruction favoring the formation of pentagonal and octagonal membered rings. In this energy range, it is also observed that nanotubes doped with two nitrogen atoms exhibit a maximal electronic band gap (see configurations V_2N_2AD, V_2N_2AB, V_1N_2BC in figure 4-8b). Notice that the canonical configuration (three nitrogen atoms occupying the pyridine-like sites, V_1N_3ABC), one of the most

studied cases in the literature, is the less stable doped system. A comparison between our work and previous reported works on the formation energy of five types of defects can be seen in table 4-1, showing that in most cases, our formation energies are in according with previous calculations.

Table 4-1: Comparison of the formation energy (E_{form}) of some defects in the (10,0) semiconductor single walled carbon nanotube calculated in our work (bold face values) and previous reported works from other groups. The different defects correspond to: one vacancy (V_1N_0), divacancy (V_2N_0), substitutional nitrogen doping (V_0N_1), three nitrogen atoms in a pyridine-like island (V_1N_3ABC), and four nitrogen atoms and double vacancy (V_2N_4ABCD).

Type of defect	E_{form} (eV)
V_1N_0	**5.53**, 5.62[34]
V_2N_0	**3.77**, 3.9[31]
V_0N_1	**0.83**, 1.04[32], 0.93[30], 1.78[11], 4.8[29]
V_1N_3ABC	**4.46**, 2.16[18], 6.46[11],4.02[30], 2.99[32]
V_2N_4ABCD	**2.24**, 2.58[32], 2.87[22]

However, little is known about chemical reactivity of the configurations shown in figure 4-8a, and therefore additional theoretical and experimental studies are needed in order to understand the capacity of nitrogen-doped carbon nanotubes for adsorbing different molecules and atoms. Along this direction, Zhao *et al.* [22] studied the hydrogen adsorption on calcium dispersed in the V_2N_4ABCD structure. The authors suggested that up to five H_2 molecules could be bound per calcium atom.

Finally, as we have mentioned above, by a selective introduction of nitrogen atoms and vacancies to a (10,0) carbon nanotube, it is possible to tune its electronic properties. In this sense, it is probable to build a *p-n* junction made of N-doped nanotubes. Figure 4-9 depicts a *p-n* junction made entirely with

one dopant within a (10,0) carbon nanotube. We have simultaneously introduced two different types of defects that modify the electronic properties of the (10,0) carbon nanotube in opposite ways.

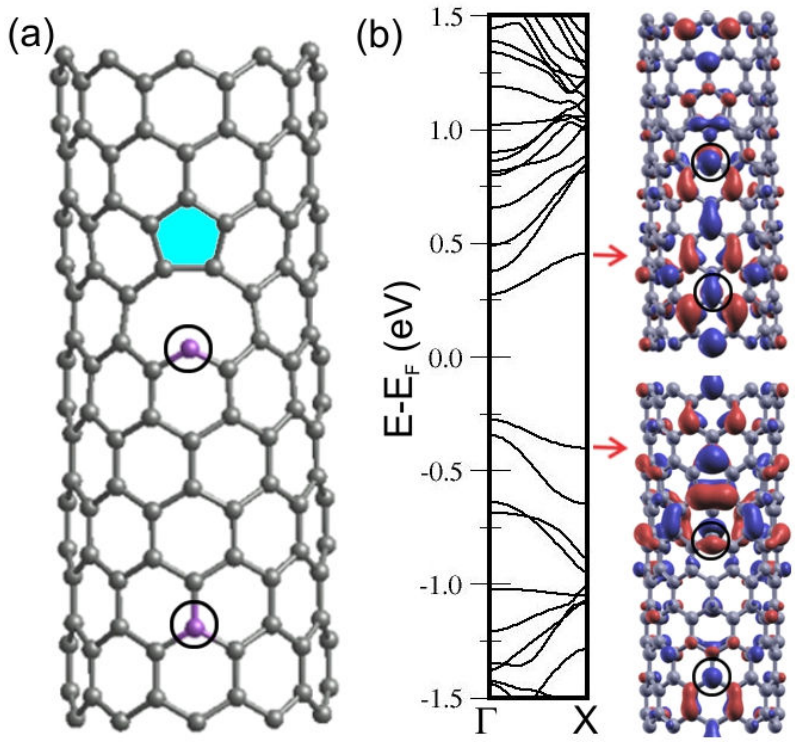

Figure 4-9: (a) Relaxed geometry of the (10,0) carbon nanotube by simultaneously introducing one nitrogen atom in a substitutional fashion (V_0N_1) and a V_1N_1B defect (such defects generate negatively and positively doped materials, respectively; the open circles illustrate the position of the nitrogen atoms). **(b)** Band structure and the corresponding HOMO and LUMO wave functions for the structure shown in **(a)**. For the band structure, the Fermi level is set to zero. The tube exhibits semiconductor properties with a band gap equal to 0.55 eV and formation energy of 3.41 eV. The wave functions are plotted at the gamma point (isosurface value of ±0.05 $Å^{-3/2}$). It is observed that the HOMO is located near the V_1N_1B defect, whereas the LUMO is mainly situated at the substitutional nitrogen atom.

First, we added one nitrogen atom in a substitutional fashion (which creates a negative doped semiconductor material) followed by the addition of a V_1N_1B defect (which generates a positively doped material, as is determined

in figure 4-3a). The resulting geometry is shown in figure 4-9a. The band structure is depicted in figure 4-9b, where the Fermi level is set to zero; we observed that the resulting material shows semiconductor properties with a band gap equal to 0.55 eV which is less than the band gap of the substitutional case (0.76 eV). The wave functions of the HOMO and LUMO are also shown in figure 4-9b, and it is observed that the HOMO is located near the V_1N_1B defect, while the LUMO is mainly situated at the substitutional nitrogen atom. This substitutional V_1N_1B defect exhibits a formation energy of 3.41 eV, which is higher than the formation energy of the isolated substitutional case, but lower than the isolated V_1N_1B case. The competitive formation energy and the interesting electronic properties obtained for this specific case (substititutional-V_1N_1B defect on the (10,0) carbon nanotube), open a theoretical and experimental challenge to tailor or improve the physical-chemical properties of carbon nanotubes by controlling and combining simultaneously two or more different ways of doping.

4.4. Conclusions

The combined effect of nitrogen doping and vacancy defects were studied in semiconductor (10,0) SWCNTs using first principle calculations. For different cases, the relative stability and the band structures were calculated. Our results demonstrated that the (10,0) semiconductor nanotube could exhibit metallicity depending on the position of the nitrogen atoms along the nanotube structure. When one vacancy and one nitrogen atom are introduced within the nanotube, the surface remains open (holey), and the bands cross the Fermi level, thus indicating metallicity. It has also been observed that one vacancy with two nitrogen atoms embedded symmetrically, exhibits a non dispersive conduction band which results in a LUMO-wave function with localized states in the defective region. In general, when two vacancies were introduced, the systems surface self-reconstructs, preserving the semiconducting feature with a reduction of the electronic band gap. All energies associated with the different systems are less stable than the pristine the (10,0) nanotube. However, we found that pyridine-like doping with three double coordinated nitrogen atoms surrounding a vacancy (V_1N_3ABC), exhibits higher formation energy than the cases with one, two and four nitrogen atoms in a pyridine-like fashion.

4.5. References

[1] B. G. Sumpter, V. Meunier, J. -M. Romo-Herrera, E. Cruz-Silva, D. A. Cullen, H. Terrones, D. J. Smith, M. Terrones," Nitrogen-Mediated Carbon Nanotube Growth: Diameter Reduction, Metallicity, Bundle Dispersability, and Bamboo-like Structure Formation" *ACS Nano* **1**, 369 (2007)

[2] C.P. Ewels, M. Glerup, "Nitrogen Doping in Carbon Nanotubes", *J. Nanosci. and Nanotech*. **5**, 1345 (2005)

[3] E. Cruz-Silva, D. A. Cullen, L. Gu, J. M. Romo-Herrera, E. Muñoz-Sandoval, F. López-Urías, B. G. Sumpter, V. Meunier, J. C. Charlier, D. J. Smith, H. Terrones, M. Terrones, "Heterodoped Nanotubes: Theory, Synthesis, and Characterization of Phosphorus−Nitrogen Doped Multiwalled Carbon Nanotubes" *ACS Nano* **2**, 441 (2008)

[4] A. Chen, Q. Y. Shao, Z. C. Lin, "Effects of phosphorus-doping upon the electronic structures of single wall carbon nanotubes" *Sci China Ser G-Phys Mech Astron*, **52**, 1139 (2009).

[5] J. M. Romo-Herrera, B. G. Sumpter, D. A. Cullen, H. Terrones, E. Cruz-Silva, D. J. Smith, V. Meunier, M. Terrones," An atomistic branching mechanism for carbon nanotubes: Sulfur as the triggering agent" *Angew Chem. Int Ed,* **47**, 2948 (2008)

[6] R. Czerw, M. Terrones, J. C. Charlier, X. Blase, B. Foley, R. Kamalakaran, N. Grobert, H. Terrones, D. Tekleab, P. M. Ajayan, W. Blau, M. Rühle, D. L. Carroll," Identification of Electron Donor States in N-Doped Carbon Nanotubes" *Nano Lett.* **1**, 457 (2001)

[7] J. W. Jang, C. E. Lee, S. C. Lyu, T. J. Lee, C. J. Lee, "Structural study of nitrogen-doping effects in bamboo-shaped multiwalled carbon nanotubes", *Appl. Phys. Lett*., **84**, 2877-2879 (2004)

[8] M. Terrones, A. Jorio, M. Endo, A. M. Rao, Y. A. Kim, T. Hayashi, H. Terrones, J. C. Charlier, G. Dresselhaus, M. S. Dresselhaus," New direction in nanotube science" *Mater. Today,* **7**, 30 (2004)

[9] M. Terrones, P. M. Ajayan, F. Banhart, X. Blase, D. L. Carroll, J. C. Charlier, R. Czerw, B. Foley, N. Grobert, R. Kamalakaran, P. Kohler-Redlich, M. Rühle, T. Seeger, H. Terrones," N-doping and coalescence of carbon nanotubes: synthesis and electronic properties" *Appl. Phys. A,* **74**, 355 (2002)

[10] M.U. Kahaly, "Defect states in carbon nanotubes and related band structure engineering: A first-principles study" *J. Appl. Phys.* ***1*05**, 024312 (2009)

[11] S. H. Lim, R. Li, W. Ji, J. Lin," Effects of nitrogenation on single-walled carbon nanotubes within density functional theory" *Phys. Rev. B,* **76**, 195406 (2007).

[12] H. S. Kang, S. Jeong,"Nitrogen doping and chirality of carbon nanotubes", *Phys. Rev. B* **70**, 233411 (2004).

[13] J. Wei, H. F. Hua, H. Zeng, Z. Zhou, W. Yang, P. Peng," Effects of nitrogen substitutional doping on the electronic transport of carbon nanotube", *Physica E* **40**, 462 (2008)

[14] J. Wei, H. Hu, Z. Wang, H. Zeng, Y. Wei, J. Jia," Effect of nitrogen-vacancy complex defects on the electronic transport of carbon nanotube" *Appl. Phys. Lett.* **94**, 102108 (2009)

[15] C. C. Kaun, B. Larade, H. Mehrez, J. Taylor, H. Guo," Current-voltage characteristics of carbon nanotubes with substitutional nitrogen", *Phys. Rev. B,* **65**, 205416 (2002)

[16] Y. Ma, A. S. Foster, A. V. Krasheninnikov, R. M. Nieminen," Nitrogen in graphite and carbon nanotubes: Magnetism and mobility" *Phys. Rev. B,* **72**, 205416 (2005)

[17] Y. S. Min, E. J. Bae, U. J. Kim, E. H. Lee, N. Park, C. S. Hwang, W. Park," Unusual transport characteristics of nitrogen-doped single-walled carbon nanotubes" *Appl. Phys. Lett.* **93**, 043113 (2008)

[18] Y. Fujimoto, S. Saito, "Energetics and electronic structures of pyridine-type defects in nitrogen-doped carbon nanotubes" *Physica* E **43**, 677 (2011).

[19] B. G. Sumpter, J. Huang, V. Meunier, J. M. Romo-Herrera, E. Cruz-Silva, H. Terrones, M. Terrones," A theoretical and experimental study on manipulating the structure and properties of carbon nanotubes using substitutional dopants" *Inter. J. of Quantum Chem.* **109**, 97 (2009)

[20] J. Akola, H. Häkkinen," Density functional study of gold atoms and clusters on a graphite (0001) surface with defects" *Phys. Rev. B,* **74**, 165404 (2006).

[21] G. Kim, S. H. Jhi, N. Park," Effective metal dispersion in pyridinelike nitrogen doped graphenes for hydrogen storage" *Appl. Phys. Lett.* **92**, 013106 (2008)

[22] J.-X. Zhao, Y. -H. Ding, X. -G. Wang, Q.-H. Cai, X.-Z. Wang," Theoretical studies of the CNx nanotube with four-nitrogen divacancy (4ND) defects" *Diamond & Related Materials,* **20**, 36 (2011)

[23] I. C. Gerber, P. Puech, A. Gannouni, W. Bacsa," Influence of nitrogen doping on the radial breathing mode in carbon nanotubes" *Phys. Rev. B,* **79**, 075423 (2009)

[24] P. Hohenberg, W. Kohn, "Inhomogeneous Electron Gas" *Phys. Rev*. **136**, B864 (1964)

[25] W. Kohn, L. J. Sham," Self-Consistent Equations Including Exchange and Correlation Effects" *Phys. Rev*. **140**, A1133 (1965)

[26] J. M. Soler, E. Artacho, J. D. Gale, A. García, J. Junquera, P. Ordejón, D. Sánchez-Portal, "The SIESTA method for ab initio order-N materials simulation" *J. Phys. Condens. Matter,* **14,** 2745 (2002)

[27] J. Kotakoski, A. V. Krasheninnikov, K. Nordlund," Energetics, structure, and long-range interaction of vacancy-type defects in carbon nanotubes: Atomistic simulations" *Phys. Rev.* B, **74**, 245420 (2006)

[28] J. E. Padilla, R. G. Amorim, A. R. Rocha, A. J. R. da Silva, A. Fazzio," Energetics and stability of vacancies in carbon nanotubes" *Solid State Commun*. **151**, 482 (2011)

[29] S. S. Yu, Q. B. Wen, W. T. Zheng, Q. Jiang," Effects of doping nitrogen atoms on the structure and electronic properties of zigzag single-walled carbon nanotubes through first-principles calculations" *Nanotechnology,* **18**, 165702 (2007)

[30] E. Cruz-Silva, F. López-Urías, E. Muñoz-Sandoval, B. G. Sumpter, H. Terrones, J. C. Charlier, V. Meunier, M. Terrones," Electronic Transport and Mechanical Properties of Phosphorus- and Phosphorus−Nitrogen-Doped Carbon Nanotubes" *ACS Nano* **3**, 1913 (2009)

[31] R. G. Amorim, A. Fazzio, A. Antonelli, F. D. Novaes, A. J. R. da Silva," Divacancies in Graphene and Carbon Nanotubes" *Nano Lett.* **7**, 2459 (2007)

[32] Y. F. Li, Z. Zhou, L. B. Wang," CNx nanotubes with pyridinelike structures: p-type semiconductors and Li storage materials" *J. Chem. Phys.* **129**, 104703 (2008)

[33] V. Krstic, G. L. J. A. Rikken, P. Bernier, S. Roth, M. Glerup," Nitrogen doping of metallic single-walled carbon nanotubes:n-type conduction and dipole scattering" *Europhys. Lett.* **77**, 37001 (2007)

[34] S. Tang, Z. Cao," Defect-induced chemisorption of nitrogen oxides on (10,0) single-walled carbon nanotubes: Insights from density functional calculations" *J. Chem. Phys.* **131**, 114706 (2009)

Chapter 5 : Synthesis, Characterization, and Theoretical Studies of Hybrid ZnO Nanoparticles and Nitrogen-Doped Carbon Nanotubes

5.1. Summary

We have synthesized ZnO nanoparticles (ZnO-NPs) anchored on the surface of nitrogen-doped multiwalled carbon nanotubes (CN_X-MWNTs). The anchoring process consisted in adding CN_X-MWNTs (previously synthesized using chemical deposition method) in a solution containing dimethylformamide, zinc acetylacetonate, and thiophene. The thiophene solvent was used as a capping agent. Different samples were obtained by varying the thiophene concentration. Scanning and transmission electron microscopy characterizations revealed that ZnO-NPs are homogeneously distributed along the CN_X-MWNTs. X-ray diffraction analysis demonstrated that the ZnO-NPs exhibit a Wurtzite crystal structure with an average diameter equal to 5nm. We found that the ZnO-NPs does not exhibit a preferential grown direction respect to the nanotube surface, and its growth is controlled by the concentration of passivating agent. First-principles density functional calculations in the local spin density approximation were performed to understand the role of the sulfur atoms (coming from the passivating agent) during the formation of ZnO-NPs and the interaction with CN_X-MWNTs. Our theoretical results on different nanoparticle sizes revealed the presence of unpaired spins on the isolated ZnO-NPs passivated with sulfur. The obtained magnetic moments were located mainly at the surface and on the sulfur atoms. In addition, a ZnO-NP was set on the surface of a N-doped (10,0) single walled carbon nanotubes. After geometry relaxation, the ZnO-NP was attached to the nanotube surface exhibiting a net total magnetic moment. The ZnO-NP was preferentially bonded to the surface of carbon nanotubes via oxygen atoms.

Chapter Content

Chapter 5 : Synthesis, Characterization, and Theoretical Studies of Hybrid ZnO Nanoparticles and Nitrogen-Doped Carbon Nanotubes

5.1. Summary 97

5.2. Introduction: Zinc Oxide Nanoparticles Anchored to Carbon Nanotubes 99

5.3. Materials and Methods: Zinc Oxide Decoration of Nitrogen Doped Carbon Nanotubes 101

5.4. Results and Discussion: N-Doped Carbon Nanotube Decoration and Material Characterization 102

5.5. Theoretical Study of Sulfur Passivated Zinc Oxide Cluster and Carbon Nanotube System 108

5.6. Conclusions 112

5.7. References 113

5.2. Introduction: Zinc Oxide Nanoparticles Anchored to Carbon Nanotubes

The properties of ZnO nanoparticles could be efficiently transferred to other materials when interacting with other surfaces such as cotton fabrics [1], carbon nanotubes [2] and polymers [3]. Over the last years, carbon nanotubes (CNTs) have been used as efficient templates to obtain ZnO-NPs. Actually, a wide variety of ZnO nanostructures have been synthesized, such as rods, flowers [4], thin films and quantum dots [2,5] on the outer wall of carbon nanotubes. Different coating techniques has been used to obtain these hybrid materials, from techniques using high temperatures and sophisticated equipment [6,7] to some simple methods which offers low control on particle size [8-10]. The resulting ZnO-CNTs nanocomposite can be employed in many applications, such as field emitters [11-13] with increased lifetimes [14] and low turn electric field [15,16], as a biological sensor [17-20], for the fabrication of super-hydrophobic surface [21], supercapacitors [22] and hybrid solar cells [23]. Despite their wide range of applications little is actually known about the interaction, electron transfer events and nucleation mechanism of the metal or metal oxide nanoparticles on carbon nanotubes. Moreover, the role of the passivating agents is not completely understood [24-26].

Nitrogen-doped multiwalled carbon nanotubes are more chemically reactive [27-31] and are suitable substrate materials for the deposition of nanoparticles, the nitrogen act as an important promoter of nanoparticle nucleation [30-33]. The use of these CN_X-MWNTs avoids the use of hazard acidic solution trying to improve its chemical reactivity and avoid damage to its mechanical end electrical properties. In this work, we have employed CN_X-MWNTs as a template to deposit ZnO nanoparticles. Far as we know,

this is the first report regarding to CN_X-MWNTs decorated with ZnO nanoparticles.

In this chapter, we synthesized and used nitrogen-doped multiwalled carbon nanotubes as an efficient substrate to deposit ZnO nanoparticles by wet chemistry. The thiophene solvent was used as a capping agent and to control the ZnO-NPs size. It is important to emphasize the CN_X-MWNTs were not functionalized or previously treated with acid solutions, thus avoiding serious structural defects on the nanotube lattice. The samples were characterized using the SEM, TEM, and X-ray techniques. We carried out first-principles density functional calculations on different sizes of ZnO-NPs passivated with sulfur. In addition, results on ZnO nanoparticle interaction with a nitrogen-doped (10,0) single walled carbon nanotube are discussed.

5.3. Materials and Methods: Zinc Oxide Decoration of Nitrogen Doped Carbon Nanotubes

Nitrogen-doped carbon nanotubes (CN_X-MWNTs) were synthesized using a chemical vapor deposition (CVD) method [34,35]. The general procedure for the decoration process consisted in adding 5 mg of CN_X-MWNTs in a solution containing 10 ml N,N-dimethylformamide (DMF), zinc acetylacetonate, ($Zn(acac)_2$) and thiophene. The thiophene is used as a capping agent. The molar ratio of carbon (from the CNTs) and zinc was kept at 10. Subsequently, the suspension was dispersed ultrasonically for 30 minutes. The flask was collocated under an argon atmosphere (Ar flow of 0.3 l/min) and it was placed in a glycerin bath to increase the temperature up to 125°C, until the solution was evaporated, the experimental setup is depicted in figure 5-1.

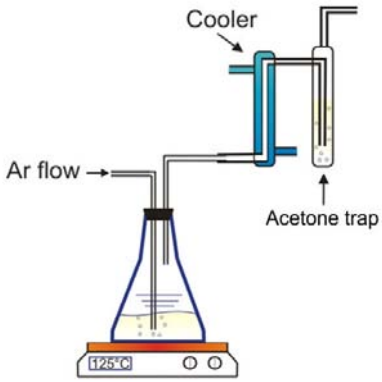

Figure 5-1: Scheme diagram of the experimental setup used to anchor ZnO nanoparticles on the surface of nitrogen-doped carbon nanotubes (CN_X-MWNTs). The suspension was prepared by mixing carbon nanotubes, zinc acetylacetonate and thiophene in N,N-dimethylformamide as solvent. The suspension was maintained under vigorous stirring at 125°C. Also an Ar flow was implemented to create a controlled atmosphere and to increase the evaporation rates.

Subsequently, a thermal treatment was carried out at 400°C for 15 minutes under an argon atmosphere. The samples were characterized by scanning electron microscopy, (SEM FEI XL30 SFEG at 18 kV), X-ray diffraction powder patterns were obtained using XRD D8 Advance–Bruker Axs, with Cu K_α radiation (λ = 1.54060 Å) operated at 35 kV and 25 mA. High-resolution transmission electron microscopy characterization was carried out using a Philips TECNAI-F30 HRTEM of 300 kV.

5.4. Results and Discussion: N-Doped Carbon Nanotube Decoration and Material Characterization

Figure 5-2 depicts scanning electron microscopy (SEM) images of the ZnO nanoparticles anchored on the surface of nitrogen-doped carbon nanotubes for different values of thiophene concentration (from 6.6 to 26.0 µl/ml) added during the coating process. Figure 5-2a depicts the sample synthesized with the lower thiophene concentration (6.6 µl/ml); by inspection it is possible to observe the low surface coverage of ZnO-NPs on the surface of the carbon nanotubes. When the thiophene concentration is increased up to 26.0 µl/ml, the CN_X-MWNTs seem to be completely coated (when compared with the lowest thiophene concentration in figure 5-2a) and it exhibits a homogeneous distribution of ZnO-NPs with smaller diameters, these results are depicted in figure 5-2b.

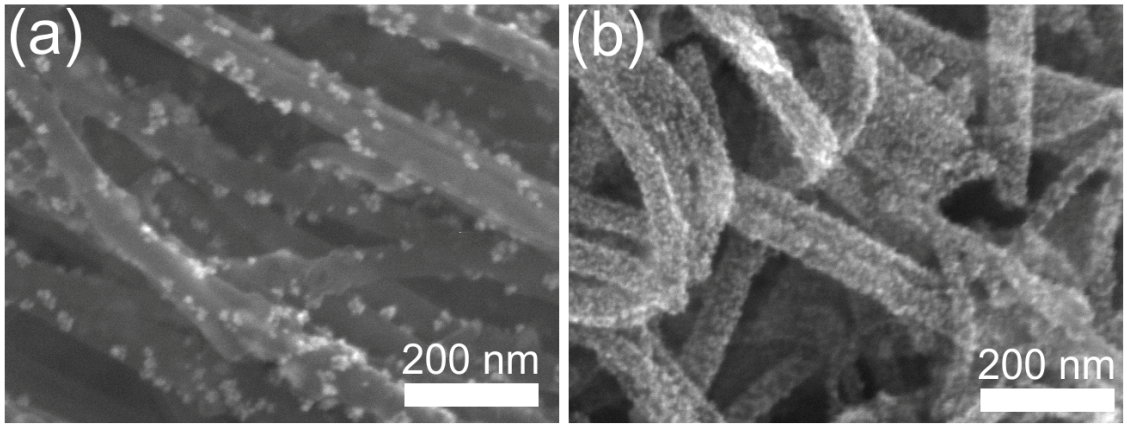

Figure 5-2: Scanning electron microscopy (SEM) images of ZnO nanoparticles anchored on the surface of nitrogen-doped multiwalled carbon nanotubes (CNX-MWNTs) by using different thiophene concentrations: **(a)** 6.6 µl/ml and **(b)** 26.4 µl/ml. Notice that the increment of the thiophene concentration inhibits the growth of large ZnO nanoparticles, thus achieving a more efficient coverage of the nanotube´s surface.

The final sulfur content of the hybrid material was determined after the heat treatment of the samples using energy-dispersive X-ray spectroscopy (EDX). In this case, the resulting sulfur is expected to be attached or related to the ZnO nanoparticles surface. We also monitored the change in diameter of the ZnO-NPs due the addition of capping agent (thiophene). Figure 5-3 shows the behavior of the nanoparticles size and the final sulfur:zinc atomic ratio as a function of the thiophene concentration. From figure 5-3a, we observed that the ZnO particle diameter decreases at higher thiophene concentrations, however, the sulfur:zinc ratio (see figure 5-3b) increases at the same time. After ~20µl/ml of thiophene, the particle diameter is almost constant and the sulfur:zinc ration does not increase substantially with further addition of thiophene. These results suggest that sulfur could be at the surface of the ZnO-NPs, thus the ZnO just reach 5nm size, apparently is the smaller size reached with this coating method. Therefore the sulfur inhibits the growth of the ZnO nanoparticles, acting as a passivating agent.

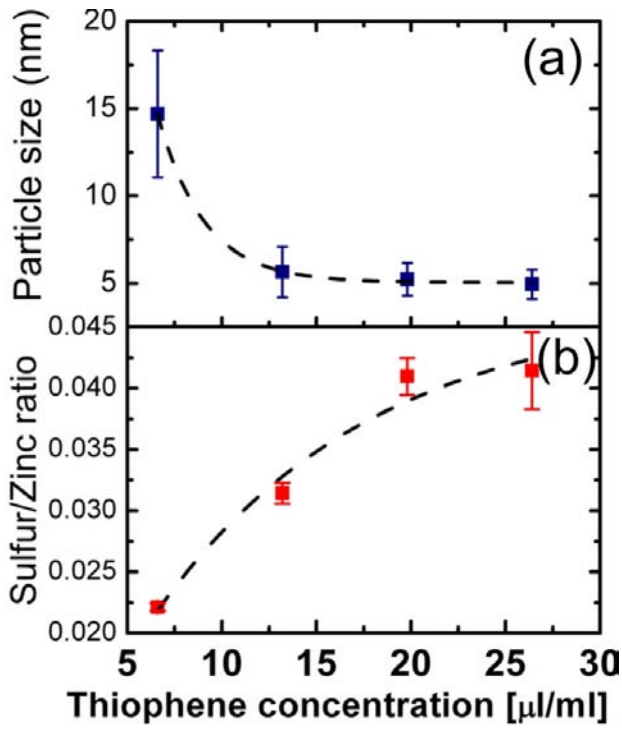

Figure 5-3: Thiophene concentration dependence of **(a)** average size of the ZnO nanoparticles anchored on nitrogen-doped multiwalled carbon nanotubes (CN_X-MWNTs) and **(b)** sulfur:zinc ratio determined by energy-dispersive X-ray (EDX) after thermal treatment. Notice that the average size curve exhibits a typical exponential decay behavior whereas the sulfur:zinc ratio curve presents a sigmoidal behavior. The decrease of the nanoparticle size and the increase of the sulfur:zinc ratio when the thiophene concentration increases could suggest that the sulfur inhibits the growth of ZnO nanoparticles acting as a passivated agent.

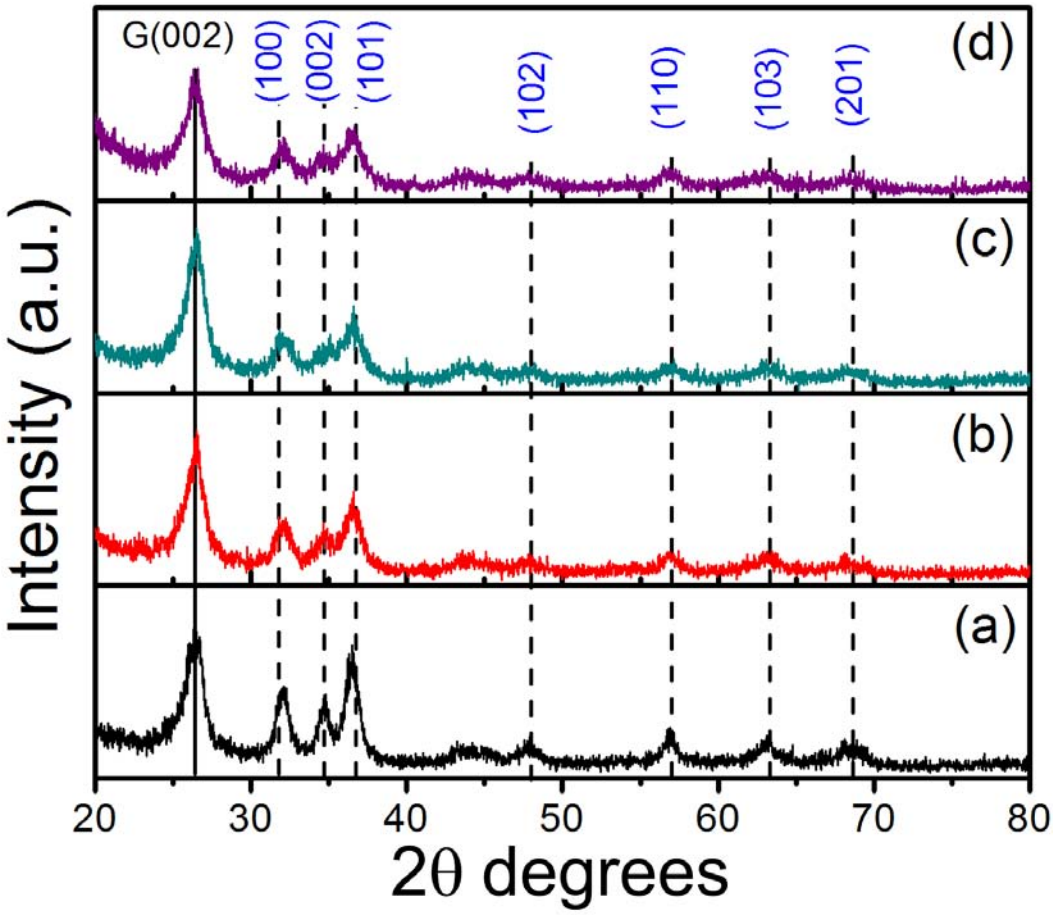

Figure 5-4: X-ray diffraction (XRD) patterns of ZnO nanoparticles anchored on the surface of nitrogen-doped multiwalled carbon nanotubes (CNx-MWNTs) for different values of the thiophene concentration: **(a)** 6.6 µl/ml, **(b)** 13.2 µl/ml, **(c)** 19.8 µl/ml, **(d)** 26.4 µl/ml. The vertical dashed lines are characteristic peaks of the bulk ZnO with Wurtzite structure. Notice that the different peaks reveal that the ZnO nanoparticles exhibit a Wurtzite-like structure whereas the peak G(002) is associated to the carbon nanotubes. The peaks around 45° belong to iron carbides. It has also observed that the width of the peaks associated to the ZnO nanoparticles increases with the thiophene concentration revealing a decrease of the nanoparticles size as it was also confirmed by scanning electron microscopy characterization.

X-ray diffraction patterns results for different values of the thiophene concentration are shown in figure 5-4. The samples exhibit different peaks associated to the ZnO nanoparticles, carbon nanotubes and iron carbide. The peak indicated by the G(002), which is characteristic of graphite,

corresponds to the carbon nanotubes. Beyond of 26 degrees, the patterns exhibit different peaks associated to the planes of the Wurtzite crystal, as the dashed line indicates, which suggest that the ZnO-NPs exhibit a Wurtzite-like structure. When the thiophene concentration is increased, the diffraction peaks becomes wider meaning that the ZnO-NPs exhibit smaller size as it was previously confirmed by SEM characterization. The peaks around 45 degrees (non indexed) could be related with iron carbide or α-iron nanoparticles inside carbon nanotubes which are produced during the chemical vapor deposition synthesis method [34,35].

Transmission electron microscopy images of CN_X-MWCNTs decorated with ZnO-NPs at 26 µl/ml of thiophene concentration are shown in figure 5-5. It can be seen, how the nanoparticles are well distributed along the CN_X-MWNTs. A higher magnification image demonstrated that the ZnO-NPs exhibit a crystalline structure (see figure 5-5b). The insets (i-iii) in figure 5-5b depict different ZnO-NPs on the surface of a CN_X-MWNT with an inter-planar distance of 0.24 nm, which correspond to the (101) plane of the Wurtzite structure. It is observed that these ZnO nanoparticles show the (101) crystal plane, however, this crystalline plane is arranged in different orientations respect to the carbon nanotube walls (i.e. in (i) is the (101) crystal plane is perpendicular to the nanotube walls, on the other hand, in (iii) is parallel). Notice that a superficial layer may cover the ZnO nanoparticles; a chemical analysis of the sample suggests that this layer contains sulfur atoms.

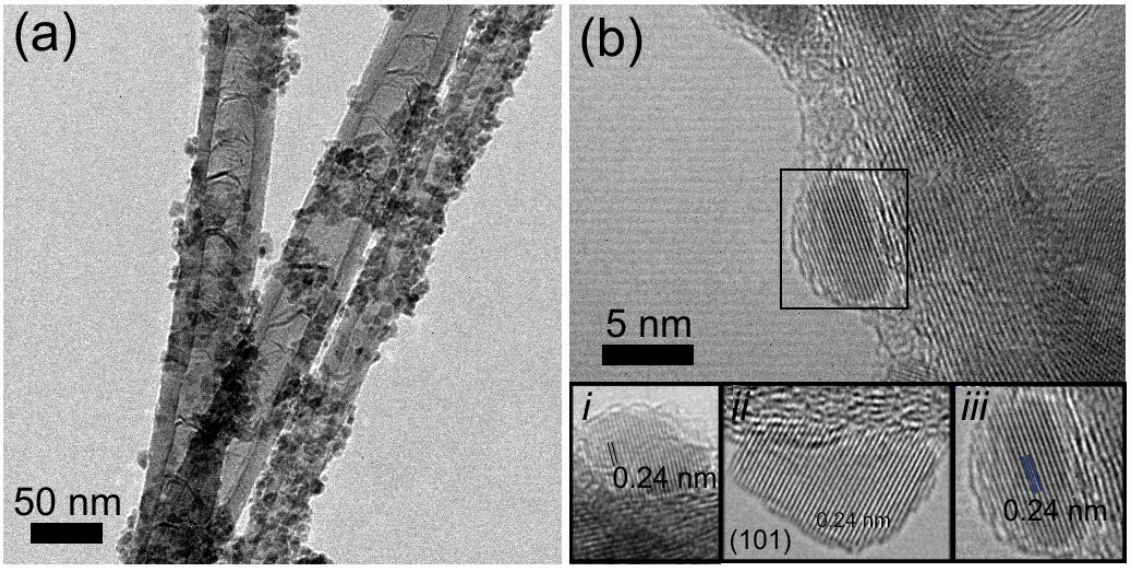

Figure 5-5: **(a)** and **(b)** Transmission electron microscopy (TEM) images of ZnO nanoparticles anchored on the surface of nitrogen-doped multiwalled carbon nanotubes (CN_X-MWCNTs). The sample was synthesized using a thiophene concentration of 26.4 µl/ml. The TEM images shown in the insets ***(i)-(iii)*** depict ZnO nanoparticles anchored to the nanotubes with different crystal orientation. Here, the ZnO nanoparticles exhibit an inter-planar distance of 0.24 nm corresponding to the (101) plane of the Wurtzite crystal. This suggests that there is no preferential orientation in the growth of the ZnO nanoparticles on the surface of carbon nanotubes.

Figure 5-6 depicts the linear mapping of a single CN_X-MWNT decorated by ZnO-NPs. This sample was synthesized with higher thiophene concentration (26 µl/ml). Atomic concentration profile of carbon, nitrogen, zinc, oxygen, and sulfur across the nanotube, derived from an EDX line scan in TEM, is depicted in figure 5-6a. The analyzed region correspons to the nanotube decorated with ZnO-NPs, is shown in figure 5-6b. In the EDX line scan, carbon and nitrogen elements are observed along linear mapping corresponding to the N-doped carbon nanotube. Whereas the zinc and oxygen are observed only in the extreme of the linear mapping; also a small trace of sulfur is observed, which correspons to two ZnO nanoparticles that are in the edges of the nanotube.

The presence of sulfur atoms match just in the region where ZnO was detected, and because the XRD analysis does not found any ZnS, it is probable that sulfur may be surrounding the ZnO nanoparticles, thus forming the disordered layer observed during TEM characterization.

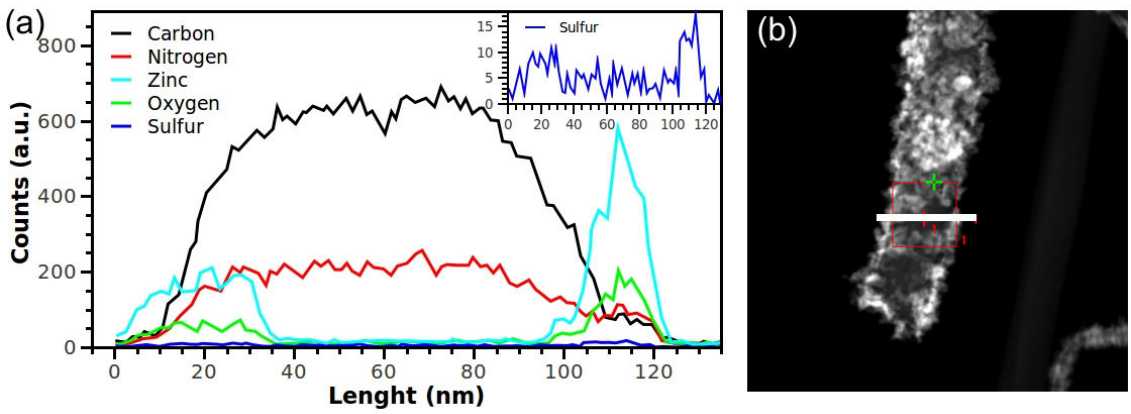

Figure 5-6: Linear mapping of a single nitrogen-doped multiwalled carbon nanotube decorated by ZnO nanoparticles. This sample was synthesized with a thiophene concentration of 26.4 µl/ml. **(a)** Concentration profile of carbon, nitrogen, zinc, oxygen, and sulfur across the nanotube, derived from Energy-dispersive X-ray spectroscopy (EDX) line scan. **(b)** Analyzed region corresponding the nanotube decorated with ZnO nanoparticles (white line). Notice that the carbon and nitrogen are observed along linear mapping whereas the zinc and oxygen are observed only in the extreme of the linear mapping; also a small trace of sulfur was detected which suggest that the ZnO nanoparticles could be passivated with sulfur.

5.5. Theoretical Study of Sulfur Passivated Zinc Oxide Cluster and Carbon Nanotube System

Density functional calculations studies were carried out to determine the role of sulfur atoms in the formation of ZnO nanoparticles. The electronic spin-polarized calculations were performed using density functional theory (DFT) [36,37] in the framework of the general gradient approximation (GGA) within the Perdew-Burke-Ernzerhof (PBE) [38,39] with a basis of linear combination of atomic orbitals (LCAO) as implemented in the SIESTA code [40]. The systems were constructed by using a supercell made of 5 unit cells of the (10,0) nanotubes (40 atoms per unit cell) and $Zn_{15}O_{15}$ cluster. For the case of the isolated $Zn_{15}O_{15}$ clusters, they were collocated in a supercell with a separation of 30 Å. For further information please see Appendix A.

The starting geometries in our calculations were constructed from the Wurtzite structure. The sulfur atoms were gradually added to the surface, mainly to low coordinated Zn atoms of the $Zn_{15}O_{15}$ cluster. After geometry optimization, it was observed that the final structures were more energetically favorable and less symmetric than the pure $Zn_{15}O_{15}$ cluster. Here, the sulfur atoms bond preferentially to others sulfur or zinc atoms. This result has been previously observed in the adsorption of sulfur-containing molecules such as H_2S, disulfides, thiophene and mercaptans in ZnO surfaces [41,42]. It has also been determined, that Zn sites of ZnO are more reactive toward S-containing molecules. Studies involving, H_2S, HS and S atoms on ZnO oriented in (0001) direction, have demonstrated that these molecules interact preferentially with unsaturated Zn atoms of the ZnO surface [41-43], thus leaving the sulfur adsorbed on Zn atoms. It has been also suggested that sulfur adatoms weaken the bonding interactions of sulfur-containing molecules on ZnO. In the same way, ZnS is also

considerably less reactive toward thiophene than ZnO [44]. These previous observations and the results obtained in this work suggest that, sulfur atoms may remain in the surface of the ZnO cluster bonded preferentially to Zn atoms, probably creating a small ZnS layer at the surface. This layer of sulfur atoms passivates the ZnO cluster, and avoids further addition of sulfur atoms to the ZnO cluster. In fact, in our calculations, sulfur atoms act as stabilizer of ZnO clusters, and this could explain our experimental results, where the sulfur avoids the further increment of ZnO nanoparticles size, acting as a passivating agent.

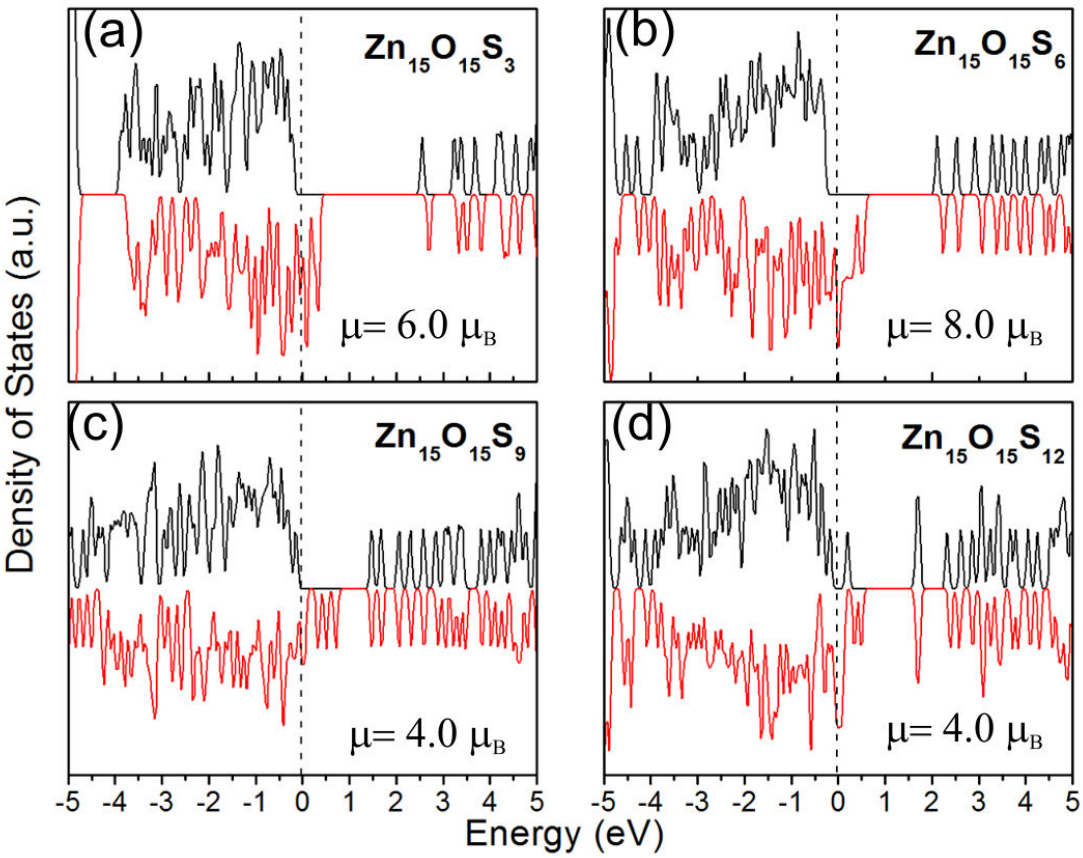

Figure 5-7: (a)-(d) Spin-polarized electronic density of states of the zinc oxide cluster passivated with sulfur atoms on the surface $Zn_{15}O_{15}S_x$ (x=3, 6, 9, and 12). In all cases, the Fermi level was set to zero (vertical dashed line). The net magnetic moment in each case is indicated in the plots. It is important to remark that the pure (without sulfur passivation) $Zn_{15}O_{15}$ cluster exhibits a null total magnetic moment.

Spin-polarized density of states calculations show that sulfur-passivated $Zn_{15}O_{15}$ cluster exhibit magnetic moment and states at the Fermi level, while the pure $Zn_{15}O_{15}$ cluster showed zero magnetic moment without states at the Fermi level, these results are depicted in figure 5-7. The magnitude of the total magnetic moment is 6.0, 8.0, 4.0, and 4.0m_B for the clusters $Zn_{15}O_{15}S_3$, $Zn_{15}O_{15}S_6$, $Zn_{15}O_{15}S_9$, and $Zn_{15}O_{15}S_{12}$ respectively. The magnetic moment in all clusters arises mainly from the sulfur and oxygen atoms. Our results on the appearance of unpaired spins in sulfur-passivated ZnO clusters are in agreement with a previous work reported by Botello-Méndez *et al* [45], where sulfur or thiol passivated ZnO cluster and nanoribbons shows an enhancement in magnetic moment.

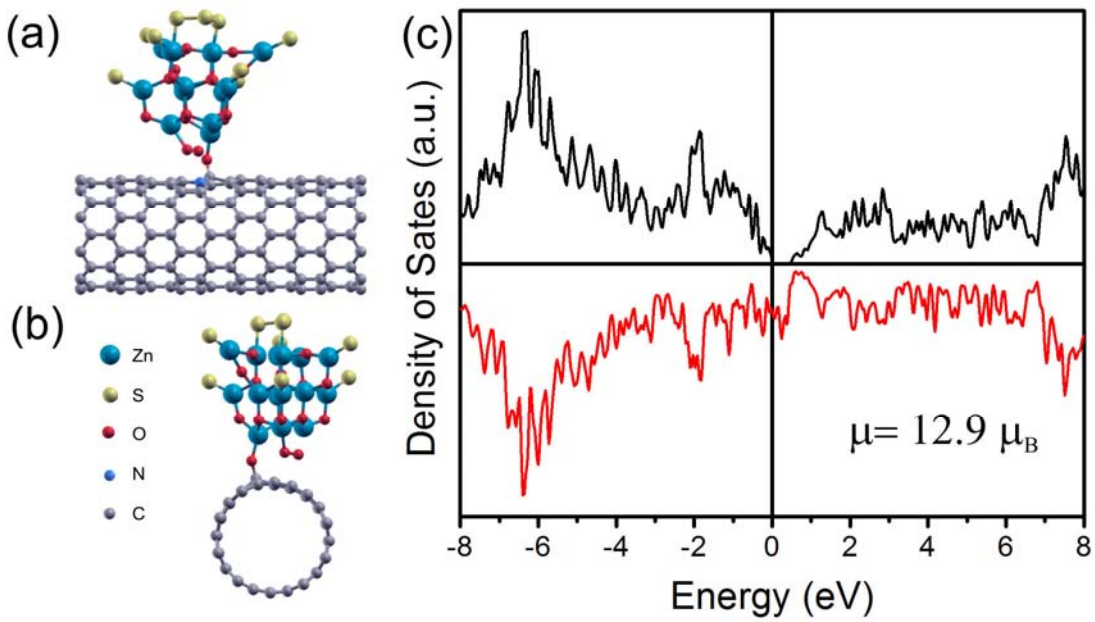

Figure 5-8: The relaxed structure (top and side views) of a sulfur passivated ZnO clusters ($Zn_{15}O_{18}S_8$) on the surface of a nitrogen-doped single walled (10,0) carbon nanotube are shown and **(a)** and **(b)**. Notice that the ZnO cluster is joined to nanotube surface by an oxygen atom (this oxygen atom makes a bond with a carbon atom neighbor of the nitrogen atom). **(c)** The corresponding spin-polarized electronic density of states (DOS). The Fermi level was set at zero energy (see the vertical line) and the nitrogen atom was introduced via a substitutional way. Notice that the DOS only exhibits states with spin down at the Fermi level, typical behavior of half-metallic systems. The obtained total magnetic moment is of 12.93 μ_B. Worth mentioning that we have performed similar calculations without the presence of sulfur passivation and we observed that the system's magnetism is lost.

In order to understand the interaction between the doped carbon nanotubes and the ZnO nanoparticles, we have performed calculations of a substitutional nitrogen-doped (10,0)-single-walled carbon nanotube (CN_x-SWNT) decorated with a $Zn_{15}O_{15}S_9$ cluster passivated with sulfur. This cluster exhibits twelve Zn superficial atoms doubly or triply coordinated, then nine of them where passivated with sulfur atoms and in the remaining three Zn atoms, an extra oxygen atom was collocated. After that, the $Zn_{15}O_{18}S_9$ cluster was collocated by the extra oxygen atoms, near the nitrogen atom of the N-doped (10,0)-SWNT (composed by 5 unit cells). The relaxed structure is depicted in figure 5-8a and b. It is observed, that the $Zn_{15}O_{18}S_9$ is covalently bonded to the nanotube via one oxygen atom. This O atom is bonded to one C atom placed just as first neighbor of the nitrogen impurity atom, and not directly to the N atom. The spin-polarized density of states (DOS) of this hybrid material is depicted in figure 5-8c. The hybrid structure exhibits a half-metallic behavior with only spin down states at the Fermi level, whereas the spin up DOS exhibits a band gap of 0.56 eV. The magnitude of the total magnetic moment is 12.93μ_B and the magnetic moment arises mainly from the sulfur and oxygen atoms. Notice that the total magnetic moment is increased regarding the corresponding isolated cluster.

5.6. Conclusions

ZnO nanoparticles (ZnO-NPs) anchored on the surface of nitrogen-doped multiwalled carbon nanotubes (CN_x-MWNTs) were synthesized using chemical wetting using the thoiphene as passivated agent. Varying the thiophene concentration was possible to control the ZnO-NPs size. Scanning and transmission electron microscopy analysis demonstrated that the ZnO-NPs are homogeneously distributed along the nanotube surface. First-principles density functional calculations demonstrated that the sulfur atoms are bound strongly to superficial Zn atoms. Concerning the magnetic properties, we found that the S-passivated ZnO nanoparticles present magnetism with important magnetic moments on the surface. The passivated ZnO clusters were set in contacting with a N-doped single walled carbon nanotube. The results demonstrated that ZnO cluster are preferentially attached to the nanotube by oxygen bonding.

5.7. References

[1] B. M.Dürr, P. Nostro, P. Baglioni," Synthesis and characterization of zinc oxide nanoparticles: application to textiles as UV-absorbers" *J. Nanopart. Res*. **10**, 679-689 (2008)

[2] L. Chen-Sha, Q. Ying-Jie, L. Yu-Ning, W. Yi-Liang, "Decorating multiwalled carbon nanotubes with zinc oxide nanoparticles by thermally decomposing Zn-oleate in an organic medium" *Sci China Ser E-Tech Sci*, **52**, 1254-1257 (2009)

[3] C.S. Lao, M.-C. Park, Q. Kuang, Y. Deng, A. K. Sood, D. L. Polla, Z. L. Wang, Giant Enhancement in UV Response of ZnO Nanobelts by Polymer Surface-Functionalization, *J. Am. Chem. Soc*. 129, 12096–12097 **(2007)**

[4] X. Wang, B. Xia, X. Zhu, J. Chen, S. Qiu, J. Li, "Controlled modification of multiwalled carbon nanotubes with Zno nanostructures" *J. Sol State Chem.* **181**, 822–827 (2008)

[5] H. Kim, W. Sigmund, "Zinc oxide nanowires on carbon nanotubes", *Appl. Phys. Lett.* **81**, 2085-2087 (2002)

[6] Y. M. Ho, J. W. Liu, J. L. Qi, W. T. Zheng, "Spectroscopic investigation on carbon nanotubes coated with ZnO nanoparticles", *J. Phys. D: Appl. Phys*., **41**, 065308 (2008)

[7] Y. S. Min, E. J. Bae, J. B. Park, U. J. Kim, W. Park, J. Song, C. S. Hwang, N. Park, "ZnO nanoparticle growth on single-walled carbon nanotubes by atomic layer deposition and a consequent lifetime elongation of nanotube field emission", *Appl. Phys. Lett.,* **90**, 263104 (2007)

[8] G. Guo, J. Guo, D. Tao, W.C.H. Choy, L. Zhao, W. Qian, Z. Wang, "A Simple method to prepare multi-walled carbon nanotube/ZnO nanoparticle composites", *Appl. Phys. A*, **89**, 525–528 (2007)

[9] N. Zhang, J. Sun, D. Jiang, T. Feng, Q. Li, "Anchoring zinc oxide quantum dots on functionalized multi-walled carbon nanotubes by covalent coupling" Carbon, **47,** 1214 –1219 (2009)

[10] J. Sun, L. Gao, M. Iwasa, "Noncovalent attachment of oxide nanoparticles onto carbon nanotubes using water-in-oil microemulsions", *Chem. Commun.*, **7**, 832-833 (2004)

[11] Y. S. Min, E. J. Bae, J. B. Park, U. J. Kim, W. Park, J. Song, C. S. Hwang, N. Park, "ZnO nanoparticle growth on single-walled carbon nanotubes by atomic layer deposition and a consequent lifetime elongation of nanotube field emission", *Appl. Phys. Lett.,* **90**, 263104 (2007)

[12] Y. Di, Y. Cui, Q. Wang, W. Lei, X. Zhang, D. Engelsen, "Field emission from carbon nanotube and tetrapod-like ZnO compound cathode fabricated by spin-coating method" *Appl. Surf. Sci.*, **255**, 4636–4639 (2009)

[13] J.Y. Pan, C.C. Zhu, Y.L. Gao, "Enhanced field emission characteristics of zinc oxide mixed carbon nano-tubes films" *Appl. Surf. Sci.*, **254,** 3787–3792 (2008)

[14] J. M. Green, L. Dong, T. Gutu, J. Jiao, J. Conley, Y. Ono, "ZnO-nanoparticle-coated carbon nanotubes demonstrating enhanced electron field-emission properties" *J. Appl. Phys.,* **99**, 094308 (2006)

[15] W. B. Choi, D. S. Chung, J. H. Kang, H. Y. Kim, Y. W. Jin, I. T. Han, Y. H. Lee, J. E. Jung, N. S. Lee, G. S. Park, J. M. Kim, "Fully sealed, high-brightness carbon-nanotube field-emission display", *Appl. Phys. Lett.*, **75**, 3129-3131 (1999)

[16] K. Yu, Y. S. Zhang, F. Xu, Q. Li, Z. Q. Zhu, Q. Wan, "Significant improvement of field emission by depositing zinc oxide nanostructures on screen-printed carbon nanotube films", *Appl. Phys. Lett.*, **88**, 153123 (2006)

[17] H. P. Bai, X. X. Lu, G. M. Yang, Y. H. Yang, *Chinese Chem. Lett.*, **19** 314–318 (2008)

[18] W. Zhang, T. Yang, Daming Huang, Kui Jiao, Guicun Li, *J. Membrane Sci*. **325**, 245–251(2008)

[19] W. Zhang, T. Yang, D. M. Huang, K. Jiao, *Chinese Chem. Lett.*, **19**, 589–591 (2008)

[20] C. S. Rout, A.R. Raju, A. Govindaraj, C.N.R. Rao, *Sol. State Commun.,* **138**, 136–138 (2006)

[21] L. Huang, S.P. Lau, H. Y. Yang, E.S.P. Leong, S.F. Yu, S. Prawer, "Stable Superhydrophobic Surface via Carbon Nanotubes Coated with a ZnO Thin Film", *J. Phys. Chem. B*, **109**, 7746-7748 (2005)

[22] Y. Zhang, X. Sun, L. Pan, H. Li, Z. Sun, C. Sun, B. K. Tay "Carbon nanotube–zinc oxide electrode and gel polymer electrolyte for electrochemical supercapacitors" *J. Alloys and Compounds*, **480**, L17-L19 (2009)

[23] S. Wu, Q. Tai, F. Yan, "Hybrid Photovoltaic Devices Based on Poly (3-hexylthiophene) and Ordered Electrospun ZnO Nanofiber", *J. Phys. Chem. C,* **114**, 6197–6200 (2010)

[24] I. Suarez-Martinez, C. P. Ewels, X. Ke, G. V. Tendeloo, S. Thiess, W. Drube, A. Felten, J.-J. Pireaux, J. Ghijsen, C. Bittencourt, "Study of the Interface between Rhodium and Carbon Nanotubes" *ACS Nano,* **4**, 1680–1686 (2010)

[25] B. Ritz, H. Heller, A. Myalitsin, A. Kornowski, F. J. Martin-Martinez, S. Melchor, J. A. Dobado, B. H. Juarez, H. Weller, C. Klinke, "Reversible Attachment of Platinum Alloy Nanoparticles to Nonfunctionalized Carbon Nanotubes", *ACSnano,* **4**, 2438-2444 (2010)

[26] D. R. Kauffman, D. C. Sorescu, D. P. Schofield, B. L. Allen, K. D. Jordan, A. Star, "Understanding the Sensor Response of Metal-Decorated Carbon Nanotubes", *Nano Lett.,* **10**, 958–963 (2010)

[27] Z. Zhang, K. Cho, "*Ab initio* study of hydrogen interaction with pure and nitrogen-doped carbon nanotubes", *Phys. Rev. B.,* **75**, 075420 (2007)

[28] E. Cruz-Silva, F. López-Urías, E. Muñoz-Sandoval, B. G. Sumpter, H. Terrones, J. -C. Charlier, V. Meunier, M. Terrones, "Electronic Transport and Mechanical Properties of Phosphorus- and Phosphorus, Nitrogen-Doped Carbon Nanotubes", *ACS nano*, **3**, 1913-1921 (2009)

[29] Fabrication of vapor and gas sensors using films of aligned CNx nanotubes " F. Villalpando-Paez, A.H. Romero, E. Muñoz-Sandoval, L.M. Martínez, H. Terrones, M. Terrones", *Chem. Phys. Lett.* **386**, 137–143 (2004)

[30] F.R. Garcia-Garcia, J. Alvarez-Rodrıguez, I. Rodrıguez-Ramos, A. Guerrero-Ruiz, The use of carbon nanotubes with and without nitrogen doping as support for

ruthenium catalysts in the ammonia decomposition reaction, *Carbon,* **48**, 267-276 (2010)

[31] A. Zamudio, A. L. Elías, J. A. Rodríguez-Manzo, F. López-Urías, G. Rodríguez-Gattorno, F. Lupo, Manfred Rühlz, D. J. Smith, H. Terrones, D. Díaz, M. Terrones. "Efficient Anchoring of Silver Nanoparticles on N-Doped Carbon Nanotubes", *Small*, **2**, 346-350 (2006)

[32] X. Lepró, E. Terrés, Y. Vega-Cantú, F. J. Rodríguez-Macías, H. Muramatsu, Y. A. Kim, T. Hayahsi, M. Endo, M. Torres R., M. Terrones, "Efficient anchorage of Pt clusters on N-doped carbon nanotubes and their catalytic activity", *Chem. Phys. Lett*. **463**, 124-129 (2008)

[33] X. Lepró, Y. Vega-Cantú, F.J. Rodríguez-Macías, Y. Bando D. Golberg, M. Terrones, "Production and Characterization of Coaxial Nanotube Junctions and Networks of CN_X/CNT" *Nano Lett.*, **7**, 2220–2226 (2007)

[34] M. Pinault, H. Mayne-L'Hermite, C. Reynaud, O. Beyssac, J.N. Rouzaud, C. Clinard, Carbon nanotubes produced by aerosol pyrolysis: growth mechanisms and post-annealing effects, *Diamond Relat. Mater*, **13**, 1266-1269 (2004)

[35] M. Mayne, N. Grobert, M. Terrones, R. Kamalakaran, M. Rühle, H.W. Kroto, D. R. M. Walton, Pyrolytic production of aligned carbon nanotubes from homogeneously dispersed benzene-based aerosols, *Chem. Phys. Lett.,* **338**, 101–107 (2001)

[36] P. Hohenberg, W. Kohn, "Inhomogeneous Electron Gas" *Phys. Rev.,* **136**, B864 (1964)

[37] W. Kohn, L.J. Sham, "Self-Consistent Equations Including Exchange and Correlation Effects" *Phys. Rev.*, **140**, A1133 (1965)

[38] J.P. Perdew, K. Burke, M. Ernzerhof, "Generalized Gradient Approximation Made Simple" *Phys. Rev. Lett.*, **77**, 3865 (1996)

[39] J.P. Perdew, K. Burke, M. Ernzerhof," Generalized Gradient Approximation Made Simple" *Phys. Rev. Lett.*, **78**, 1396 (1997)

[40] J. M. Soler, E. Artacho, J.D. Gale, A. García, J. Junquera, P. Ordejón, D. Sánchez-Portal, "The SIESTA method for ab initio order-N materials simulation" *J. Phys.: Condens. Matter*, **14**, 2745 (2002)

[41] J. A. Rodriguez, A. Maiti, "Adsorption and Decomposition of H2S on MgO(100), NiMgO(100), and ZnO(0001) Surfaces: A First-Principles Density Functional Study" *J. Phys. Chem. B,* **104**, 3630-3638 (2000)

[42] J. A. Rodriguez, J. Hrbek, "Interaction of Sulfur with Well-Defined Metal and Oxide Surfaces: Unraveling the Mysteries behind Catalyst Poisoning and Desulfurization" *Acc, Chem Research*., **32**, 719-728 (1999)

[43] J. A. Rodriguez, T. Jirsak, J. Hrbek, "Reaction of SO_2 with Cesium and Cesium-Promoted ZnO and MoO_2" *J. Phys. Chem. B,* **103**, 1966-1976 (1999)

[44] T. Jirsak, J. Dvorak, J. A. Rodriguez, "Chemistry of Thiophene on ZnO, S/ZnO, and Cs/ZnO Surfaces: Effects of Cesium on Desulfurization Processes" *J. Phys. Chem. B*, **103**, 5550-5559 (1999)

[45] R. Botello-Méndez, F. López-Urías, M. Terrones, H. Terrones, "Enhanced Ferromagnetism in ZnO Nanoribbons and Clusters Passivated with Sulfur" *Nano Res.,* **1**, 420-426 (2008)

Chapter 6 : Conclusions and Perspectives

6.1. Conclusions

During the doctoral research, we have contributed meanly in the development of nanostructured carbon science. We center our research on the study of different properties of functionalized and doped carbon nanotubes. We contributed to understand the interaction of these composite materials with their surrounded environment. We also fabricated two electronic devices, in this way, we increased the opportunity for the introduction of electronic devices based on carbon nanostructures in day life situations.

In Chapter 2 we have studied the electrical properties of random network composed of functionalized SWCNTs, we demonstrated the potential of the inkjet printing technique for the fabrication of practical electronic devices made of nanostructures. We studied their current-voltage characteristics and field effect properties of various functionalized nanotubes, and by applying the generated knowledge, we finally achieved the fabrication of an entirely SWCNT field effect transistor over a flexible substrate. Here we have contributed to increase the opportunity for the incorporation of carbon nanotubes in low-cost electronic devices.

As we have observed, the introduction of functional groups in the carbon nanotube results in different electrical properties. Similar phenomena occur when we add a small cluster of a metallic or semiconductor material. Composites of metal-decorated carbon nanotubes have been widely used on different devices, however, a little is known about the electronic

phenomena that occur in those systems. In this case, we fabricated a vapor-sensor device, by decorating CN_X-MWNTs with Ag nanoparticles and studying the interaction with different organic molecules and the effect of the temperature on the sensor performance. Using density functional theory we also carried out a systematic study to understand the interaction between the molecules and the composite system. Finally, based on these results we proposed the probable detection mechanism.

Nanotubes are one of the most studied carbon nanostructures and they have been doped by the introduction of different elements to the carbon lattice. Actually there are different theoretical studies about doped nanotubes, using their own doped-configurations as models to study different properties, such as electrical transport or their chemical reactivity. Some of the most studied doped nanotubes are the nitrogen-doped; they have shown better performance for gas detection, anchorage of nanoparticles, enhanced biocompatibility and a better performance as adsorbent materials for heavy metals in aqueous environment. We believe that there are different ways to dope a nanotube, thus their electronic, chemical and mechanical properties strongly depend of these doping-configurations. A long this lines, we decide studied different nitrogen-doping configurations, and we wanted to really understand the individual behavior of these doped systems. Our results suggest that all the proposed configurations could coexist at room temperature. All the doped configurations exhibit different electronic structures and different chemical reactivity. Thus each individual doped configuration can be responsible for different behaviors in N-doped nanotubes. In order to understand better their electronic properties, all this configurations could be extended to other types of doped nanotubes such as boron, sulfur or phosphorous doped nanotubes.

In the final chapter, we also studied a composite material, we decorated carbon nanotubes with ZnO nanoparticles, and we controlled the nanoparticles size by adding a sulfur-containing capping agent. As we mentioned before, these composite materials has been used in different applications, but there is not a deep compression on the interaction between these nanostructures. We wanted to contribute by understanding the interaction between nanoparticles and carbon nanotubes. We tried to solve some basic questions, such as, why the nanoparticle is attached to the nanotube? What is on the surface of the nanoparticles? Guided by those questions, we carried out systematic experimental and theoretical studies. Within this chapter, we have contributed to understand the interaction of the nanoparticle with their surrounding media, because now we may suggest what is in their surfaces and the interface between the nanotube and the nanoparticle. We also found a magnetic response generated by the addition of sulfur to the ZnO, which is in great concordance with the recent observation of ferromagnetic response in ZnO nanoparticles at room temperature.

6.2. Perspectives

Fabrication nanotube-based field effect transistors that we have done in this thesis, open the possibility to test other carbon nanomaterials with different functional groups, and as we assume from our results, polymeric composite could be better candidates for their use in the channel on FET devices. It would be also desirable to improve the ink preparation, to enhance the nanostructures printability. After the optimization process on fabrication, we would like to fabricate more complicated electronic circuit and test the performance of nanotube-FET devices in a “real” life situation. There are other carbon nanostructures such as graphene, carbon nanoribbons or a combination of them, which we could use to improve the performance of the electronic devices. We also wanted to compare different thin-films deposition technique for different applications.

For the vapor-sensor based on metal-decorated carbon nanotubes, it would be desirable to test different nanocomposites by varying the metallic nanoparticle, and controlling what is on the surface of the nanoparticles. In this way, we can improve their selectivity and sensitivity. After their optimization, it would be desired to test the sensor devices in a real life situation. In this way we go closer to the final application of these low-cost sensor devices. We can also use other carbon nanostructures decorated with different metal or semiconductor materials to detect different vapors or gases, and by varying their working temperature we could improve its selectivity. In this way we want to contribute to obtain a functional product based on carbon nanostructures.

In order to deeply understand the behavior of the doped nanosystems, in chapter 4 we analyzed different nitrogen-doping configuration, the resulting

structures may be used as a model for different phenomena, such as electronic transport, metal adsorption, gas/vapor detection, etc. It is well know that, defects are a rule in carbon nanotubes, and talking about doped nanotubes, the formation of such defects is enhanced for the introduction of foreign atoms. For these reason, we also want to study similar doping configurations with other elements, such as boron, sulfur, phosphorous, etc.

In the last chapter, we analyzed a semiconductor-nanotube system, N-doped carbon nanotubes decorated with zinc oxide nanoparticles. We studied the role of the passivating agent, and the interface between the nanostructures. These results open the possibility to study, in a more real situation, the interaction of this hybrid-material with other molecules for possible sensor applications, or to study the electronic transport or optical properties of this composite.

Appendix A : Electronic Structure Calculations and Computational tools

A.1. Electronic Structure Calculation

The role of computational materials science has become of fundamental importance not only for the advancement of basic research but also in the applied field of nanotechnology. Theoretical modeling and computer simulations can directly access with high accuracy the shortest length and time scales of nanoscopic systems. Nanoscale simulations have thus become a predictive tool for the design of novel devices and now modeling is an integral part of interdisciplinary materials research. In order to study the electronic behavior of carbon materials, one has to solve the basic equation of quantum mechanics, the many electrons Schrödinger equation. However, in spite of the impressive computer power at our disposal, solving this equation remains a difficult task and requires a deep physical and chemical understanding of many-electrons systems. Wide ranges of computational methods are available for the theoretical modeling and simulation of carbon materials properties. These methods are actually based on approximations at various level of detail of the complicate many-body problem, thus they can be considered a compromise between efficiency and accuracy. In general, they can be classified into three groups: *ab initio*, semi-empirical, tight-binding and effective methods.

Ab initio methods allow the computation of materials properties from first principles, without the need of parameters to be adjusted or fitted to experimental input data, apart from the fundamental physical constants and atomic masses. The general advantage of *ab initio* methods is the high

accuracy of the quantitative results. The main disadvantages are represented by the high computational cost and the difficulty of getting a deeper understanding of the calculated phenomena. They can be further classified into *wavefunction methods* and *density functional methods*.

Wavefunction methods solve self-consistently, in a mean-field approximation, the many electron Schrödinger equation by expanding the many-electron antisymmetrized wavefunction in Slater determinants, formed by a set of orthonormal one-electrons orbitals φi (r). This constitutes the basics of Hartree-Fock (HF) method. HF theory is less appropriate for systems with high electron density such as transition metal systems or with highly delocalized states and fails completely to account for the collective Coulomb screening in a perfect metal. Inclusion of correlation effects reduces the system size accessible to calculation to few hundred atoms, depending on the level of theory. The most accurate correlated methods are restricted to molecules with just a few atoms and are also too slow for performing dynamical simulations even for small molecules and time-scales in the pico-second range.

Density functional theory (DFT) is another independent-particle method, whose basics were formulated in two fundamental papers, the first published in 1964 by P. Hohenberg and W. Kohn [1], and the second in 1965 by W. Kohn and J. L. Sham [2]. The basic idea behind these works is that the ground-state electronic energy (and therefore all other related ground-state properties) is a functional of the electronic density. Then a set of single-particle equations, the so-called Kohn-Sham equations, are derived by applying a variational principle to the electronic energy. Electron-electron interactions are again treated in an average way according to several available approximations to the functional dependence of the exchange-

correlation energy on density, which actually constitutes the main source of variations in DFT calculations. Actually, the Hohenberg-Kohn theorem doesn't specify the form of the functional to be used, but just confirms that it exists. Starting from a trial density given by the square modulus of guessed wavefunctions, the energy functional of the Kohn-Sham hamiltonian is obtained and then minimized until self-consistency is reached for the input and output ground state charge densities.

DFT calculations can be considered the workhorse of all *ab initio* methods, as they can provide accurate predictions of structural, electronic, vibrational and magnetic properties for a wide range of systems, from molecules and clusters to periodic and amorphous solids, either metals, semiconductors or insulators. Density functional calculations are possible for systems of the order of 100 atoms, but by exploiting symmetry also calculations for clusters of over 1000 atoms can be performed [3]. Although DFT is computationally less demanding than HF methods, it has to be pointed out that in DFT calculations the number of variational parameters needed for the expansion of the wavefunction adopted for constructing the trial ground-state density is quite large, thus other methods are required for achieving more efficient calculations and treating systems with larger size. Soon after the discovery of carbon nanotubes in 1991, the electronic properties of singlewalled nanotubes were investigated by density functional methods [4,5], before the electronic density of states could be actually measured by STS in 1998 by Odom. Subsequently, calculations were performed also for more complex systems such as double- and multi-wall nanotubes and bundles of single-wall nanotubes [6,7].

A.2. Computational Tools: The SIESTA Code

Within the last two decades, the first-principles simulation of condensed matter systems has expanded spectacularly, from physics and chemistry into life, earth, nanoscale and materials sciences. This success has been based on both the steady growth of computing power and the development of methods based on density-functional theory (DFT). The SIESTA method [8] relies on periodic boundary conditions (PBC) in the three directions of space, and so, clusters, molecules or point defects (0D), chains, tubes or line defects (1D), and surfaces, interfaces or plane defects (slabs, 2D) are treated with 3D supercells. The basic goal is thus finding the quantum-mechanical groundstate energy of the electrons in the system for given nuclear positions. To deal with the many-electron problem, the density functional theorem is employed [1] which asserts that the energy of the ground state of a many-body system can in principle be obtained as a functional of its particle density. The local density approximation [2] provides a practical implementation of that functional. It proposes an alternative system of formally non-interacting particles under the influence of a local potential, which depends on the electron density at the point where it is evaluated, and which includes the electron–electron interaction in an effective way. The essentially non-local effects of electron exchange and correlation are described by an effective local potential obtained by fitting [9] to the result of an independent, very accurate calculation for the full many-body problem of the free electron gas [10]. The original many-particle problem is thus approximated by a one-particle problem that has to be solved self-consistently (the potential depends on the density which, in turn, depends on the solution). The generalized-gradient approximated (GGA) functionals represent a step towards the exact DFT functional, by considering that the exchange-correlation potential at a point depends not

only on the electronic density but also on its gradient and (in some cases) on higher derivatives.

The inclusion of core electrons in the calculation increases the computational load since the number of electrons is higher, and their wave functions vary very rapidly. They are, however, very insensitive to variations in the chemical environment. Therefore, core electrons are not explicitly considered in the calculations but are replaced by non-local norm-conserving pseudopotentials, also calculated from first principles. Numerical atomic orbitals (NAO's) are more flexible in this respect. Different ideas have been proposed in the literature, originally within tight-binding contexts concentrating on minimal (single ζ) bases. They are obtained by finding the eigenfunctions of the isolated atoms confined within spherical potential wells of different shapes, or directly modifying the eigenfunctions of the atoms. These schemes give strictly localized orbitals, i.e., orbitals that are strictly zero beyond given cutoff radii r_c [11]. After all these considerations, the problem to be solved is a one-particle quantum-mechanical problem with an effective potential. This problem is solved by expanding the one-particle wave functions in a finite basis and diagonalizing the Hamiltonian matrix that results.

In the SIESTA program, the building of the Hamiltonian and overlap matrices is performed using a combination of two techniques [12,13]. On one hand, the overlap matrix and some terms of H including the kinetic energy (the so-called two-centre integrals) allow a very efficient numerical integration in one single variable and as a function of just the distance between every two atoms. The remaining terms are calculated by replacing the three-dimensional integrals by summations over a finite grid, a discretization of 3-D space. One parameter controls the precision of these integrations,

namely, the fineness of the grid, usually expressed as an energy cutoff, an index borrowed from PWs, the square root of which gives the inverse of that fineness.

A.3. SIESTA Computational Details

The electronic calculations were performed using Density Functional Theory (DFT) [1,2] within the Local Spin Density Approximation (DFT-LSDA) using the general gradient approximation (GGA) with the Perdew-Burke-Ernzerhof (PBE) [14,15] functional as implemented in the SIESTA code [3]. The wave functions for the valence electrons were represented by a linear combination of pseudo-atomic numerical orbitals using a double-ζ with additional polarization orbitals basis (DZP) [11], while core electrons were represented by norm-conserving Troullier-Martins pseudopotentials in the Kleynman-Bylander non-local form [16,17]. The real-space grid used for charge and potential integration is equivalent to a planewave cut-off energy of 150Ry in the majority of the systems. The pseudo-potentials (pp's) were constructed as follow:

Atom	*Valence electrons*	*Electronic configuration*
H	1	$1s^1$
C	4	$2s^2 2p^2$
N	5	$2s^2 2p^3$
O	6	$2s^2 2p^4$
S	6	$3s^2 3p^4$
Cl	7	$3s^2 3p^5$
Zn	12	$4s^2 3d^{10}$
Ag	11	$5s^1 4d^{10}$

In all cases, the structures were relaxed by conjugate gradient minimization until the maximum force was less than 0.04 eV/Å. Periodic boundary conditions were used and the inter-cell distance was kept to a minimum of 30 Å to avoid lateral interactions. The studied systems were constructed in different ways according to our necessities; here we explain how they were built and some additional details:

In Chapter 3, the systems were built by using a supercell of 100 atoms taking 5 unit cell of (5,5) carbon nanotube and different organic molecules. For the case of Ag_{13} clusters, they were collocated in a supercell with a separation of 30 Å. The molecular dynamic simulations of the $Ag_{55}C_{80}$ cluster was carried out during 1 picosecond with 1 femtosecond steps, using the same parameters described above. For Chapter 4, the systems were constructed by using a supercell of 160 atoms taking 4 unit cell of the (10,0) nanotubes. The inter-tube distance was kept to a minimum of 40 Å to avoid lateral interactions. Finally, in Chapter 5 the clusters were created from a bulk-structure ZnO. For the case of $Zn_{15}O_{15}$ clusters, they were collocated in a supercell with a separation of 30 Å. In this case, the real-space grid used was equivalent to a planewave cut-off energy of 300Ry. The hybrid carbon nanotube-ZnO cluster system was built using 5 unit-cells of (10,0)-SWCNT (200 atoms) and a $Zn_{15}O_{18}S_3$ cluster (36 atoms).

Along the chapters, we calculate the binding, formation and adsorption energies of different systems; here we show the used formula:

1. The **binding energy (*E_b*)** is defined by

$$E_b = \frac{\sum E_i N_i - E_{SC}}{N_{total}}$$

Where E_{SC} is the energy of the super cell, N_i is the number of *i* atoms in the super cell and E_i is the energy of the isolated atom, the subindex *i* mean the different atomic species that may contain the system under study.

2. The **formation energy (E_f)** is defined by

$$E_f = E_b - \sum_i N_i \mu_i$$

Where E_b is the binding energy of the system, N_i is the number of atoms of species *i*, and the μ_i is the cohesive energy of the corresponding atom.

3. The **Adsorption energy (E_{ads})** is given by:

$$E_{ads} = E_{SC} - E_{substrate} - E_{adsorbate}$$

Where E_{SC} is the energy of the entire system (substrate material and adsorbed molecules or atoms); $E_{substrate}$ is the energy of the pure substrate material (carbon nanotube or metallic cluster) and $E_{adsorbate}$ is the energy of the isolated adsorbed material (organic molecule).

Appendix B : Carbon Nanotube Growth Methods and Principles of Characterization Techniques

B.1. Carbon Nanotubes Growth Methods

B.1.1. Arc-discharge and Laser Ablation

In arc-discharge, carbon atoms are evaporated by plasma of helium gas ignited by high current passed through opposing carbon anode and cathode (see Fig). Arc-discharge has been developed into an excellent method for producing both high quality multi-walled nanotubes and single-walled nanotubes. MWNTs can be obtained by controlling the growth conditions such as the pressure of inert gas in the discharge chamber and the arcing current. In 1992, a breakthrough in MWNTs growth by arc-discharge was first made by Ebbesen and Ajayan, who achived growth and purification of high quality MWNTs at the gram level [18]. The synthesized MWNTs have lengths on the order of ten microns and diameters in the range of 5-30 nm. The nanotubes are typically bounded together by strong van der Waals interactions and form tight bundles. MWNTs produced by arc-discharge are very straight, indicative of their high crystallinity. For as grown materials, there are few defects such as pentagons or heptagons existing on the sidewalls of the nanotubes. The by-product of the arc-discharge growth process is multi-layered graphitic particles in polyhedron shapes. Purification of MWNTs can be achieved by heating the as grown material in an oxygen environment to oxidize away the graphitic particles [18]. The polyhedron graphitic particles exhibit higher oxidation rates than MWNTs; nevertheless, the oxidation purification process also removes an appreciable amount of nanotubes.

For the growth of single-walled tubes, a metal catalyst is needed in the arc-discharge system. The first success in producing substantial amount of SWNTs by arc-discharge was achieved by Bethune in 1993 [19]. They used a carbon anode containing a small percentage of cobalt catalyst in the discharge experiment, and found abundant SWNTs generated in the soot material. The growth of high quality SWNTs at the 1-10g scale was achieved by Smalley using laser ablation (laser oven) method [20]. The method utilized intense laser pulses to ablate a carbon target containing 0.5 atomic percent of nickel and cobalt. The target was placed in a tubular furnace heated at 1200°C. During laser ablation, a flow of inert gas was passed trough the growth chamber to carry the grown nanotubes downstream to be collected on a cold finger. The produced SWNTs are mostly in the forma of ropes consisting of tens of individual nanotubes close-packed into hexagonal crystals via van der Waals interactions. In SWNTs growth by arc-discharge and laser ablation, typical by-products include fullerenes, graphitic polyhedrons with enclosed metal particles, and amorphous carbon in the form of particles or overcoating on the sidewalls of nanotubes.

B.1.2. Chemical Vapor Deposition

Chemical vapor deposition (CVD) methods have been successful in making carbon fibers, filament and nanotubes materials. The growth process involve heating a catalyst material to high temperatures in a tube furnace and flowing a hydrocarbon gas through the tube reactor for a period of time. Materials grown over the catalyst and are collected upon cooling the system to room temperature. They key parameters in nanotube CVD growth are the hydrocarbon, catalyst and growth temperature. The active catalytic species are typically transition metal nanoparticles formed on a supported material such as alumina. The general nanotube growth mechanism in CVD process

involves the dissociation of hydrocarbon molecules catalyzed by the transition metal, and dissolution and saturation of carbon atoms in the metal nanoparticle. The precipitation of carbon from the saturated metal particle leads to the formation of tubular carbon solids in sp^2 structure. Tubule formation is favored over other forms of carbon such as graphitic sheets with open edges. This is because a tube contains no dangling bonds and therefore is in a low energy form. MWNT growth, most of the CVD methods employ ethylene or acetylene as the carbon feedstock and the growth temperature is typically in the range of 550-750°C. Iron, nickel or cobalt nanoparticles are often used as a catalyst. The rationale for choosing these metals as a catalyst for CVD growth of nanotubes lies in the phase diagram for the metals and carbon. At high temperatures, carbon has finite solubility in these metals, which leads to the formation of metal-carbon solution and therefore the aforementioned growth mechanism. Noticeably, iron, cobalt and nickel are also the favored catalytic metals used in laser ablation and arc-discharge. This simple fact may hint that laser, discharge and CVD growth methods may share a common nanotube growth mechanism, although very different approaches are used to provide carbon feedstocks.

A major pitfall for CVD grown MWNTs has been the high defect densities in their structure. The defective nature of CVD grown MWNTs remains to be thoroughly understood, but is most likely be due to the relatively low growth temperature, which does not provide sufficient thermal energy to anneal nanotubes into perfectly crystalline structures [21].

B.2. Characterization Techniques

B.2.1. X-ray powder diffraction

X-rays are electromagnetic waves, and as such are accompanied by a periodically changing electrical field as they proceed outward from their source. An electron in the path of such a wave is excited to periodic vibrations by the changing field, and itself becomes a source of electromagnetic waves of the same frequency and wavelength. There thus arise from the interaction a new spherical wave front of X-rays, with the electron as its origin, deriving its energy from the impinging beam. By this procedure the electron is said to scatter the original beam. The X-ray powder diffractometer is designed to disperse X-rays of a single wavelength by diffracting them from planes of different spacing. Furthermore, and X-ray powder diffraction is characterized by the use of a local intensity-measuring receiver

If the presence of lattice strains or other imperfections are non-significant, under these circumstances the breadth β of pure diffraction profile can be ascribed solely to small crystallite size:

$$L = \frac{K\lambda}{\beta_{1/2}\cos\theta} \qquad \textbf{(B-1)}$$

Wherein θ is the diffraction angle, λ is the wavelength of the X-rays, L is the mean dimension of crystallites composing the powder, $\beta_{1/2}$ is the breadth at half-maximum intensity of the pure diffraction profile, and K a constant approximately equal to unity and related to crystallite shape, this is the Scherrer equation [22].

B.2.2. Electron microscopy

The particle-wave duality of quantum mechanics states that a particle can behave like a wave with a wavelength called the *de Broglie wavelength* that is inversely proportional to its momentum. Hence, an electron accelerated at 50keV would have a wavelength of l=0.005nm. In the case of electron microscopes, the spatial resolution is limited by the aberration of the electromagnetic lenses. In a transmission electron microscope (TEM), electrons pass through a rather thin sample and are then imaged by appropriate electromagnetic lenses into a fluorescent screen or a CCD, in analogy to a regular optical microscope. The electrons are accelerated to voltages between 50kV and 300kV. The spatial resolution is around 0.2nm, although recent spherical aberration-corrected TEMs have achieved better resolution at even lower acceleration voltages [23].

Unless the sample is very thin, the electrons of a TEM are strongly scattered within the specimen, or absorbed rather than transmitted. Therefore, for examining bulk samples it is desirable to use reflected, or secondary electrons (absorbed and then emitted). However, when the electrons are emitted, they do so with a variety of energies and directions, making them difficult to focus and project into a screen. Instead, a scanning approach is used: First, the source electrons are focused into a small-diameter electron probe that is scanned throughout the sample, and then, the secondary electrons of each of the scanning steps or pixels are collected and amplified. The intensity or number of electrons reaching the collector specifies the brightness of a given pixel of an image. This is the principle of a scanning electron microscope (SEM). The acceleration voltage of a SEM is usually between 5 to 30 kV, and the spatial resolution is of c.a. 1nm. In moderate

acceleration voltages, the information observed in the SEM image is mostly of the surface of the sample. As the acceleration voltage increases, information of deeper in the sample is obtained.

B.2.3. Energy Dispersive X-ray Analysis

Energy Dispersive X-ray (EDX) analysis is a technique used for identifying the elemental composition of the specimen, or an area of interest. The EDX analysis system works as an integrated feature of an electron microscope, and cannot operate on its own without the latter. During EDX analysis, the specimen is bombarded with an electron beam inside the scanning electron microscope. The bombarding electrons collide with the specimen atoms' own electrons, knocking some of them off in the process. A position emptied by an ejected inner shell electron is eventually occupied by a high-energy electron from an outer shell. To be able to do so, however, the transferring outer electron must give up some of its energy by emitting an X-ray. The amount of energy released by the transferring electron depends on which shell it is transferring from, as well as which shell it is transferring to. Furthermore, the atom of every element releases X-rays with unique amounts of energy during the transferring process. Thus, by measuring the amounts of energy present in the X-rays being released by a specimen during electron beam bombardment, the identity of the atom from which the X-ray was emitted can be established.

Appendix C : Published Works During the Ph. D. Thesis

During this Ph. D. thesis various research works were presented and published in different international conferences and scientific journals, a complete list of the published work is listed below:

Published Research Papers

1. E. Gracia-Espino, F. López-Urías, H. Terrones, and M. Terrones, “Doping (10, 0)-Semiconductor Nanotubes with Nitrogen and Vacancy Defects”, *Mater Express,* **1**, 127-135 (2011)

2. A. B. Castle, E. Gracia-Espino, C. Nieto-Delgado, H. Terrones, M. Terrones, and S. Hussain, “Hydroxyl Functionalized and N-doped Multi-Walled Carbon Nanotubes Decorated with Silver Nanoparticles Preserve Cellular Function”, *ACSnano*, **5**, 2458–2466 (2011)

3. E. Gracia-Espino, G. Sala, F. Pino, N. Halonen, J. Luomahaara, J. Makin, G. Toth, K. Kordas, H. Jantunen, M. Terrones, P. Helisto, H. Seppa, P. M. Ajayan and R. Vajtai, "Electrical Transport and Field-Effect Transistors Using Inkjet-Printed SWCNT Films Having Different Functional Side Groups," *ACSNano*, **4**, 3318 – 3324 (2010)

4. J, Kukkola, A. Rautio, G. Sala, F. Pino, G. Tóth, A.-R. Leino, J. Mäklin, H. Jantunen, A. Uusimäki, K. Kordás, E. Gracia, M. Terrones, A. Shchukarev, J.-P. Mikkola, “Electrical transport through single-wall carbon nanotube–anodic aluminum oxide–aluminum heterostructures” *Nanotechnology*, **21**, 035707 (2010)

5. X. Jia, J. Campos-Delgado, E. Gracia-Espino, M. Hofmann, H. Muramatsu, Y. A. Kim, T. Hayashi, M. Endo, J. Kong, M. Terrones, M. S. Dresselhaus, "Loop formation in graphitic nanoribbon edges using furnace heating or Joule heating" *J. Vac. Sci. Technol. B*, **27** 1996-2002 (2009)

6. H. Rosas-Hernández, S. Jiménez-Badillo, P. P. Martínez-Cuevas, E. Gracia-Espino, H.Terrones, M.Terrones, S.M. Hussain, S. F. Ali, C. González, "Effects of 45-nm silver nanoparticles on coronary endothelial cells and isolated rat aortic rings" *Toxicology Letters*, **191**, 305–313 (2009)

7. E. E. Gracia-Espino; D. Hernández-Cruz; M. Terrones; E. Alvarado-Méndez; Monica Trejo-Durán; J. A. Andrade-Lucio, "Self-diffraction properties in nanotubes (CNTs)" (Proceedings Paper), Photonics North, **7386** (2009) doi: 10.1117/12.839517

Published Patents

1. J Campos-Delgado, M. S. Dresselhaus, M. Endo, E. Gracia-Espino, X. Jia, J.M Romo-Herrera, H. Terrones, M. Terrones. "CVD-grown graphite nanoribbons" Pub. No. US 2009/0226361 A1. Pub. Date: Sep. 10 (2009)

Poster Presentation in International Conferences

1. E. Gracia-Espino, F. Lopez Urias, H. Terrones, M. Terrones. "Quantum Transport Theoretical Study on Narrow Doped Armchair Graphene Nanoribbons: DFT Calculations". Poster presentation, *International Conference on the Science and Application of Nanotubes*, Cambridge, UK (2011)

2. E. Gracia-Espino, F. Lopez Urias, H. Terrones, M. Terrones. "Synthesis, Characterization, and Theoretical Studies of Hybrid ZnO Nanoparticles and Nitrogen-Doped Carbon Nanotubes". Poster presentation, *International Conference on the Science and Application of Nanotubes*, Cambridge, UK (2011)

3. E. Gracia-Espino, F. Lopez Urias, H. Terrones, M. Terrones. "Vacancies and Nitrogen-Doped Effects on the Electronic and Structural Properties of the (10,0) Semiconducting Carbon Nanotube". Poster presentation, *International Conference on the Science and Application of Nanotubes,* Montréal, Québec, Canada (2010)

Appendices References

[1] P. Hohenberg, W. Kohn. "Inhomogeneous electron gas". *Phys. Rev. B* **136**, 864 (1964).

[2] W. Kohn, L. J. Sham." Self-consistent equations including exchange and correlation effects". *Phys. Rev.* **140**, A1133 (1965).

[3] J. M. Soler, E. Artacho, J. D. Gale, A. Garcıa, J. Junquera, P. Ordejon, D. Sanchez-Portal. "The SIESTA method for ab initio order-N materials simulation". *J. Phys.: Cond. Matter,* **14**, 2475 (2002).

[4] J. W. Mintmire, B. I. Dunlap, C. T. White. "Are fullerene tubules metallic?" *Phys. Rev. Lett.* **68**, 631 (1992).

[5] J. W. Mintmire, C. T. White. "First-principles band structures of armchair nanotubes". *Appl. Phys. A* **67**, 65 (1998)

[6] D. Östling, D. Tomanek, A. Rosen. "Electronic structure of single-wall, multiwall, and filled carbon nanotubes". *Phys. Rev. B* **55**, 13980 (1997)

[7] Y.-K. Kwon, D. Tomanek. "Electronic and structural properties of multiwall carbon nanotubes". *Phys. Rev. B* **58**, R16001 (1998)

[8] E. Artacho, E. Anglada, O. Dieguez, J.D. Gale, A. Garcıa, J. Junquera, R.M. Martin, P. Ordejon, J. M. Pruneda, D. Sanchez-Portal, J. M. Soler, "The SIESTA method; developments and applicability", *J. Phys.: Condens. Matter*, **20** 064208 (2008)

[9] J.P. Perdew, A. Zunger "Self-interaction correction to density functional approximations for many-electron systems". *Phys Rev B*, **23**, 5048–5079 (1981)

[10] D.M. Ceperley, B.J. Alder "Ground state of the electron gas by a stochastic method". *Phys Rev Lett* **45**, 566–569 (1980)

[11] J. Junquera, O. Paz, D. Sanchez-Portal, E. Artacho, "Numerical atomic orbitals for linear-scaling calculations", *Phys Rev B*, **64**, 235111 (2001)

[12] P. Ordejon, E. Artacho, J. M. Soler, "Self-consistent order-*N* density-functional calculations for very large systems", *Phys Rev B*, **53** (1996)

[13] D. Sanchez-Portal, P. Ordejon, E. Artacho, J.M. Soler "Density functional method for very large systems with LCAO basis sets". *Int J Quantum Chem,* **65**, 453–461 (1997)

[14] J. P. Perdew, K. Burke, M. Ernzerhof, "Generalized Gradient Approximation Made Simple," Phys. Rev. Lett. ,**77**, 3865 (1996)

[15] J. P. Perdew, K. Burke, M. Ernzerhof, "Generalized Gradient Approximation Made Simple," Phys. Rev. Lett., **78**, 1396 (1997)

[16] N. Troullie, J.L. Martins, "Efficient pseudopotentials for plane-wave calculations" *Phys. Rev. B*, **43**, 1993 (1991)

[17] L. Kleinman, D.M. Bylander, "Efficacious form for model pseudopotentials" *Phys. Rev. Lett.* **48**, 1425 (1982)

[18] T.W. Ebbesen, P.M. Ajayan, "Large-scale synthesis of carbon nanotubes" *Nature*, **358**,220-222 (1992)

[19] D.S. Bethune, C.H. Kiang, M. DeVries, G. Gorman, R. Savoy, J. Vazquez, R. Beyers, “Cobalt-catalysed growth of carbon nanotubes with single-atomic-layer walls” *Nature*, **363**, 605-607 (1993)

[20] A. Thess, R. Lee, P. Nikolaev, H. J. Dai, P. Petit, J. Robert, C. H. Xu, Y. H. Lee, S.G. Kim, A.G. Rinzler, D.T. Colbert, G.E. Scuseria, D. Tomanek, J.E. Fisher, R.E. Smalley, “Crystalline Ropes of Metallic Carbon Nanotubes” *Science,* **273**, 483-487 (1996)

[21] M.S. Dresselhaus, G. Dresselhaus, Ph. Avouris (eds), “Carbon nanotubes, syhtnesis, structure, properties, and applications”, Springer (2001)

[22] H.P. Klug, L.E. Alexander, “X-ray difraction procedures, for polycristalline and amorphous materials” 2nd edition, USA, Wiley-intersience (1974)

[23]